Molecular basis for SH3 domain regulation of F-BAR-mediated membrane deformation

Inaugural-Dissertation
to obtain the academic degree
Doctor rerum naturalium (Dr. rer. nat.)
submitted to the Department of Biology, Chemistry and Pharmacy
of Freie Universität Berlin

By

Yijian Rao

From Fujian, China

November, 2010

Die vorliegende Arbeit wurde in der Zeit von März 2007 bis November 2010 unter Anleitung von Prof. Dr. Volker Haucke am Institut für Chemie-Biochemie der Freien Universität Berlin im Fachbereich Biologie, Chemie, Pharmazie durchgeführt.

1st Reviewer: Prof. Dr. Volker Haucke

2nd Reviewer: Prof. Dr. Wolfram Saenger

Date of defence: 13-01-2011

Acknowledgements

I would like to thank all people who have helped and inspired me during my doctoral study.

First and foremost, I would like to express my deep and sincere gratitude to my supervisor Prof. Dr. Volker Haucke. Thank you for giving me the opportunity to enter the world of biological science and perform my research in his lab. His contagious enthusiasm for science has motivated all people in his lab, including me. In addition, I am thankful for his understanding, encouraging and personal guidance.

I would like to thank all former and current members of AG Haucke's lab for my thesis support and for creating a homey place to work. Special thanks to Dr. Arndt Pechstein and Dr. Dmytro Puchkov for their contribution to my project. Special thanks also to Dr. Tanja Maritzen and Dr. Arndt Pechstein for their critical reading of this dissertation manuscript. In particular, I am deeply grateful to Julia Mössinger, "my neighbor in the lab" and a very nice lady. You are always accessible and willing to help me. Thank you, Julia.

I gratefully thank Prof. Dr. Wolfram Saenger, Dr. Qingjun Ma and Dr. Ardeschir Vahedi-Faridi for your wonderful collaboration and contribution to my project. Without your contribution, we cannot publish the *Syndapin* story so fast. I also thank Prof. Dr. Wolfram Saenger for his assistance and support as my thesis committee member.

I would like to thank Prof. Dr. Oleg Shupliakov and Dr. Anna Sundborger at Department of Neuroscience, Linné Center in Developmental Biology and Regenerative Medicine, Karolinska Institutet. Thanks for your collaboration and contribution to my project.

I would like to thank all my friends in Berlin for spending so much happy time with me!

My deepest gratitude goes to my parents and my family for their unflagging love and support throughout my life. This dissertation is simply impossible without them. Last but not least, thanks to my wife Lifeng Yang for her patience, love and support.

Directory

Summary

Eukaryotic cells are characterized by a diverse array of membraneous structures including vesicles, tubules, and pleiomorphic vacuoles that enable cellular processes such as organelle biogenesis, cell division, cell migration, secretion, and endocytosis. In many cases, dynamic membrane remodeling is accomplished by the reversible assembly of membrane-sculpting or deforming proteins, most notably by members of the BAR (Bin/amphiphysin/Rvs) domain superfamily. Members of this protein superfamily are involved in membrane remodeling in various cellular pathways ranging from endocytic vesicle and T-tubule formation to cell migration and neuromorphogenesis. Membrane curvature induction and stabilization are encoded within the BAR or F-BAR (Fer-CIP4 homology-BAR) domains, alpha-helical coiled coils that dimerize into membrane-binding modules. BAR/F-BAR domain proteins often contain also an SH3 domain, which recruits binding partners such as the oligomeric membrane-fissioning GTPase dynamin. How precisely BAR/F-BAR domain-mediated membrane deformation is regulated at the cellular level is unknown. Here we present the crystal structures of full-length syndapin 1 and its F-BAR domain. The crystal structures show that the F-BAR domain of syndapin 1 dimerizes into an elongated “S” shape with a wedge loop in each monomer, which is required for the membrane-deforming activity of syndapin. Importantly, our data also show that syndapin 1 F-BAR-mediated membrane deformation is subject to autoinhibition by its SH3 domain. Release from the clamped conformation is driven by association of syndapin 1 SH3 domain with the proline-rich domain of dynamin 1, thereby unlocking its potent membrane-bending activity. We hypothesize that this mechanism might be commonly used to regulate BAR/F-BAR domain-induced membrane deformation and to potentially couple this process to dynamin-mediated fission. Our data thus suggest a structure-based model for SH3-mediated regulation of BAR/F-BAR domain function.

Zusammenfassung

Eukaryotische Zellen enthalten eine große Vielfalt membranöser Strukturen wie z.B. Vesikel, Röhren und pleiomorphe Vakuolen, die an so unterschiedlichen Prozessen wie der Biogenese zellulärer Organellen, der Zellteilung, Zellmigration, Sekretion und Endozytose beteiligt sind. In den vielen Fällen wird die dynamische Umformung der Membran durch die reversible Zusammenlagerung von Membran-verformenden Proteinen bewirkt, ganz besonders durch Mitglieder der BAR (Bin/amphiphysin/Rvs) Domänen Proteinfamilie. Mitglieder dieser Proteinfamilie sind beteiligt am Membranumbau im Rahmen verschiedenster zellulärer Prozesse, von der Generierung endozytotischer Vesikel und T-Röhren bis hin zu Zellmigration und Neuromorphogenese. Ihre Fähigkeit zur Induzierung einer bestimmten Membrankrümmung und zur Stabilisierung von gekrümmten Membranen resultiert aus der Struktur ihrer BAR oder F-BAR (Fer-CIP4 Homologie-BAR) Domänen. Hierbei handelt es sich um alpha-helikale “coiled coils”, die zu Membran-bindenden Modulen dimerisieren können. BAR/F-BAR Proteine enthalten zudem oft eine SH3 Domäne, die Bindepartner wie die oligomere GTPase Dynamin, die an Membranabtrennungsprozessen beteiligt ist, rekrutieren kann.

Wie genau die BAR/F-BAR Domänen vermittelte Membranverformung in der Zelle reguliert wird, ist bislang unbekannt. Die in dieser Doktorarbeit präsentierten Kristall-Strukturdaten von komplettem Syndapin 1 Protein und seiner F-BAR Domäne können zur Aufklärung dieser Frage beitragen. Die Kristallstrukturen zeigen, dass die F-BAR Domäne von Syndapin 1 dimerisiert. Des resultierende Dimer hat die Form eines verlängerten “S”, wobei jedes Monomer eine Keil-artige Schleife enthält, die notwendig ist für die Fähigkeit Syndapins, Membranen zu deformieren. Von großer Bedeutung für das Verständnis der Regulation dieser Fähigkeit ist die aus den Strukturdaten gewonnene Erkenntnis, dass die Syndapin 1 F-BAR-vermittelte Membranverformung durch eine in Syndapin enthaltene SH3 Domäne autoinhibiert wird. Erst wenn diese SH3 Domäne durch die Prolin-reiche Domäne von Dynamin 1 gebunden wird, kommt es zu einer intramolekularen Konformationsänderung in Syndapin, die die Keil-artigen Schleifen freilegt und es ihm so ermöglicht, Membranen zu krümmen. Wir stellen die Hypothese auf, dass diese Art der Autoinhibition ein genereller Mechanismus zur Regulation der BAR/F-BAR

Domänen vermittelten Membrankrümmung sein könnte, der möglicherweise diesen Prozess zugleich an die Dynamin-vermittelte Membranabtrennung koppelt. Unsere Daten schlagen ein Struktur-basiertes Modell für die SH3-vermittelte Regulation der BAR/F-BAR Domänenfunktion vor.

1 Introduction

1.1 Mechanisms of membrane curvature gerenation and membrane deformation

Eukaryotic cells are characterized by a diverse array of membraneous structures including vesicles, tubules, Golgi, ER, endosomes, lysosomes, mitochondria and pleiomorphic vacuoles. The bilayer membrane can be considered as a highly regulated and heterogeneous environment which not only functions as an active participant to interact with the outside world but also provides a highly dynamic platform to control its own local morphology by regulating assembly of stabilizing cytoskeletal elements (Doherty and McMahon, 2008). Cellular activity, such as organelle biogenesis, cell division, cell migration, secretion, exocytosis and endocytosis, depends to a large extent on dynamic membrane bilayer remodelling. Dynamic membrane remodeling is achieved by an intricate interplay between lipids and proteins. The concept of protein-mediated membrane curvature generation in cells has attracted much attention in recent years. McMahon and Gallop suggested five mechanisms that could generate membrane curvature (Figure1-1) (McMahon and Gallop, 2005).

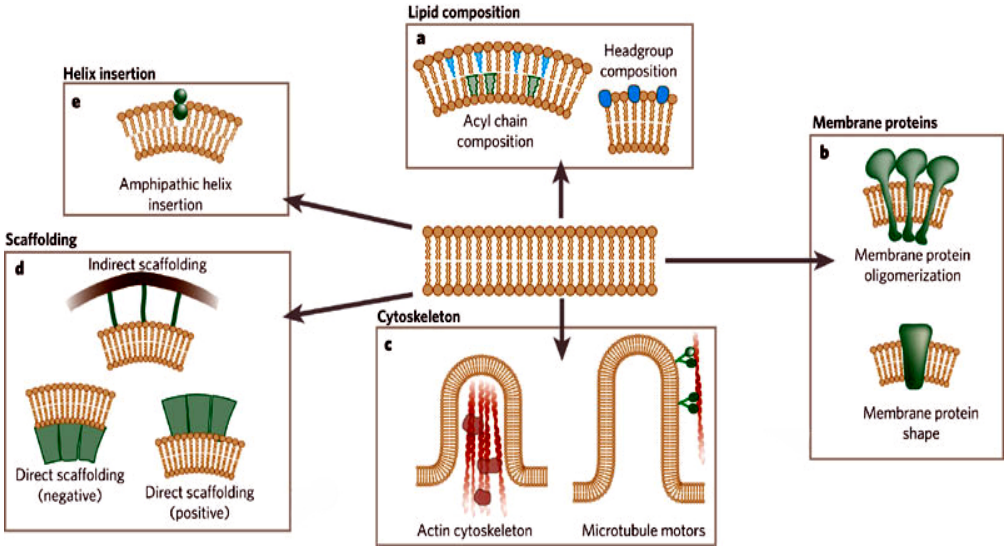

Figure 1-1 Mechanisms of membrane deformation. Membrane curvature can be generated by five mechanisms. **a**, changes of lipid composition; **b**, influences of integral membrane proteins; **c**, cytoskeletal proteins and microtubule motor activity; **d**, scaffolding by peripheral membrane

proteins; **e**, active insertion of amphipathic helices into the membrane (Taken from McMahon, HT & Gallop, JL, 2005).

1.1.1 Changes in lipid composition

The chemical properties of different lipid acyl chains or headgroups make them perfer different membrane curvatures. For example, lysophosphatidic acid and phosphatidic acid associate with opposite membrane curvatures (Brown et al., 2003; Kooijman et al., 2005; Shemesh et al., 2003) (Figure 1-1a). Addtionally, lipid headgroups are attachment sites for the recruitment of peripheral membrane proteins and can therefore generate membrane curvature. Phosphatidylinositol and its phosphorylated derivatives (referred to as phosphoinositides, PIs) have been implicated in numerous membrane trafficking and cellular signalling events. Different phosphoinositide species have been shown to exhibit distinct and characteristic subcellular distribution patterns. For example, the presence of PtdIns(4,5)P2 in the plasma membrane is essential for the budding of clathrin-coated vesicles, largely because the budding machinery binds to PtdIns(4,5)P2 (Ford et al., 2002; Ford et al., 2001; Honing et al., 2005; Kinuta et al., 2002; Wenk and De Camilli, 2004). PIs can directly associate with a variety of different proteins including cytoplasmic factors, such as membrane trafficking proteins, cell signalling adaptors, and membrane integral channels and transporters. A variety of structurally different PI binding domains have been identified, including PH (pleckstrin homology), FYVE (Fab1, YOTB, Vac1 (vesicle transport protein), and EEA1 domain), PX (Phox homology), ENTH (Epsin N-terminal homology domain), ANTH (AP180 N-terminal homology domain), C2 (protein kinase C conserved region 2, involved in calcium-dependent phospholipid binding), PTB (Phosphotyrosine binding-domain), and FERM domains (4.1-ezrin, radixin, and moesin homology domain) (Krauss and Haucke, 2007). The recruitment of these binding domains to the membrane can induce local membrane deformation.

1.1.2 Influence of integral membrane proteins

Based on crystal structures of membrane proteins, transmembrane proteins with a conical shape naturally favor curvatures that mould around their shapes. This shape has been illuminated by crystal structures of the voltage-dependent K^+-channel (Mackinnon, 2004), the amino acid antiporter AdiC (Gao et al., 2009; Gao et al., 2010b), the formate transporter FocA (Wang et al., 2009b), the transmembrane

domains of the nicotinic acetylcholine receptor (Fertuck and Salpeter, 1974; Unwin, 2005) and AMPA-subtype glutamate receptor (Sobolevsky et al., 2009). However, given that only a few structures of transmembrane proteins are known, the contribution of their intrinsic shape to membrane curvature remains largely unexplored.

1.1.3 Cytoskeletal proteins and microtubule motor activity

Filamentous cytoskeletal elements associate intimately with the plasma membrane at a wide variety of cellular locations, including highly curved regions of the plasma membrane and sites of adhesion to the cellular surroundings (Figure 1-2). Previous studies have shown that cytoskeletal changes affect membrane remodelling in cell motility and in tubule and vesicle carrier formation (Allan and Vale, 1994; Bretscher, 1996; Merrifield, 2004). The cytoskeleton also plays a role in directing the location of fusing and endocytosed vesicles and in localizing receptors and signalling complexes (Zakharenko and Popov, 1998). The ability of the cytoskeleton to influence membrane-shape changes is affected by membrane tension (Raucher and Sheetz, 2000), and decreases in tension can induce local curvature. This membrane tension can be generated by two mechanisms: actin polymerization and microtubule motor activity.

Actin polymerization has been shown to play a very important role in the remodeling of many areas containing high membrane curvature, including filopodia, lamellipodia, macropinocytic ruffles, adherens junctions, endocytic pits and phagocytic cups (Figure 1-2) (Doherty and McMahon, 2008). During endocytic processes, actin polymerization occurs once the required nucleation initiators, including Arp2/3 complex, formins, Cordon-bleu (Cobl), Leiomodin (Lmod-2), and Spire proteins are recruited to vesicle buds. The generated actin filaments are thought to push the vesicles off from the plasma membrane (Figure 1-3) (Ahuja et al., 2007; Carroll et al., 2003; Engqvist-Goldstein et al., 2004; Merrifield et al., 2005; Qualmann and Kelly, 2000; Qualmann and Kessels, 2009; Renault et al., 2008; Shupliakov et al., 2002; Takano et al., 2008; Winckler and Schafer, 2007; Yamada et al., 2009; Yarar et al., 2005). According to the specific architecture of nucleation initiators, they use different manners to catalyze actin polymerization as shown in Figure 1-3. The Arp2/3 complex for example, the first actin nucleator to be identified can form a

template for actin nucleation and thereby enable efficient filament formation. This complex is activated by the members of the WASP/WAVE superfamily through their direct interation (Takenawa and Suetsugu, 2007; Vartiainen and Machesky, 2004). WASP proteins form a family of five proteins in mammals, Wiskott–Aldrich Syndrome Protein (WASP), Neural-WASP (N-WASP) and Scar/WAVE1, 2 and 3 (Suppressor of a cyclic AMP receptor mutation/WASP Verprolin homologous) (Higgs and Pollard, 1999; Takenawa and Suetsugu, 2007; Vartiainen and Machesky, 2004) After activation, Arp2 and Arp3 are arranged to form a complex which mimics an actin dimer. Afterwards, an actin monomer is added onto the Arp2/3 complex with the help of WASP proteins. The Arp2/3 complex furthermore interacts with the sides of pre-existing actin filaments, which increases its nucleation activity and generates new filament branches at a characteristic 70^{o} angle (Figure 1-3A). The Arp2/3 complex thereby gives rise to a rapidly expanding, branched network of filaments (Campellone and Welch, 2010; Qualmann and Kessels, 2009). Actually, many BAR domain containing-proteins have been linked to the nucleation of actin polymerization and are thus able to coordinate actin polymerization and membrane remodeling events (discussed later).

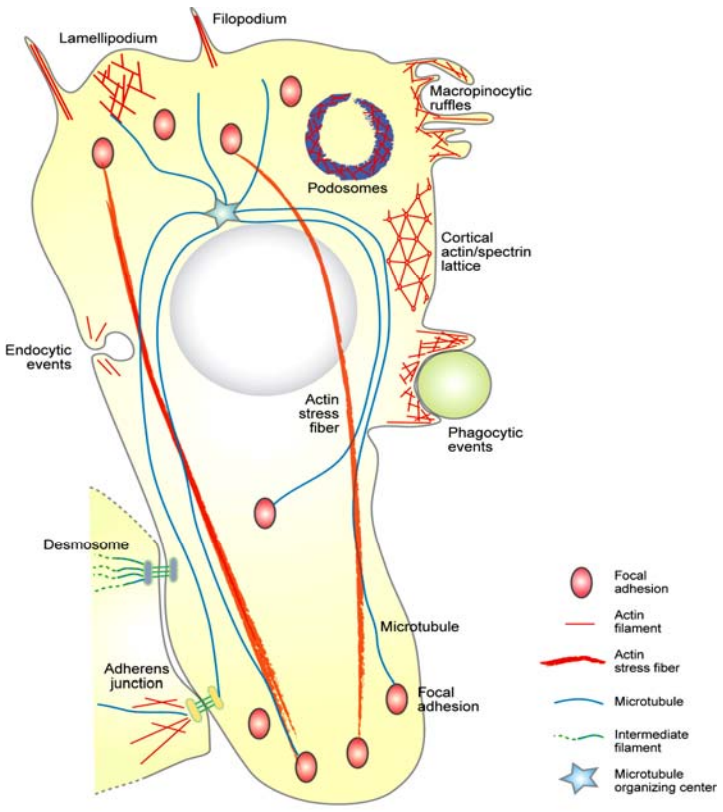

Figure 1-2 The array of membrane-cytoskeleton interactions in mammalian cells. Schematic

diagram showing the main types of cellular locations where membrane-cytoskeleton interactions are formed (Taken from Doherty, GJ & McMahon, HT, 2008).

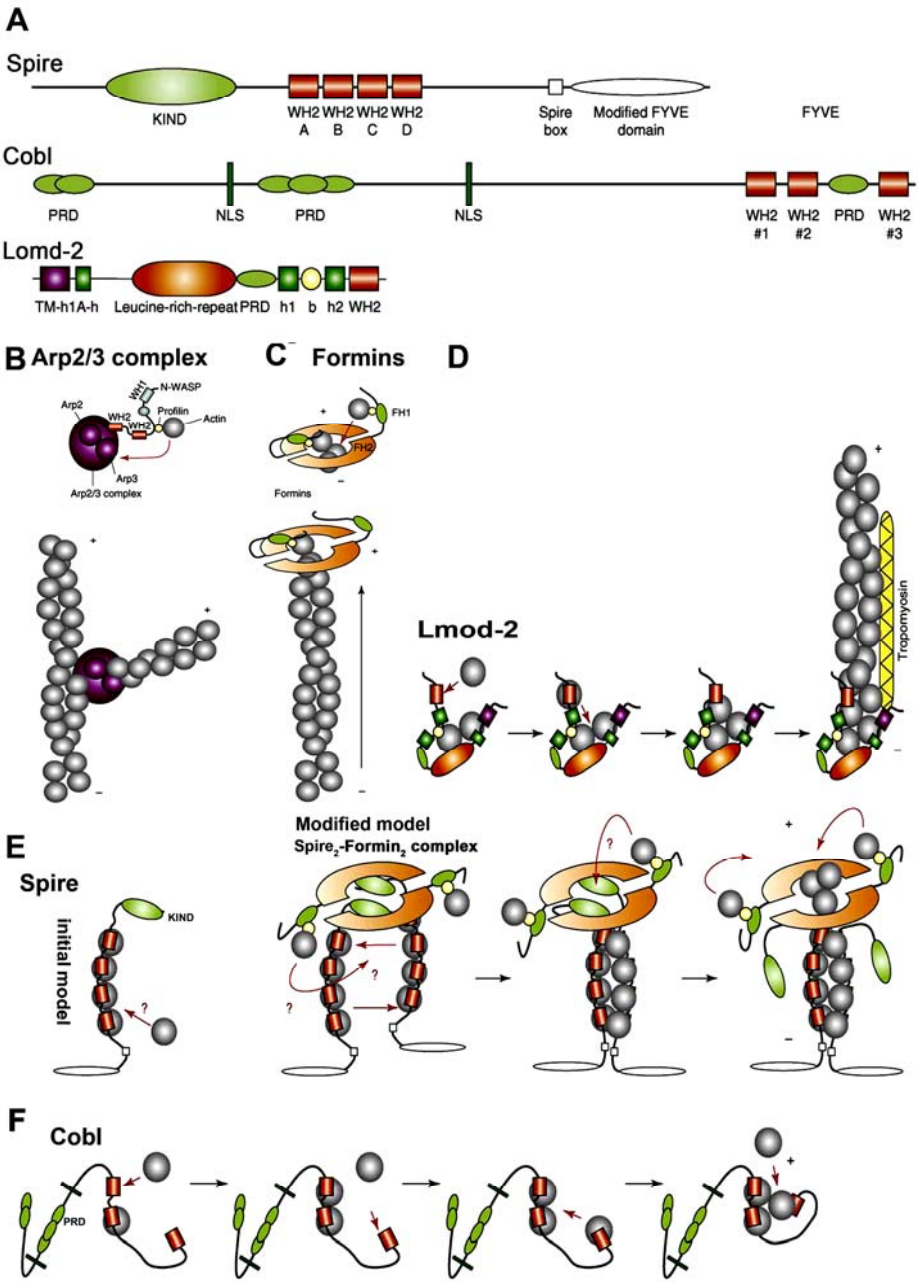

Figure 1-3 The initiation mechanisms of actin polymerization by the Arp2/3 complex, formins, Spire, Lmod-2 and Cobl. (A) Domain architecture of the nucleation initiators of Spire, Cobl and Lmod-2. A-h, actin-binding helix; b, basic stretch; h1 and h2, helix 1 and 2; KIND, kinase non-catalytic C-lobe domain; NLS, nuclear localization signal; PRD, proline-rich domain; Sec, type II secretion/translocation signal; TM-h1, tropomyosin-binding helix 1. **(B)** The Arp2/3 complex mimicks an actin dimer after activation by members of the WASP superfamily of proteins (N-WASP is depicted). WASP superfamily proteins interact with G-actin by means of one or two WH2 domain(s) and recruit profilin–actin complexes by associating with their proline rich

domain (PRD). **(C)** Formins nucleate using their dimerized doughnut-shaped formin-homology 2 (FH2) domain, to which profilin–actin is recruited by binding to the neighboring proline-rich FH1 domain. During elongation, formins move processively along with the barbed end. **(D)** Lmod-2 directly binds two actin monomers using its different domains to form an actin dimer; the third actin is recruited by the WH2 domain of Lmod-2 and translocated to the actin dimer which initiates actin polymerization. **(E)** For Spire, both the initial model (Quinlan et al., 2005) (left side) and a model (right side) based on newer data from Quinlan et al. are shown. The left model: four actin monomers are recruited by Spire using its four WH2 domains; after that, the monomer actin is added. The right model: Spire directly binds to Formin and forms a $Spire_2$-$Formin_2$ complex; four actin monomers are recruited by each Spire (the right side model); the dimerization of Spire-$actin_4$-Formin complex allows monomer actin to be added to start actin polymerization. (F) In the case of Cobl two actin monomers directly bind to two of its adjacent WH2 domains of Cobl and form an actin dimer; the third actin is recruited by the third WH2 domain and is translocated to the actin dimer which initiates actin polymerization. '+' indicates filament plus ends whereas '_' indicates filament minus ends (modified from (Qualmann and Kessels, 2009)).

Microtubule motor activity also has been known to play an important role in membrane traffic, not only by transporting vesicles along microtubule tracks, but also by directly deforming membranes (Farsad and De Camilli, 2003). Many intracellular membrane tubules are generated in this fashion. For example, microtubule motors along a preformed microtubule track can generate a developing membrane tubule in vitro (Dabora and Sheetz, 1988; Robertson and Allan, 2000; Roux et al., 2002). Microtubule-dependent mechanisms, possibly in cooperation with other cytosolic factors (Dreier and Rapoport, 2000), have also been suggested to play a role in vitro and in vivo for the tubular dynamics of the ER (Dabora and Sheetz, 1988; Klopfenstein et al., 1998; Vale and Hotani, 1988; Waterman-Storer and Salmon, 1998), as well as for Golgi and endosome tubulation events following treatment with the fungal metabolite brefeldin A (BFA) (Lippincott-Schwartz et al., 1991).

1.1.4 Scaffolding by peripheral membrane proteins

Peripheral membrane proteins can participate in membrane deformation in different ways. First, coat proteins such as clathrin, COPI and COPII which are essential components for vesicle formation, can also be considered as exoskeletons that affect membrane bending by polymerizing into curved structures. However, these coat proteins do not directly associate with membranes and are supposed to act in

conjunction with other proteins (Antonny et al., 2003; Bi et al., 2002; Bi et al., 2007; Hughson, 2010; Lee and Goldberg, 2010; Low et al., 2008; Nossal, 2001; Russell and Stagg, 2009). The crystal structures or structures determined by electron microscopy of COPI, COPII and clathrin show that they share a similar architecture and functional organization (Fath et al., 2007; Fotin et al., 2004; Lee and Goldberg, 2010; Stagg et al., 2006; Stagg et al., 2008) (Figure 1-4). The COPII cage composed of the small GTPase Sar1, the Sec23/Sec24 complex and the Sec13/Sec31 complex is built by α-solenoid and β-propeller protein domains. The COPII cage assembly unit, two copies of Sec13/31, has a central α-solenoid dimer capped by two β-propeller domains at each end (here called the rod structure). The rod builds the edge of a cuboctahedron cage, and four other rods converge to form the vertex with no interdigitation of assembly units. The clathrin cage is generated by triskelion assembly units - trimers of clathrin heavy chains that are centered on the vertices of the cage, and the long α-solenoid legs curves towards and interdigitate with neighboring legs as they extend to the adjacent vertices. COP I consists of seven subunits, α-COP, β-COP, β′-COP, γ-COP, δ-COP, ε-COP and ζ-COP (Suntio et al., 1999). The recently reported crystal structure of the αβ′-COP core of coatomer shows a triskelion conformation in which three copies of aβ′-COP β-propeller domain converge via their axial ends. Each copy comprises two β-propeller domains at one end followed by an extended α-solenoid (Lee and Goldberg, 2010). The arrangement of αβ′-COP shares similar features with clathrin which suggests a similar mechanism to form the COP I cage.

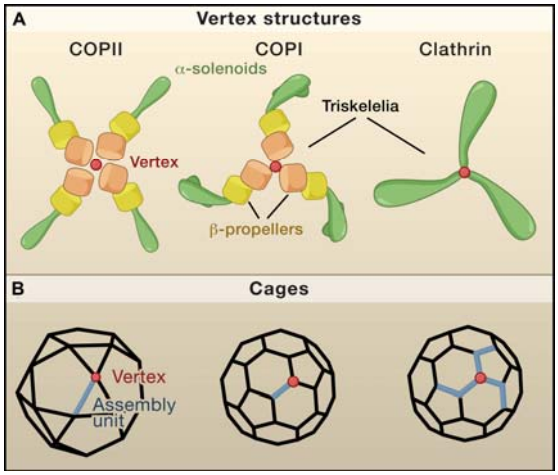

Figure 1-4 The three archetypal vesicle coats. (A) COPI, COPII and clathrin drive the formation of transport vesicles by polymerization. **(B)** COPII polymerizes into a polyhedral lattice

with triangular and pentagonal faces. In contrast, COPI is proposed to form clathrin-like truncated icosohedra with hexagonal and pentagonal faces (modified from (Hughson, 2010)).

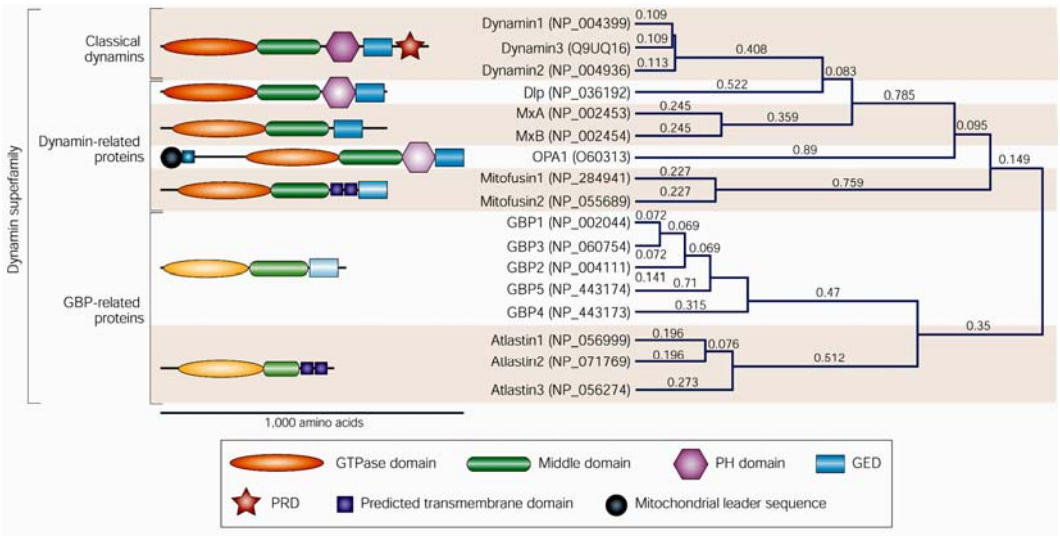

Figure 1-5 Domains of the human dynamin superfamily. All dynamins have a GTPase domain, a middle domain and a GTPase effector domain (GED) (except for Atlastin family proteins). Most dynamins also have a PH domain for interactions with membranes. Classical dynamins carry a proline-rich domain (PRD) at the carboxyl terminus that binds Src-homology-3 (SH3) domains. Human dynamin-superfamily members are grouped according to their domain structure and their accession numbers are shown. DLP1, dynamin-like protein1; GBP1, guanylate-binding protein 1; OPA1, optic atrophy 1 (taken from (Praefcke and McMahon, 2004)).

Second, proteins of the dynamin family interact with lipid membranes via their PH domain and form helical oligomers which constrain the membrane topology into a tubular shape (Gao et al., 2010a; Hinshaw and Schmid, 1995; Marks et al., 2001; Roux et al., 2006). All dynamins contain a GTPase domain that binds and hydrolyses GTP, a middle domain and a GTPase effector domain (GED) that are involved in oligomerization and stimulation of GTPase activity (Figure 1-5) (Ramachandran et al., 2007; Zhang and Hinshaw, 2001). Additionally, most dynamins carry a PH domain for interactions with lipid membranes. Classical dynamins contain a proline-rich domain (PRD) at the carboxyl terminus which recruits dynamin for vecsicle formation by interacting with Src-homology-3 (SH3) domains. Based on electron microscopy, dynamin tubulates liposomes and forms T-bar-like structures in which the PH domain is at the base of the T-bar (Figure 1-6A) (Zhang and Hinshaw, 2001). Although the crystal structure of full-length dynamin 1 is still unknown, crystal structures of isolated domains (except its PRD domain which forms a flexible

loop structure) have been determined. By combining this data with electron microscopy, a dynamin model has been recently deduced by Gao S et al (Figure 1-6) (Gao et al., 2010a), which provides details for understanding dynamin's biological function. Accumulating evidence supports the hypothesis that the GTPase dynamin functions as a mechanochemical enzyme, which plays an essential role in endocytosis by catalyzing the fission of nascent clathrin-coated vesicles from the plasma membrane. Its hydrolysis of GTP provides the energy to generate a large conformational change within dynamin which helps clathrin-coated vesicles to be pinched off from the plasma membrane (Marks et al., 2001; Stowell et al., 1999; Zhang and Hinshaw, 2001). Recent studies suggest that dynamin is recruited for vesicle formation by BAR domain containing-proteins, such as endophilin, amphiphysin, sorting nexin 9 and syndapin, particularly for assembling around necks of clathrin-coated pits (Ferguson et al., 2009; Habermann, 2004; Ren et al., 2006). The biological function of dynamin together with BAR domain containing-proteins will be dicussed later in this study.

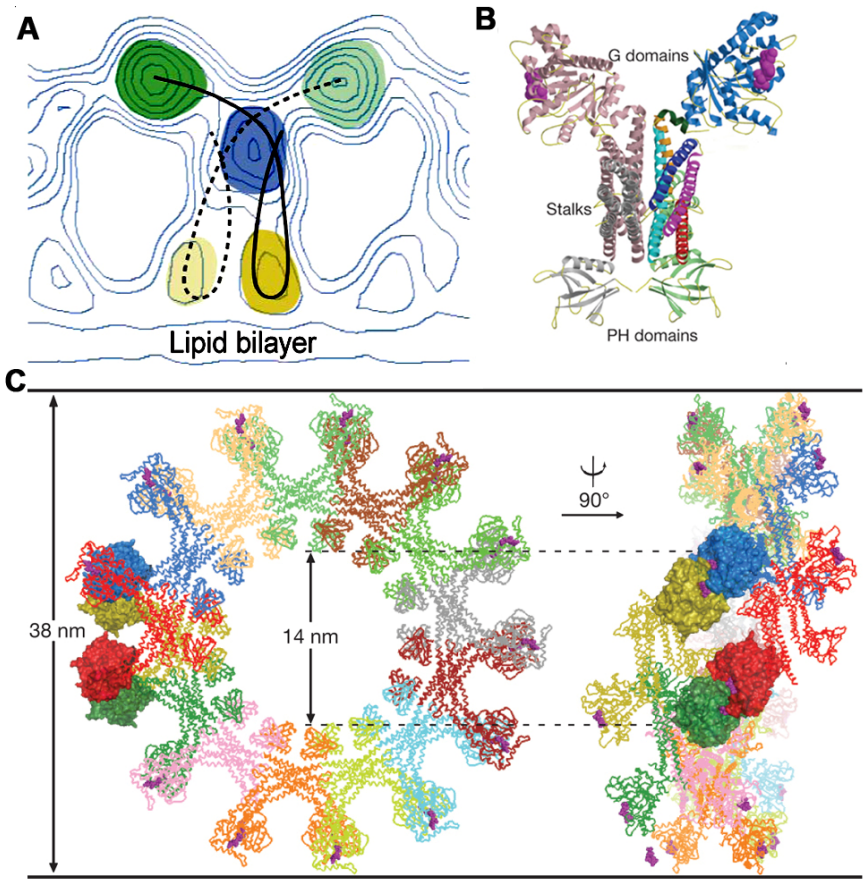

Figure 1-6 Model of a dynamin oligomer. (A) The typical T-bar shape of dynamin is shown by

an EM electron density map. The locallization of differents domains are coloured (taken from (Zhang and Hinshaw, 2001)). **(B)** The crystal structure model of dynamin is shown. PH domain, stalks region and G domain are indicated. **(C)** Two views of a complete turn of the dynamin helix composed of 13–14 dimers according to the EM electron density map of oligomerized dynamin in the constricted state. Only after one complete turn is formed the G domains of neighbouring helical turns (shown in green–red and yellow–blue surface representations) can approach each other (modified from (Gao et al., 2010a)).

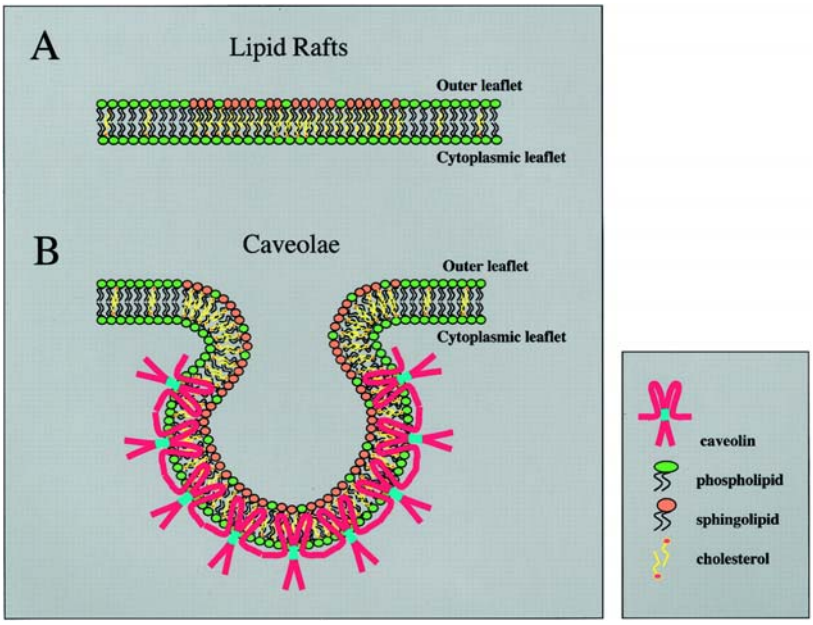

Figure 1-7 The organization of lipid rafts and caveolae membranes. (A) Lipid rafts are enriched in cholesterol within the liquid-ordered phase (yellow) and exoplasmically oriented sphingolipids (pink) in the outer leaflet. In contrast, the liquid-disordered phase is composed essentially of phospholipids (shown in green). **(B)** The caveolae structure is generated within lipid rafts. Upon integration of the caveolin-1 protein, liquid-ordered domains form small flask-shaped invaginations called caveolae. Caveolin-1 monomers assemble into discrete homo-oligomers (shown as dimers for simplicity) containing 14 to 16 individual caveolin molecules (taken from (Razani et al., 2002)).

Third, membrane bending is generated by caveolae structures. These flask-shaped membrane invaginations were first identified by electron microscopy (Palade, 1953). Caveolae form a stable functional unit at the cell surface and are generated by oligomerized caveolin and associated proteins and lipids (Figure 1-7) (Parton and Simons, 2007; Razani and Lisanti, 2001). The caveolin gene family has three members in vertebrates: caveolin-1, caveolin-2, and caveolin-3. Unlike COP and clathrin-coated vesicles, caveolins are a family of integral membrane proteins which

are the principal components of caveolae membranes and possibly involved in receptor-independent endocytosis (Scherer et al., 1996; Tang et al., 1996; Williams and Lisanti, 2004). Lastly, BAR domains are modules that sense and generate membrane curvature as part of both clathrin-dependent and clathrin-independent pathway (BAR domains will be discussed later).

1.1.5 Helix insertion into membranes

Amphipathic helices are stretches of α-helix with a charged (polar) side and a hydrophobic side. The most important feature of an amphipathic helix is its effect on membrane curvature. In many cases the α-helix forms only when the protein is tightly associated with the membrane. The helices are predicted to sit flat on the membrane surface with the hydrophobic residues dipping into the hydrophobic phase of the membrane (Campelo et al., 2008; Ford et al., 2002; McMahon and Gallop, 2005; Peter et al., 2004). This asymmetric insertion into one leaflet of the membrane results in membrane bending. Amphipathic helices are found in trafficking proteins as diverse as small G proteins (like Arf and Sar1 (Bi et al., 2002; Bielli et al., 2005; Huang et al., 2001; Liu et al., ; Liu et al., 2010; Memon, 2004; Rao et al., 2006)), epsins, BAR domains as well as others (Cui et al., 2009; Gallop et al., 2006; Low et al., 2008; Peter et al., 2004). For example, folding of the ‘0-helix’ (according to crystal structure of ENTH domain, 0-helix stands for the flexible loop at N-terminus.) is induced upon the interaction between the ENTH domain of epsin and a PI(4,5)P2-enriched membrane surface (Ford et al., 2002). The newly formed helix is amphipathic in nature. Positively charged residues on one side of the helix are engaged in lipid headgroup binding, whereas hydrophobic residues on the other face insert into the cytoplasmic face of the lipid bilayer. Actually, amphipathic α-helices not only induce membrane curvature, but are also believed to act as sensors of membrane curvature, thus facilitating the assembly of protein complexes on curved membranes. (Bhatia et al., 2010; Bhatia et al., 2009; Drin and Antonny, 2010; Epand et al., 1995)

1.2 BAR domains

In most cases, dynamic membrane remodelling is accomplished by the reversible assembly of membrane-sculpting or deforming proteins (Hatzakis et al., 2009; Hui et

al., 2009). Recently, increasing numbers of membrane-deforming proteins connecting the actin cytoskeleton and the plasma membrane have been indentified. These proteins contain a BAR, or EFC/F-BAR and or IMD/I-BAR domain (Figure 1-8). The BAR (**B**in, **a**mphiphysin, **R**vs) domain was originally identified as an evolutionary conserved region shared by the yeast proteins Rvs161, Rvs167 and the metazoans amphiphysins (the splice variants of which are also called Bin1) (David et al., 1996; Lichte et al., 1992; Sakamuro et al., 1996; Sivadon et al., 1995) It was predicted to have a coiled-coil domain structure and was shown to act as homo- and heterodimerization domain (Ramjaun et al., 1999; Slepnev et al., 1998; Wigge et al., 1997). The first crystal structure of the Arfaptin elucidated how these domains are able to generate finely organized membrane microstructures (Tarricone et al., 2001). BAR domains are dimerized via α-helical coiled coils and the dimerization module forms a positively charged surface that associates with the negatively charged inner surface of the plasma membrane, mostly through interaction with negatively charged phospholipids (Peter et al., 2004; Tarricone et al., 2001). BAR domain superfamily proteins deform membranes to a geometry that corresponds to the structures of the membrane-binding surface of the protein (a crescent-shaped dimer or/ banana-shaped dimer) (Figure 1-9).

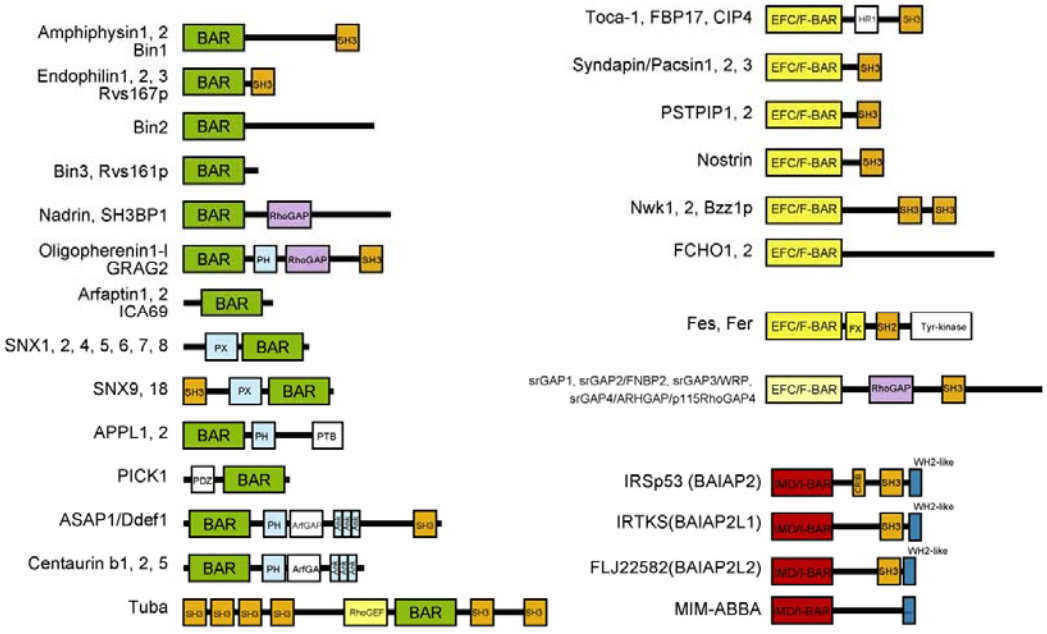

Figure 1-8 Schematic diagram of the domain structures of BAR-, EFC/F-BAR- and IMD/I-BAR-domain-containing proteins. Besides BAR domain, EFC/F-BAR and IMD/I-BAR domains, other domains are indicated for each protein (Taken from Suetsugu, S., 2010).

In vitro, liposome tubulation assay has been generally used to study the membrane tubulation activity of BAR domain. Pervious studies have shown that BAR domain containing-proteins, such as amphiphysin, endophilin, FBP17 and CIP4, are able to bind lipids and to induce tubulation of liposomes (Figure 1-10, Figure 1-11A-D) (Farsad et al., 2001; Frost et al., 2008; Gallop et al., 2006; Henne et al., 2007; Itoh et al., 2005; Takei et al., 1999). A recent cryo-EM analysis of a CIP4 F-BAR domain illustrated how BAR domain can associate with membranes to form cylindrical tubules (Frost et al., 2008) (Figure 1-10). To form membrane tubule structure, F-BAR domain is self-assembled/oligomerized into a helical coat. Besides the tip-to-tip interactions, the broad contacts between laterally-adjacent dimmers are also required for the oligomerization of F-BAR domain (Figure 1-10C,D). By fitting crystal structure of CIP4 F-BAR domain into cryo-EM reconstructions of membrane tubules, a cluster of positive residues (R/K) on the concave surface of the F-BAR module are necessary to bind the membrane bilayer and enable rigid F-BAR dimers to deform membrane (Frost et al., 2008). *In vivo,* overexpression of BAR/F-BAR domain or BAR/F-BAR domain containing proteins also generates membrane tubules in cells (Figure 1-11E-G), but BAR domain and F-BAR domain proteins segregate within distinct areas within the tubules (Figure 1-11H) (Itoh et al., 2005; Kamioka et al., 2004; Lee et al., 2002; Shimada et al., 2007; Tsujita et al., 2006).

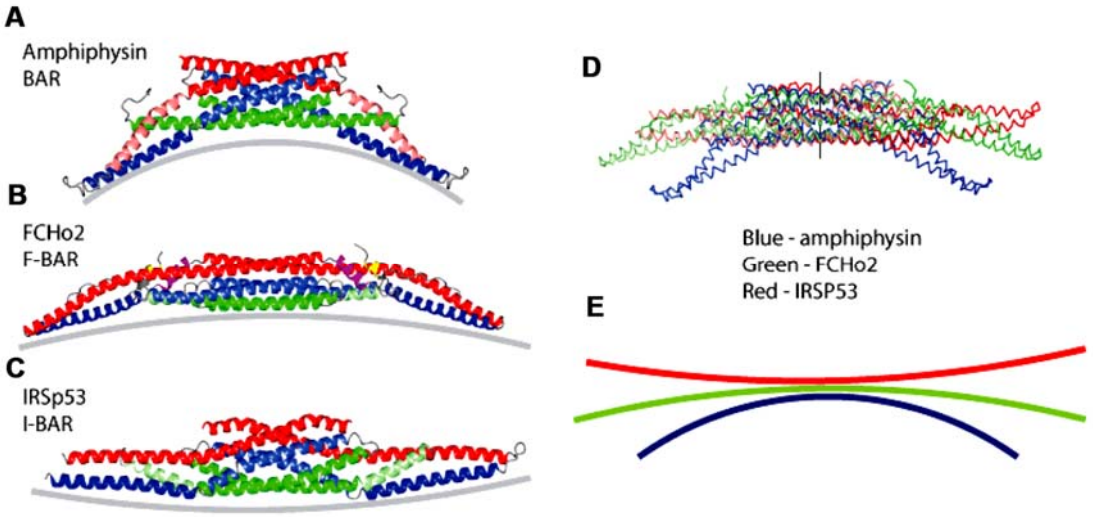

Figure 1-9 The architecture of BAR domains and the resulting membrane deformation. Crystal structures of the amphiphysin BAR domain **(A),** the FCHo2 F-BAR domain **(B)** and IRSp53 I-BAR domain **(C)** and the resulting membrane deformations are indicated. **(D)** Comparison of BAR domain, F-BAR domain and I-BAR domain. **(E)** BAR and F-BAR domains

cause positive membrane curvature whereas I-BAR domains generate negative membrane curvature (modified from http://www.endocytosis.org/F-BAR_proteins/BAR-Superfamily.html).

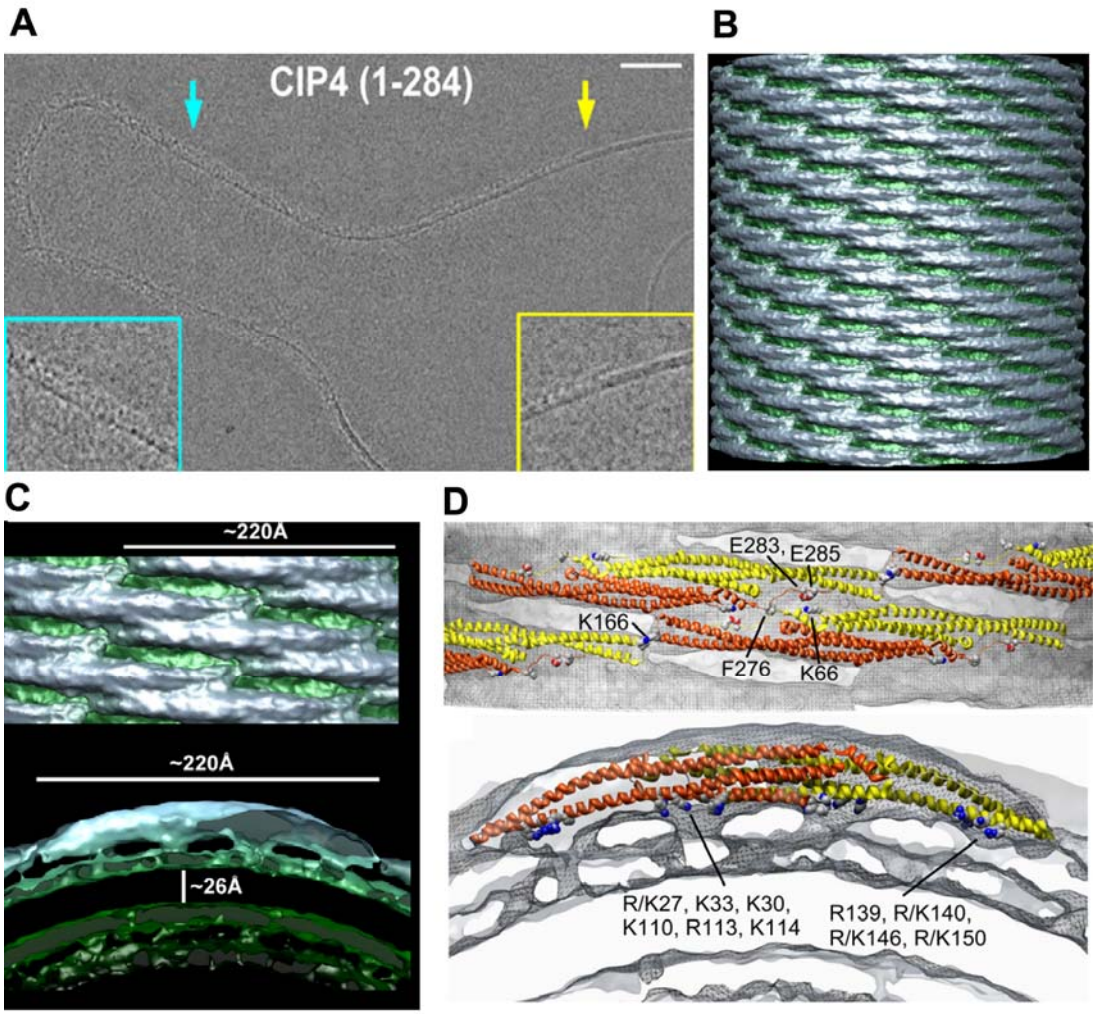

Figure 1-10 3D reconstruction of a CIP4 F-BAR domain-induced membrane tubule. (A) Electron micrograph of a membrane tubule was generated when liposomes were incubated with human CIP4 F-BAR domains (residues 1–284). The yellow arrow indicates the demarcation between the membrane surface with and without F-BAR domains, while the cyan arrow shows the membrane tubule bound to proteins. F-BAR domain self-assembled into a helical coat along the tubule. Enlarged inset surrounded by the cyan or yellow box. Scale bar, 300 Å. **(B)** Surface of a 67 nm diameter membrane tubule after 3D reconstruction. The protein coat is colored blue-gray and the membrane is green. **(C, D)** Zoom in on the lattice seen orthogonal to the cylindrical axis. Crystal Structures of the F-BAR domain were fit into the CryoEM Map. The hydrophobic core of the phospholipid bilayer is 26 Å and the length of one monomer is 22 nm. Cationic residues involved in membrane binding are found along the concave faces. The R/K indicates the amino acid found in CIP4 or FBP17, respectively. The residues involved in the tip-tip interaction are indicated (Modified from (Frost et al., 2008)).

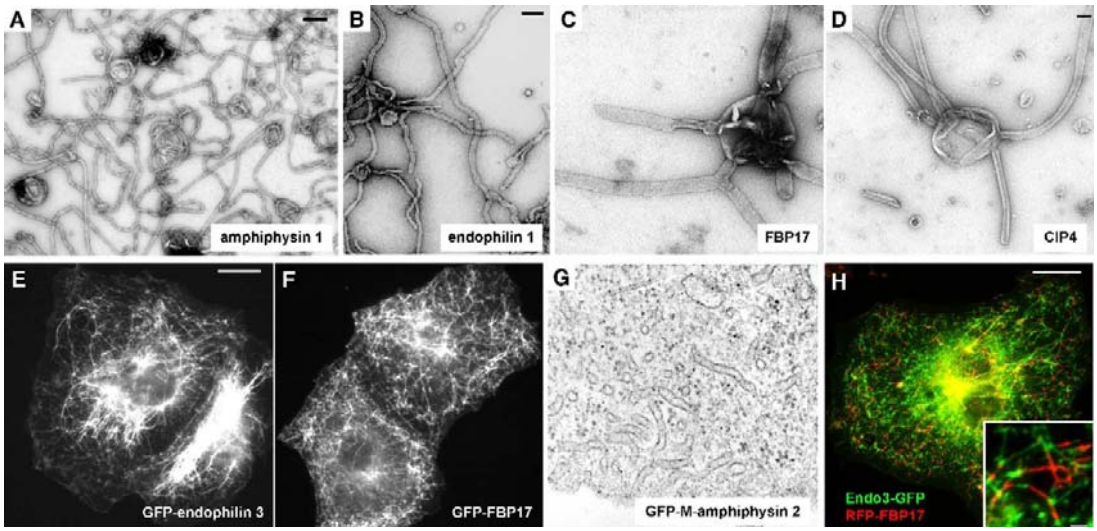

Figure 1-11 Membrane tubulation by BAR/F-BAR domains. Tubules were generated when liposomes were incubated with purified amphiphysin 1 **(A)**, endophilin 1 **(B)**, FBP17 **(C)** or CIP4 **(D)**. **(E, F)** Numerous membrane tubules in Cos7 cells were generated from the plasma membrane by the expression of endophilin3-GFP **(E)** and GFP-FBP17 **(F)**. (G) Numerous narrow tubules are detected using electron microscopy in the COS7 cells transfected with GFP-M-amphiphysin2. (H) Coexpression of endophilin3-GFP (green) and RFP-FBP17 (red) generated a tubular network in which the two proteins segregated to distinct portions of the tubules. Bars, 500 nm **(A)**, 100 nm **(B–D)**, 10 μm **(E, F and H)** and 1 μm (inset in **H**) (Taken from (Itoh and De Camilli, 2006)).

A common feature of endocytosis-linked BAR proteins is the presence of a Src homology 3 (SH3) domain (Figure1-8), which is able to interact with dynamin, synaptojanin and members of the WASP family of proteins that regulate actin polymerization (Ayton et al., 2009; Casal et al., 2006; Cui et al., 2009; Dawson et al., 2006; Frost et al., 2009; Habermann, 2004; Low et al., 2008; Masuda and Mochizuki, 2010; Ren et al., 2006; Saarikangas et al., 2009; Shimada et al., 2007; Suetsugu et al., 2009; Takano et al., 2008). The multidomain scaffold protein amphiphysin, for instance is a recently identified example of a BAR protein that couples to endocytic and actin-regulatory proteins, including dynamin and N-WASP (Dawson et al., 2006; Yamada et al., 2009).

Based on their different curvature preferences, the BAR superfamily can be subdivided into BAR/N-BAR (N-BAR: a BAR domain with an N-terminal amphipathic helix) modules that bind to membranes of high positive curvature, EFC/F-BAR domain modules that bind to a different range of positive curvature membranes, and I-BAR modules ("I"-Inverting fitting to different membrane

curvature) that bind to negatively curved membranes.

1.2.1 BAR/N-BAR

BAR/N-BAR domains are diverse in sequence and organization. However, they have in common that they are usually present at sites of dynamic membrane remodeling. BAR domains are frequently found in conjunction with a second membrane binding sequence such as an amphipathic α-helix, a PH domain, or a PX domain. The PH domain mainly binds to PtdIns(4,5)P2 or PtdIns(3,4,5)P3 (Wang and Shaw, 1995). PX domains can interact with various phosphoinositides, most notably PtdIns(3)P (Ago et al., 2003; Karathanassis et al., 2002). BAR domains exhibit relatively non-specific binding to negatively charged phospholipid membranes, but a neighboring PH or PX domain can confer specificity (Figure 1-8) (Peter et al., 2004). The PH or PX domains could thus assist BAR domain-containing proteins to target to a specific membrane compartment, where they could induce local membrane deformation.

BAR domain containing-proteins frequently contain an N-terminal amphipathic helix (referred to as AH) preceding the consensus BAR domain; this combination is referred to as an N-BAR domain. As discussed before, amphipathic helices are often unstructured until they insert into lipid membranes. The amphiphatic helices together with BAR domains emerge as an important means for proteins to sense membrane curvature and to participate in membrane insertion and bending. Thus, N-BAR domain containing-proteins not only can induce membrane curvature using their N-terminal amphipathic helices but also stabilize the curved membrane by the banana-like shape of the BAR domain, suggesting a dual role for BAR domain proteins in regulating membrane curvature. Well-studied examples of N-BAR proteins are the endophilin and amphiphysin families which are involved in synaptic vesicle recycling (Dickman et al., 2005; Jao et al., 2010; Mizuno et al., 2010). Endophilin and amphiphysin interact with dynamin, N-WASP and synaptojanin through their SH3 domain. Amphiphysin can also bind to clathrin and the AP2 adaptor complex (David et al., 1996; Ramjaun and McPherson, 1998; Slepnev et al., 2000; Yoshida et al., 2004). Interestingly, the crystal structure of endophilin N-BAR reveals the presence of an additional insert helix within the BAR domain, which is conserved between endophilin proteins (Gallop et al., 2006; Jao et al., 2010; Masuda

et al., 2006). This additional structure is an amphipathic helix located in the centre of the banana shape of the domain. Recent studies show that this extra amphipathic helix inserts into the lipid bilayer in a similar way as N-terminal amphipathic helices to induce membrane curvature (Cui et al., 2009; Jao et al., 2010; Masuda et al., 2006). N-BAR domains can thus impose a positive feedback loop on themselves by bending membranes and still associates with the bent membrane surface.. The extra amphipathic helix in endophilin could confer faster tubulation or increase the time that endophilin remains associated with the membrane compared with amphiphysin, reflecting differences in the functions of these proteins (Cui et al., 2009; Dawson et al., 2006). This may also explain why different BAR domains are acting at different stages of vesicle formation.

BAR domain proteins with adjacent PH/PX domains tabulate liposome less efficiently compared with BAR domains having an amphipathic helix and the interaction between the BAR-PH domain and liposomes is sensitive to membrane curvature (Peter et al., 2004). However, PH and PX domains bind to specific phosphoinositides which will increase the specificity of membrane targeting of BAR domain proteins. For example, the BAR and PX domains of SNX1 (Sorting Nexin) have been shown to target SNX1 to a highly curved microdomain in early endosomes that contains PtdIns(3)P and to mediate tubulation of early endosomes (Carlton et al., 2004). Sorting nexins are a large family of proteins grouped according to the presence of a SNX–PX phosphoinositide-binding domain and are largely involved in regulating vesicle trafficking between intracellular compartments (Carlton et al., 2004; Carlton et al., 2005).

1.2.2 F-BAR (EFC) domain

F-BAR proteins were formerly referred to as Pombe *Cdc15 homology* (PCH) proteins. Owing to primary sequence similarity, a domain with a distant relation to BAR domains was indentified within them (Itoh et al., 2005). The archetypal feature of this protein family is their *Fer/CIP4 homology* (FCH) domain, which constitutes a functional unit with a neighboring coiled-coil region, together forming the F-BAR domain. F-BAR domain-containing proteins often contain various combinations of SH3 domains, SH2 domains, tyrosine kinase domains and RhoGAP domains at their C-terminal part (Figure1-8). The mammalian F-BAR proteins have been grouped into

several subfamilies: FES/FER tyrosine kinases, the CIP4 subfamily, the srGAP subfamily, the PSTPIP subfamily, the FCH domain-only (FCHO) subfamily and the Syndapin/Pacsin subfamily (which will be discussed in detail in section **1.4**) (Figure 1-12) (Fricke et al., 2010; Heath and Insall, 2008).

The Fes/Fer proteins, consisting of an amino-terminal F-BAR domain, a central SH2 domain and a carboxy-terminal kinase domain, are a distinct family of non-receptor tyrosine kinases with prominent roles in regulating cell adhesion and cytoskeletal reorganisation through the modification of adherens junctions (Greer, 2002; Murray et al., 2006). Fer localizes to microtubule ends and is involved in phosphorylation of adhesion molecule platelet/endothelial cell adhesion molecule 1 (Kogata et al., 2003; Udell et al., 2006). Fer has also been linked to actin dynamics through the interaction with cortactin (Fan et al., 2004). Interestingly, the interaction between Fer and p120 catenin is required for normal neuronal polarization and neurite development (Lee, 2005).

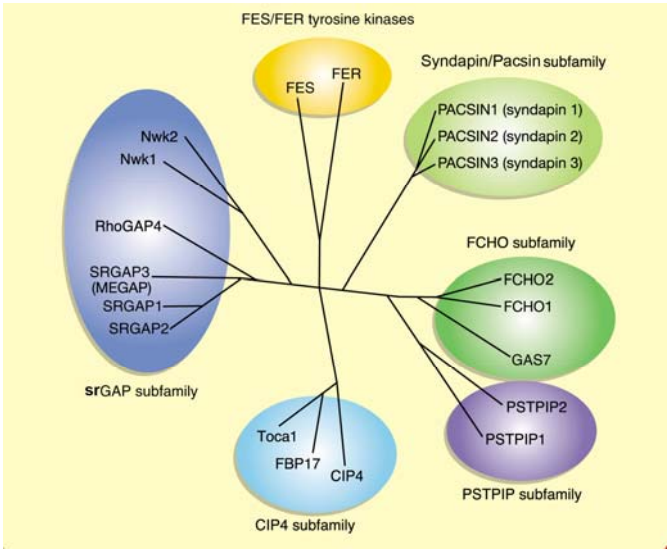

Figure 1-12 The subfamily of F-BAR domain containing-proteins. F-BAR domain containing-proteins are divided into six groups: FES/FER tyrosine kinases, the CIP4 subfamily, the srGAP subfamily, the PSTPIP subfamily, the FCH domain-only (FCHO) subfamily and the Syndapin/Pacsin subfamily (modified from (Heath and Insall, 2008)).

The CIP4 subfamily contains Cdc42-interacting protein-4 (CIP4), formin-binding protein-17 (FBP-17) and transactivator of cytoskeletal assembly-1 (Toca-1). These proteins are composed of an F-BAR domain at the N-terminus, an HR1 domain

(Cdc42 binding site) in the middle and a C-terminal SH3 domain. They form a complex with WASP and SCAR/WAVE using their SH3 domain to promote membrane invagination. FBP17 and CIP4 bind to dynamin via their SH3 domain which antagonizes their tubulation activity (Bu et al., 2009; Chang et al., 2002; Feng et al., 2010; Fricke et al., 2009; Hartig et al., 2009; Ho et al., 2004; Insall and Machesky, 2004; Leung et al., 2008; Suetsugu, 2009; Tsuboi et al., 2009). Accumulating evidence suggests that the CIP family proteins coordinate the membrane-cytoskeleton events associated with endocytosis.

The srGAP subfamily consists of the three isoforms srGAP1-3 (**S**lit-Robo **R**ho **G**TPase **a**ctivating **p**rotein) which contain an EFC/F-BAR domain, a GAP domain for small GTPases and an SH3 domain (Guerrier et al., 2009; Itoh et al., 2005; Tsujita et al., 2006; Wong et al., 2001). Like in the case of CIP family proteins, the SH3 domain of srGAP often binds to WASP/WAVE proteins. All srGAP proteins are linked to a signal transduction pathway from extracellular guidance cues to intracellular actin polymerization. The activity of Cdc42 is negatively regulated by srGAP1, which plays an important role in neuronal migration (Wong et al., 2001). srGAP2 negatively regulates neuronal migration and induces neurite outgrowth and branching through the ability of its F-BAR domain to induce filopodia-like membrane protrusions resembling those induced by I-BAR domains in vivo and in vitro (Guerrier et al., 2009). However, the mechanism by which srGAP F-BAR is able to induce filopodia-like membrane protrusions still needs to be investigated. srGAP3 binds directly to WAVE-1 through its SH3 domain and specifically inhibits Rac function in vivo (Soderling et al., 2002). RhoGAP4 (also called ARHGAP4) has the same architecture as srGAP: an F-BAR domain at the N-terminus, a central GTPase activating (GAP) domain and a C-terminal SH3 domain (Demura et al., 2002). The F-BAR domain is important for spatially localizing RhoGAP4 to the leading edges of migrating NIH/3T3 cells and to axon growth cones, whereas GAP domain and C-terminus are necessary for ARHGAP4-mediated inhibition of cell and axon motility (Vogt et al., 2007). The protein Nervous Wreck (Nwk 1 and Nwk2) also belongs to the srGAP subfamily. Nwk1/2 is a conserved neuronal F-BAR/SH3 protein that localizes to periactive zones at the Drosophila larval neuromuscular junction (NMJ) and is required for regulation of synaptic growth via bone morphogenic protein signaling (Collins and DiAntonio, 2004; Coyle et al., 2004).

Nwk interacts functionally and physically with the endocytic proteins dynamin and Dap160/intersectin and functions together with Cdc42 to promote WASP-mediated actin polymerization and to regulate synaptic growth (O'Connor-Giles et al., 2008; Rodal et al., 2008).

PSTPIP 1 and PSTPIP 2 (**p**roline-**s**erine**t**hreonine **p**hosphatase-**i**nteracting **p**roteins 1 and 2) contain an F-BAR domain and an SH3 domain. PSTPIP1 interacts with WASP via its SH3 domain, which implies that PSTPIP proteins are linked to actin dynamics. The interaction is regulated by tyrosine phosphorylation of the PSTPIP SH3 domain (Cote et al., 2002; Spencer et al., 1997; Wu et al., 1998a; Wu et al., 1998b). PSTPIP has been linked to filopodia formation through its putative F-actin bundling activity (Chitu et al., 2005; Spencer et al., 1997). However, the role of its F-BAR domain in filopodia formation is still unknown.

The FCH domain-only (FCHO) subfamily consists of two isoforms, FCHO1 and FCHO2 (homologous to the yeast protein Syp1). They contain an F-BAR domain and a μHD domain with a Proline-rich region in between (Reider et al., 2009). Previous studies have shown that Syp1 is recruited early to sites of actin-dependent endocytosis (Reider et al., 2009), inhibits Las17/WASP dependent activation of Arp2/3 complex-mediated actin assembly, and localizes to cortical sites of endocytosis (Boettner et al., 2009). More recently, the crystal structures of the F-BAR domain of Syp1 and FCHO2 have been solved. Similar to other BAR domains, they dimerize into a crescent-shape conformation (Henne et al., 2007; Reider et al., 2009). The FCHO1/2 F-BAR membrane-bending activity was suggested to sculpt the initial vesicle bud site and to recruit the clathrin machinery for CCV formation with the help of the endocytic proteins eps15 and intersectin (Henne et al., 2010). Gas7 (growth arrest-specific gene 7), another member of the FCHO family, is predominantly expressed in neurons and required for the maturation of primary cultured neurons as well as for neuron-like differentiation of PC12 cells upon nerve growth factor stimulation (Chao et al., 2003; Ebinger et al., 2006; Lazakovitch et al., 1999; She et al., 2002). Gas 7 also physically interacts with N-WASP and regulates the neurite outgrowth of hippocampal neurons (You and Lin-Chao, 2010).

The F-BAR domain containing-proteins have many properties which are similar to BAR proteins. They can dimerize and bind to the membrane lipid phosphatidylserine

in a manner that is enhanced by the presence of PtdIns(4,5)P2 (Itoh et al., 2005; Tsujita et al., 2006). F-BAR proteins (e.g. FBP-17 or CIP4) can tubulate membranes and form higher-order oligomers (Figure 1-11D, F, H) (Frost et al., 2008; Henne et al., 2007; Itoh et al., 2005; Kamioka et al., 2004; Shimada et al., 2007; Tsujita et al., 2006). However, the tubules produced by F-BAR domain have clearly distinct characteristics. They are larger and appear less flexible than tubules produced by BAR domains (Itoh et al., 2005). Furthermore, when co-expressed in cells, BAR and F-BAR domains produce an interconnected system of tubules, but segregate to distinct parts of the tubules (Itoh et al., 2005). Like other BAR domain containing proteins, most F-BAR domain containing-proteins also have an SH3 domain at their C-terminus, which interacts with dynamin, synaptojanin and N-WASP (Itoh et al., 2005), implying that these proteins are involved in vesicle recycling and endocytosis.

1.2.3 I-BAR domain

The I-BAR domain (inverse BAR) was first identified in IRSp53 based on sequence homology as an F-actin crosslinking domain at the N-terminal region of mammalian IRSp53 and MIM (missing-in-metastasis) proteins (Habermann, 2004; Yamagishi et al., 2004). The IRSp53 protein family comprises IRTKS (insulin receptor tyrosine kinase substrate; also known as BAIAP2L1), MIM/ABBA (missing in metastasis/actin-bundling protein with BAIAP2 homology), and FLJ22582 (BAIAP2L2) (Ahmed et al., 2010). Crystal structure analysis of the I-BAR domain of IRSp53 shows strong structural similarity to the BAR domain family. One monomer consists of three α helices that dimerize into an antiparallel structure which resembles a distinct, rather flat, cigar shaped curvature (Figure 1-9) (Millard et al., 2005) and the positively charged lipid-binding surface of I-BAR domains displays a convex geometry (Mattila et al., 2007; Saarikangas et al., 2009; Suetsugu et al., 2006b). Like BAR/F-BAR domains, the I-BAR domains of MIM and IRSp53 also can directly bind and deform membranes into tubules in vitro (Mattila et al., 2007; Saarikangas et al., 2009; Suetsugu et al., 2006b). However, I-BAR modules stabilize tubules that penetrate into liposomes when bound to the membrane (Figure 1-13) (Mattila et al., 2007). Strikingly, different I-BAR domains deform PI(4,5)P2-rich membranes through distinct mechanisms. The I-BAR domains of IRSp53 and IRTKS bind membranes mainly through electrostatic interactions, whereas I-BAR domains of

MIM and ABBA insert an additional amphipathic helix into the membrane bilayer, resulting in a larger tubule diameter in vitro and more efficient filopodia formation in vivo (Saarikangas et al., 2009).

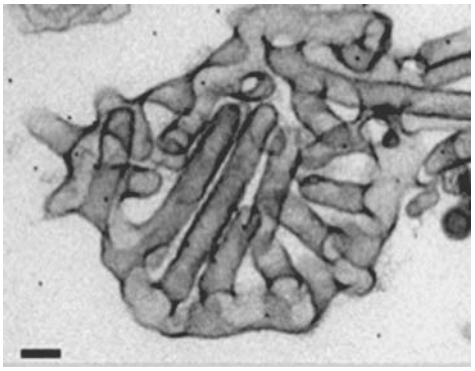

Figure 1-13 3D electron tomography analysis of I-BAR domain induced tubular network. Membrane tubules generated by MIM I-BAR (diameter of 78 nm) penetrate liposome. Bar, 0.1 μm (taken from (Mattila et al., 2007)).

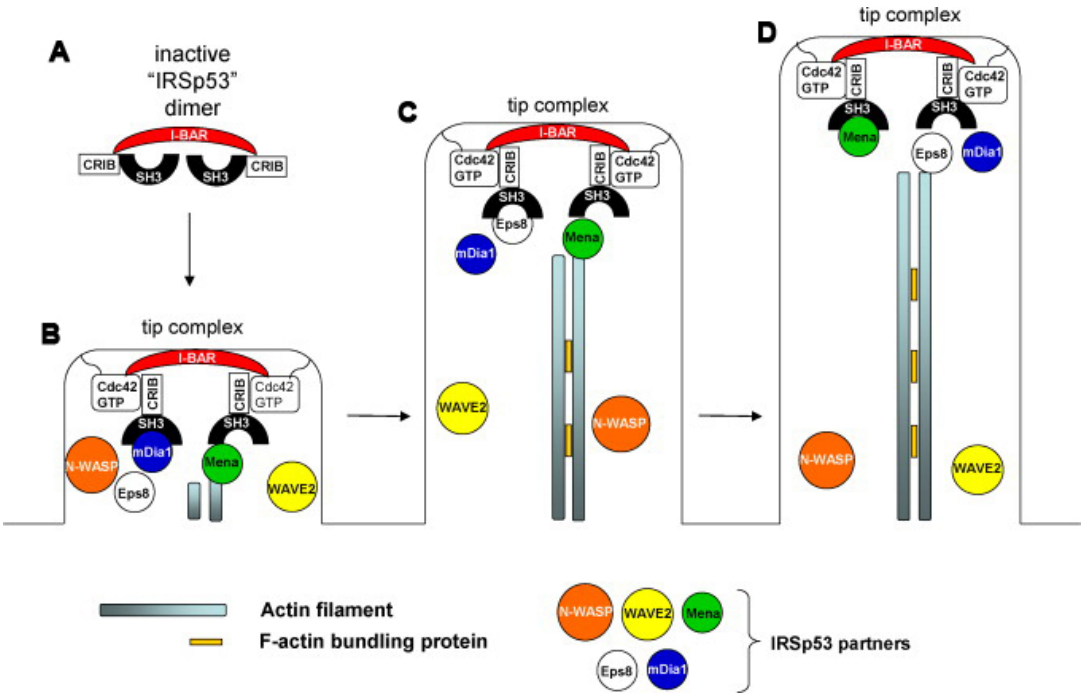

Figure 1-14 Actin filament formation via the SH3 domain binding partners of IRSp53. (A) Dimmerization of IRSp53 results in an autoinhibitory conformation, called inactive IRSp53. **(B)** Cdc42 binding to IRSp53 releases it from its autoinhibitory conformation and recruits it to the plasma membrane. There, the I-BAR domain of IRSp53 induces negative membrane curvature and its SH3 domain recruits mDia1 and Mena to acitivate the formation of actin filaments, but not N-WASP or WAVE2. **(C)** Replacement of mDia1 by Eps8 blocks one side for the formation of actin filaments, but the other one is still available. **(D)** Interaction between actin and Eps8 blocks

the further addition of actin at the barbed ends of actin filaments (modified from (Ahmed et al., 2010)).

A prominent feature of I-BAR domains is their ability to induce filopodia formation. A possible mechanism underlying this ability was proposed by Ahmed et al in the convergent elongation model for filopodia formation (Ahmed et al., 2010). Figure 1-14 illustrates this model using IRSp53 as an example. This protein has an autoinhibitory comformation in its "inactive" state (Krugmann et al., 2001). The interaction of IRSp53 with the GTP-bound state of the small GTPases Rac or Cdc42 releases IRSp53 from its autoinhibitory conformation and recruits it to the plasma membrane (Figure 1-14A); There, the IPSp53 I-BAR domain induces membrane deformation while the available SH3 domain recruits its specific binding partners mDia (a downstream effector of the small GTPase Rho implicated in stress fiber formation and cytokinesis (Fujiwara et al., 2000)) and Mena (Abou-Kheir et al., 2008; Disanza et al., 2006; Funato et al., 2004; Krugmann et al., 2001; Lim et al., 2008; Miki and Takenawa, 2002; Miki et al., 2000; Nakagawa et al., 2003; Suetsugu et al., 2006a). The recruitment of Mena initiates actin filament assembly into filopodia (Figure 1-14B). The selective interactions with mDia and Mena block the barbed ends of selected Arp2/3-nucleated lamellipodial microfilaments from capping proteins. Eps8, an actin-binding and regulatory protein, has barded-end capping activity which is mainly regulated by an amphiphathic helix that binds the hydrophobic pocket at the barbed ends of actin filaments, thus blocking the further addition of actin monomers (Figure 1-14C,D) (Disanza et al., 2004; Higgs, 2004). The replacement of mDia1 by Eps8 blocks one side (called "blocked site") for the formation of actin filaments, while the other one is still available. Interchange of Eps8 and Mena at the barbed ends of actin filaments initiates the formation of actin filaments at the previously blocked site. Recent studies show that Cdc42 binding of IRSp53 regulates the cellular distribution of the IRSp53-Eps8 complex and that the removal of either IRSp53 or Eps8 inhibits Cdc42-induced filopodia formation. These data imply that the synergistic bundling activity of the IRSp53-Eps8 complex regulated by Cdc42 contributes to the generation of actin bundles and thus promotes filopodial protrusions (Disanza et al., 2006; Funato et al., 2004).

1.3 Membrane deformation in the endocytic pathway

The endocytic pathway is essential for the delivery of membrane components, receptor-bound ligands, and soluble molecules to different intracellular organelles. Mammalian cells have at least five endocytic pathways: clathrin-dependent endocytosis, caveolae-dependent endocytosis, clathrin- and caveolae-independent endocytosis, macropinocytosis and phagocytosis (Engqvist-Goldstein et al., 2004; Le Roy and Wrana, 2005). In central nervous system synapses, multiple synaptic vesicle retrieval pathways are necessary for the recycling of synaptic vesicle (SV) membrane after exocytosis to maintain synaptic transmission (Figure 1-15). These pathways are a still somewhat controversial "Kiss and Run" mechanism, bulk endocytosis and clathrin-memdiated endocytosis. In the "kiss and run" model, synaptic vesicles are believed to form transient fusion pores in the presynaptic membrane, thereby releasing only part of their contents. Then they are immediately retrieved by a clathrin-independent process without ever fully collapsing into the plasma membrane (Burgoyne et al., 2001; Fesce et al., 1994; Hanna et al., 2009; Palfrey and Artalejo, 2003; Rizzoli and Jahn, 2007; Schneider, 2001; Tsuboi and Rutter, 2003). Bulk endocytosis is activated by strong stimulation and leads to the invagination of a large area in the presynaptic membrane, thereby forming "endosome-like structures". These endosome-like structures can remain attached to the plasma membrane for a considerable length of time while synaptic vesicles constantly bud (Clayton et al., 2009; Clayton and Cousin, 2009a; Clayton and Cousin, 2009b; Clayton et al., 2007; Clayton et al., 2008; Cousin, 2009).

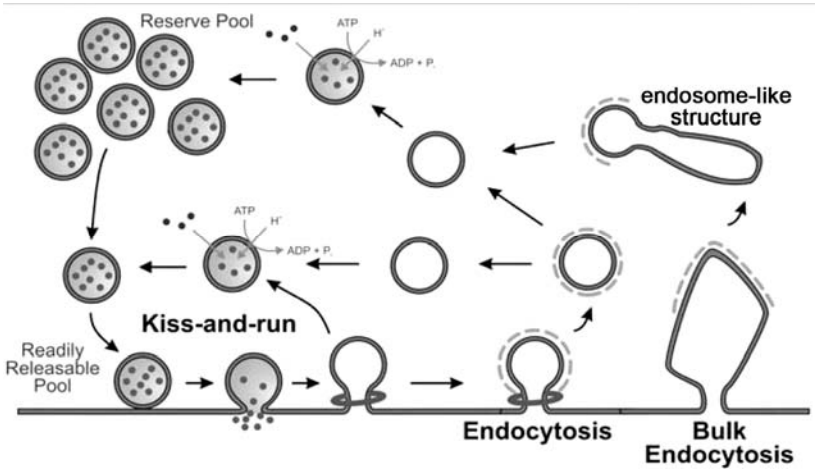

Figure 1-15 Synaptic vesicle retrieval pathways in central nerve terminals. Three different

mechanisms are suggested to retrieve synaptic vesicle (SV) membrane after exocytosis in nerve terminals. In the "Kiss-and-run" mechanism, SVs never fully fuse with the plasma membrane and are retrieved intact. In the classical clathrin-dependent endocytosis a clathrin-coated bud invaginates from the plasma membrane before its fission and uncoating. Bulk endocytosis refers to the process that large areas of nerve terminal membrane are invaginated to produce endosomes-like structures from which SVs can bud (updated from (Clayton et al., 2007)).

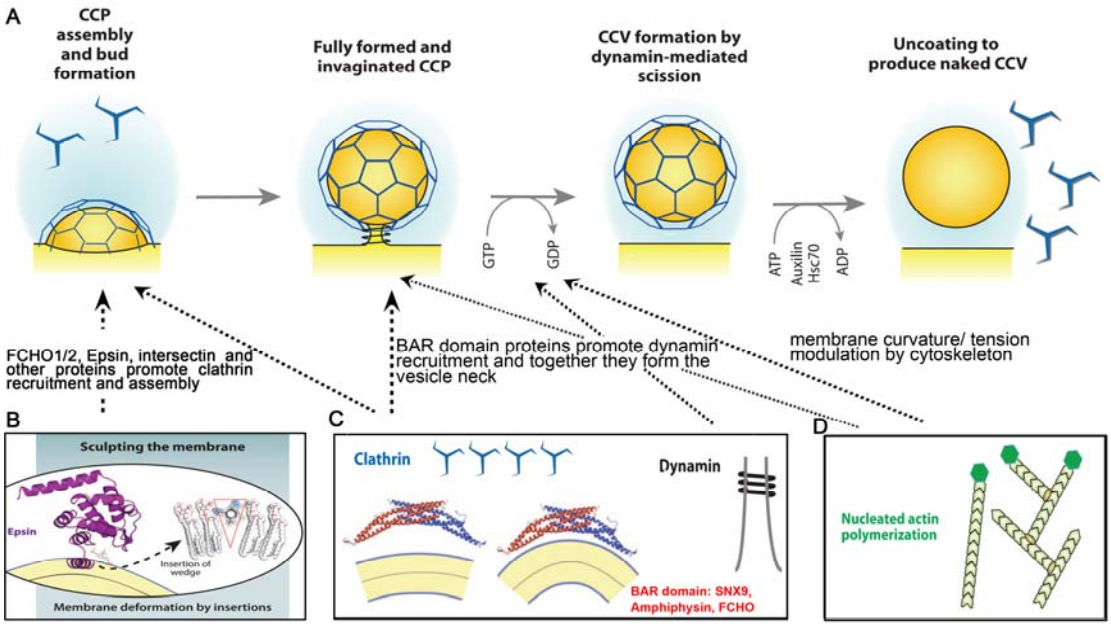

Figure 1-16 Membrane curvature modulation during endocytosis. (A) Schematic diagram illustrating the stages of clathrin mediated endocytosis and some of the key protein players in the budding and scission of clathrin-coated pits (CCPs). After budding to form a clathrin-coated vesicle (CCV), the clathrin basket is removed by uncoating proteins yielding a naked vesicle. Different mechanisms of membrane curvature generation and stabilization are illustrated in **B, C and D** (modified from (Doherty and McMahon, 2009)).

Clathrin-dependent endocytosis is the major pathway for the uptake of nutrients and signaling molecules in higher eukaryotic cells and important for the recycling or degradation of transmembrane receptors. According to the classical model, clathrin-mediated endocytosis results in the reformation of synaptic vesicles at the presynaptic membrane to allow to reuse of synaptic vesicle components (Brodin et al., 2000; Granseth et al., 2007; Jung and Haucke, 2007; Sato et al., 2009; Teng and Wilkinson, 2000). A clathrin coat is assembled on the cytoplasmic face of the plasma membrane, which then invaginates into a coated pit. The developing clathrin-coated pits constrict at the neck and finally pinches off from the membrane (Figure 1-16). The newly formed vesicles are moved into the cytoplasm where they are uncoated

and can undergo further sorting. The proper formation and fission of clathrin-coated pits from the plasma membrane requires the large GTPase dynamin and many scaffolding and accessory proteins, such as the adapter proteins AP2, DAB2/ARH, β-arrestin, Epsin, intersectin, eps15 as well as BAR domain containing-proteins (see also in Section 1.3.2). Most of these scaffolding and accessory proteins have membrane binding regions or membrane deformation elements which are necessary for vesicle formation and fission (Figure 1-16). To describe the mechanism of clathrin-coated vesicle (CCV) formation at the plasma membrane, the process can be subdivided into three stages: (1) vesicle budding, (2) vesicle formation (4) vesicle fission.

1.3.1 Vesicle budding

When a nascent vesicle buds, the membrane must deform. But how do changes in the membrane bilayer generate curvature during bud formation? Recent studies show that FCHO1/2 proteins bind specifically to PtdIns(4,5)P2-enriched membranes and sculpt the initial vesicle bud site by their F-BAR membrane-bending activity. FCHO1/2 via their μHD domains associate with the scaffold proteins eps15 and intersectin, which in turn engage the adaptor complex AP2 and clathrin (Henne et al., 2010).

Eps15 contains several functional protein domains: three EH domains which recognize Asn-Pro-Phe peptides (NPF motifs) (Diril et al., 2006; Maritzen et al., 2010; McPherson et al., 1998; Rumpf et al., 2008; van Bergen En Henegouwen, 2009), a coiled-coil region (which serves as the interacting surface for the constitutive oligomerization of Eps15 and can additionally interact with other proteins (Tebar et al., 1997)), a DPF repeat domain (needed for the association with AP2) (Mishra et al., 2004), and two consecutive UIMs (ubiquitin-interaction motifs which bind to ubiquitin-modified proteins) (Figure 1-17) (Fallon et al., 2006; Klapisz et al., 2002; Regan-Klapisz et al., 2005).

Intersectin contains two Eps15 homology (EH) domains, a central coiled-coil region, and five SH3 domains (Figure 1-17) (Yamabhai et al., 1998). Its long splicing variant also contains a Dbl homology domain (DH domain) which catalyzes nucleotide exchange for Rho family GTPases (Hussain et al., 2001)), a PH domain, and a C2 domain (Figure 1-17) (Guipponi et al., 1998). Similar to Eps15, the EH domain of

intersectin recognizes NPF motif. The central coiled-coil region of intersectin is used for its oligomeriztion and possibly complex formation with Eps15. The C-terminal five SH3 domains of intersectin recognize proline-rich motifs, such as the ones present in dynamin 1 (Evergren et al., 2007; Pechstein et al., 2010b). More recent studies show that intersectin binds to AP2 alpha- and beta-appendage domains (AP2 complex is described later) using the SH3A-B linker region and that this interaction inhibits binding of the inositol phosphatase synaptojanin 1 to intersectin 1, suggesting that the intersectin-AP2 complex acts as an important regulator of clathrin-mediated SV recycling (Pechstein et al., 2010a).

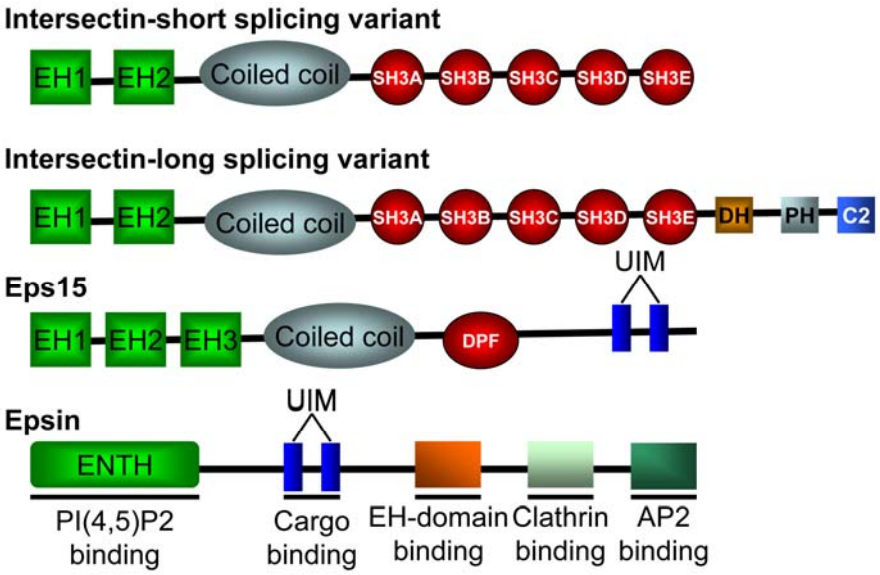

Figure 1-17 Schematic representation of the domain organization of Intersectin, Eps15 and Epsin.

1.3.2 Vesicle formation

At the clathrin coat formation step, the scaffolding proteins Eps15 and intersectin recruit other accessory protein, such as Epsin1 and the AP2 complex. The AP2 complex consists of two large α and β2 subunits (110 kD), a μ2 subunit (50 kD), and a small σ2 subunit (15 kD). The large subunits can be subdivided into an N-terminal trunk domain of 70 kD, which forms parts of the core and a C-terminal appendage domain of about 30 kD (also called "ear" domain) (Jackson et al., 2010). The AP2 core binds to PtdIns(4,5)P2-enriched membranes (Gaidarov et al., 1996; Gaidarov and Keen, 1999; Jackson et al., 2010). Epsin1 has many different domains to interact

with various proteins related to endocytosis (Figure 1-17). The ENTH domain of Epsin1 binds PtdIns(4,5)P2-enriched membranes. Insertion of an amphipathic helix from the ENTH domain into the membrane induces membrane curvature (Figure 1-16B). Mutating residues within the hydrophobic region of this helix abolishes its ability to curve membranes (Chen et al., 1998; Ford et al., 2002; Gabernet-Castello et al., 2009; Hussain et al., 2003; Jakobsson et al., 2008; Kweon et al., 2006; Wang et al., 2006; Yoon et al., 2010). The C-terminus of Epsin1 contains multiple binding sites for proteins involved in CCV formation (Figure 1-17), such as clathrin and the AP2 complex. Upon recruitement to the membrane, clathrin triskelia which are composed of three clathrin heavy and three light chains (Figure 1-16C) form a polyhedral lattice of hexagons and pentagons (Figure 1-16).

Additionally, more recent studies suggest that F-BAR domain containing-protein FBP17 has a dual role in shaping and stabilizing membrane curvature using their F-BAR domain and in recruiting machinery for actin polymerization (Wu et al., 2010). The latter may provide the force to push vesicle buds away from the plasma membrane. Blocking clathrin polymerization prevents deep membrane invaginations even in the presence of abundant membrane-tubulating proteins in the cytosol, thereby inhibiting clathrin-coated pit maturation at an early stage (Wu et al., 2010). Actually, FBP17 may also aid membrane fission by generating longitudinal tension along the neck of the fissing vesicle.

1.3.3 Vesicle fission

Deep clathrin-coated membrane invaginations finally undergo dynamin-mediated fission. Dynamins recruited to “neck region” of late stage clatthrin-coated pits via SH3 domain proteins bind to the PtdIns(4,5)P2-enriched plasma membranes via their PH domain. The hydrolysis of GTP by dynamin generates a conformational change within the protein causing scission of the clathrin-coated vesicles (Figure 1-16C) (Danino and Hinshaw, 2001; De Camilli et al., 1995; Hinshaw, 2000; Hinshaw and Schmid, 1995; Kelly, 1995; Lenz et al., 2008; Liu and Robinson, 1995; McFadden and Ralph, 2003; Sever, 2002; Shpetner et al., 1996; Shpetner and Vallee, 1989; Takei et al., 1995; Warnock et al., 1995). Dynamins function together with BAR-SH3 domain proteins, such as amphiphysin, endophilin and sorting nexins in membrane fission. Dynamins binding to narrow tubules has the similar diameter as amphiphysin

and endophilin (Farsad et al., 2001; Takei et al., 1999; Wu et al., 2010). Interestingly, although endophilin and amphiphysin have a similar morphology, endophilin cooligomerizes with dynamin-rings on lipid tubules and inhibits dynamin's GTP-dependent vesiculating activity (Farsad et al., 2001), while amphiphysin enhances liposome-fragmenting activity when it assembles with dynamin 1 into ring-like structures around tubules in the presence of GTP (Takei et al., 1999). Additionally, another BAR domain-containing protein sorting nexin 9, which contains an additional membrane binding phox homology (PX) domain right after its BAR domain and specifically binds to membrane phosphoinositides, has a similar function as endophilin in stabilizing dynamin 1 on the membrane even at the onset of stimulated GTP hydrolysis (Ramachandran and Schmid, 2008). A burst of sorting nexin 9 transiently recruited to CCPs during the late stages of vesicle formation coincides spatially and temporally with a burst of dynamin (Soulet et al., 2005). Furthermore, actin filaments may provide part of the force to puch vesicles or membrane tubules away from the plasma membrane (Suetsugu, 2009) (Figure 1-16D). However, the importance of actin for clathrin-mediated endocytosis may depend on the sits of coated pits and the cell type.

1.4 Syndapins/Pacsins

F-BAR-SH3 domain proteins, Syndapins (synaptic dynamin-associated proteins) are, a family of proteins also referred to as PACSINs (Protein kinase C and casein kinase 2 substrate in neurons), first identified in the brain. Syndapins show a remarkably high degree of conservation of both their domain structure and their amino acid sequence in species as diverse as worms, insect, fish, birds and mammals (Kessels and Qualmann, 2004). Their putative F-BAR module has been proposed to deform membreanes. In mammals, there are three syndapin isoforms, syndapin I, syndapin II and syndapin III. All of them are composed of an N-terminal F-BAR domain, a flexible stretch that contains up to three NPF motifs, and a C-terminal SH3 domain (Braun et al., 2005; Kessels and Qualmann, 2004). Several studies suggest that syndapins play an important role in the structural organization and functional coordination of the endocytic process at synapses (Andersson et al., 2008; Anggono and Robinson, 2007; Anggono et al., 2006; Clayton et al., 2009; Da Costa et al., 2003; Dharmalingam et al., 2009; Kessels and Qualmann, 2004; Kessels and Qualmann, 2006; Kim et al., 2006; Qualmann and Kelly, 2000; Qualmann et al., 1999).

1.4.1 Interactions of the syndapin protein family

Previous studies have demonstrated that the N-terminal F-BAR domain of syndapins mediates self-association (Halbach et al., 2007; Kessels and Qualmann, 2006) as well as the stabilization of curved membrane domains, similar to what has been reported for other BAR family proteins (Itoh et al., 2005). This proposal is also in agreement with the recently reported crystal structures of the F-BAR domains of FBP 17 and CIP14 (Shimada et al., 2007). The SH3 domain of syndapin I is responsible for its interaction with dynamin (Anggono et al., 2006; Kessels and Qualmann, 2006; Qualmann et al., 1999) as well as with several molecules implicated in membrane trafficking and organization of the actin cytoskeleton. These include the phosphatidylinositol 5-phosphatase synaptojanin, a protein that plays a crucial role in the uncoating of clathrin-coated vesicles (Cremona et al., 1999), synapsin I, a protein associated with the reserve pool of synaptic vesicles (Hilfiker et al., 1999), N-WASP (Kessels and Qualmann, 2002; Nikki et al., 2002; Qualmann et al., 1999), Cordon-Bleu, a brain-enriched nulceator of unbranched actin filaments (Ahuja et al., 2007), and EHD proteins (Eps15 homology domain containing-proteins) which mediate vesicle endocytosis and recycling (Figure 1-18) (Braun et al., 2005).

Additionally, syndapins have been linked to signalling pathways, development and to Huntington's disease (Figure 1-18). The interaction between syndapin and Son-of-sevenless (mSos), a guanine nucleotide exchange factor for Ras, implicates syndapins in regulating signalling to mitogen-activated protein kinases (Wasiak et al., 2001). Syndapin contains phosphorylation sites for protein kinase C and casein kinase 2 (Plomann et al., 1998), implying that syndapin function is regulated by signaling cascades. Syndapin binds to the cytoplasmic tails of members of the ADAM family proteins (A Metalloprotease And Disintegrins) and to NR3A-containing NMDA receptors (Cousin et al., 2000; Howard et al., 1999; Mori et al., 2003; Perez-Otano et al., 2006), suggesting roles in development and synaptic transmission. CD95L is a member of the tumour necrosis factor (TNF) family of death factors and induces apoptosis (Janssen et al., 2003). The association of syndapin with CD95L implicate syndapins in apoptosis (Ghadimi et al., 2002). Huntington's disease is a progressive neurodegenerative genetic disorder, which affects muscle coordination and leads to cognitive decline and dementia caused by a CAG/polyglutamine repeat expansion in the first exon of the gene coding for

huntingtin (Mangiarini et al., 1996). The specific interaction between huntingtin and neuronal syndapin 1 is enhanced in the case of mutant huntingtin and changes its intracellular distribution in pathological tissue, implying that syndapin 1 plays a role in the neuropathology of Huntington's disease (Modregger et al., 2002).

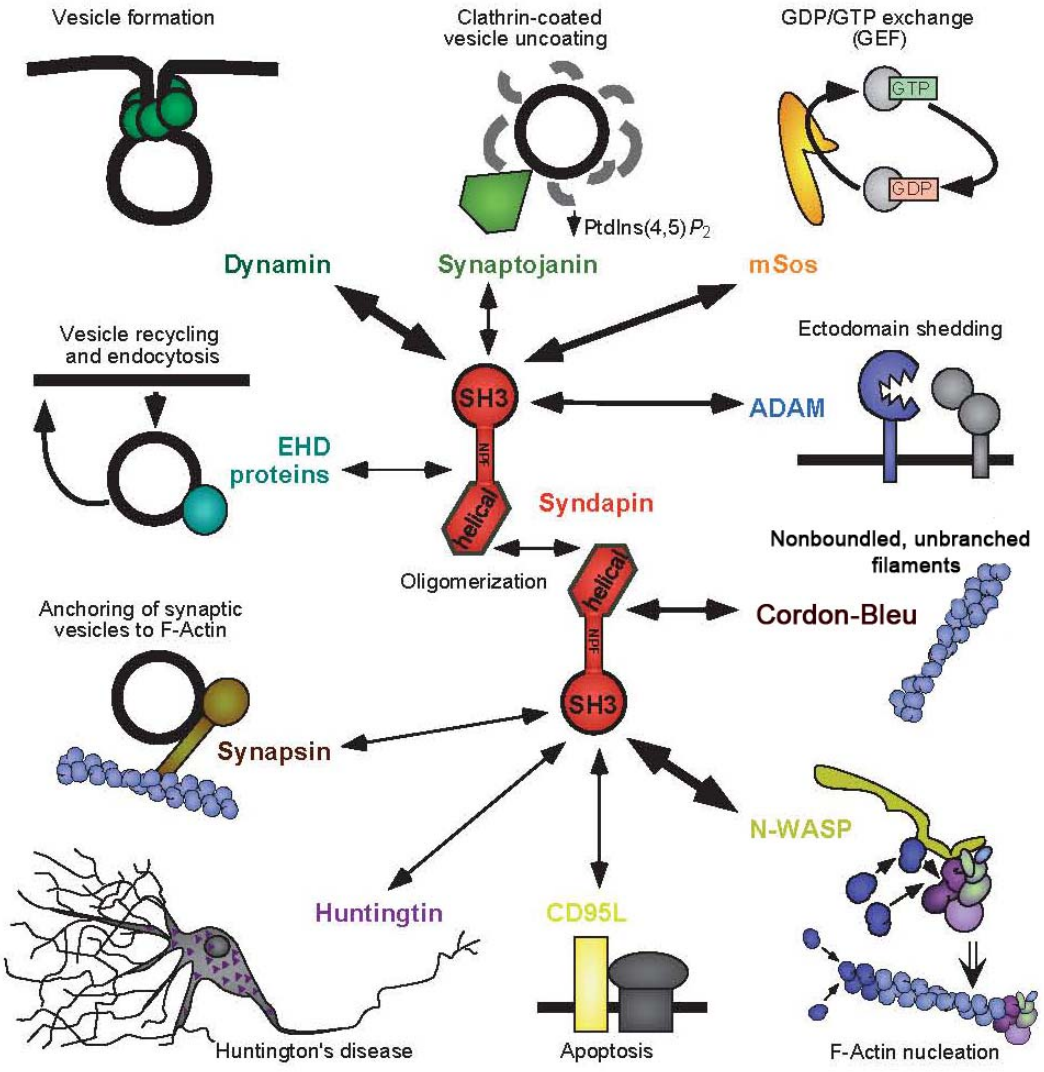

Figure 1-18 Interactions of the syndapin protein family. Depicted are all syndapin interaction partners described, irrespective of species, syndapin isoform or splice variant (modified from (Kessels and Qualmann, 2004)).

1.4.2 Syndapins play a role in endocytic pathway

The NPF motifs of syndapins are recognized by the EH domain proteins, such as EHD1 (Braun et al., 2005). Recent studies show that syndapin 1 directly and selectively binding to the carboxy-terminal domain of NR3A (a subunit of the

NMDA receptor) via its two NPF motifs assembles a protein complex comprising dynamin and clathrin (Perez-Otano et al., 2006). NMDA receptors (*N*-methyl-D-aspartate receptors) are glutamate-gated ion channels that are pivotal in the regulation of synaptic function in the CNS (cental nervous system). NMDARs are heteromeric assemblies of NR1, NR2 and NR3 subunits. NR3A is expressed primarily during a narrow time window of postnatal development during which synaptic circuitry is established (Wong et al., 2002) Mice lacking NR3A show increased dendritic spine density (Das et al., 1998), suggesting a potential role for this subunit in synapse maturation or elimination. NR3A shares only limited sequence homology with NR1 and NR2 and is equipped with a unique C-terminal domain that is different from other NMDAR subunits. Heteromeric receptors containing NR3A (NR1/NR2/NR3A) possess unique channel properties, including reduced calcium (Ca^{2+}) permeability and low sensitivity to magnesium (Mg^{2+}) blockade (Das et al., 1998; Perez-Otano et al., 2006; Tsujita et al., 2006). The interaction between NR3A and syndapin 1 mediates robust endocytosis and synaptic removal of NR3A-containing NMDA receptors (Perez-Otano et al., 2006). Syndapin 1 may function as an adaptor mediating endocytosis of NR3A-containing NMDA receptors endocytosis at distinct developmental stages.

Similar to other BAR/F-BAR domain containing-proteins, syndapins not only generate membrane curvature/deformation using the F-BAR module but also bind via their SH3 domain to endocytic proteins such as dynamin and N-WASP. Like other BAR/F-BAR domain containing-proteins, syndapin 1 binds to synaptically enriched dynamin 1. The interaction between syndapin 1 and dynamin 1 is specifically regulated by phosphorylation/dephosphorylation of dynamin 1 (Anggono et al., 2006). Dynamin 1 dephosphorylation is mediated by the calcium-dependent protein phosphatase calcineurin during intense neuronal activity (Cousin and Robinson, 2001; Cousin et al., 2001). Both dynamin 1 dephosphorylation and its downstream interaction with syndapin 1 are necessary for synaptic vesicle endocytosis (Anggono et al., 2006). Perturbation of the interaction between dynamin 1 and syndapin 1 specifically inhibits activity-dependent bulk endocytosis (Clayton et al., 2009). In lamprey reticulospinal synapses, perturbation of syndapin has no effect on vesicle recycling under conditions of low-frequency stimulation in lamprey reticulospinal synapses, but disrupts synaptic vesicle recycling activated by intense stimulation

(Andersson et al., 2008). Interestingly, perturbation of syndapin in lamprey reticulospinal synapses massively increases membranous cisternae and invaginations around release sites like “endosome-like structure”, but not of coated pits at the plasma membrane (Andersson et al., 2008). These data suggest that syndapin 1 may increase the capacity of bulk retrieval of SV membranes during intense stimulation (Cheung et al., 2010). However, this raises the question how syndapin invaginates and stabilizes the “endosome-like structures”? Syndapin is composed of an F-BAR domain and an SH3 domain. Like other BAR domains, the dimerization of syndapin F-BAR is supposed to form a crescent-shaped module which could preferentially bind and stabilize “endosome-like structure” resulting from bulk endocytosis. The crystal structure of syndapin or its F-BAR domain may provide an explanation. Given that dynamin contains a membrane binding PH domain and the GTPase activity, dynamin together with syndapin may play a role in membrane shaping and membrane fission in the bulk endocytosis pathway.

1.4.3 Syndapin 1 shapes the plasma membrane

Although syndapin 1 binds to dephosphorylated dynamin 1 and triggers bulk endocytosis during intense neuronal activity, its interaction with the actin nucleation promoting factor N-WASP plays an additional role in altering neuronal morphology during neuromorphogenesis and neuronal network formation (Dharmalingam et al., 2009)**.** Recent studies show that overexpression of syndapin 1 in neurons highly increases the neurite number and dendrite branching. Both the SH3 domain and the F-BAR domain are necessary for this syndapin 1-induced phenotype (Dharmalingam et al., 2009). Importantly, the influence of syndapin 1 on neuronal morphology depends on both N-WASP and the N-WASP-activating GTPase Cdc42 (Dharmalingam et al., 2009). Interestingly, knockdown of syndapin 1 does not change neurite number and dendrite branching, but rather increases aberrant axon branching, a phenotype also seen upon knockdown of either N-WASP or Arp2/3 complex (Dharmalingam et al., 2009). How precisely syndapin regulates neuromorphogenesis remains unknown.

.

2 Aims of this study

The aim of this work was to dissect the functions of syndapin in membrane deformation by combined structural, biochemical and cell biological approaches. Furthermore, we aimed at elucidating the precise molecular mechanism by which syndapin-mediated membrane deformation is coupled to dynamin-catalyzed membrane fission.

3 Materials and Methods

3.1 Materials

3.1.1 Chemicals and consumables

Chemicals were purchased from Invitrogen, GE Healthcare, Merck, Pierce, Roth, Serva and Sigma. Disposables were obtained from Amersham, Greiner, Millipore, Sarstedt, Schott and Whatman.

3.1.2 Enzymes and kits

Enzymes and Kits were purchased from the following companies:

Restriction enzymes, T4 DNA polymerase, VENT polymerase, Calf intestinal phosphatase (CIP): New England Biolabs (NEB)

Taq polymerase: Genaxxon

T4 DNA ligase: Roche

Wizard Plus SV miniprep kit: Promega

E.Z.N.A. Cycle pure and gel extraction kits: PeqLab

Plasmid midi prep kit (standard and endotoxin free): Qiagen

3.1.3 Markers and loading dyes

DNA markers were purchased from Fermentas (GeneRuler 1kb DNA ladder) and Genaxxon (100 bp + 1.5 kb ladder), protein markers from NEB (broad range protein marker, pre-stained broad range protein marker). 6x sample buffer for SDS-PAGE was prepared in a total volume of 50 ml containing 375 mM Tris, 60 % (v/v) glycerol, 30 % (v/v) β-mercaptoethanol, 18 % (w/v) SDS and a “tip of a spatula” bromphenol blue (no water added). 6x DNA loading dye solution was prepared as follows: 0.05 % bromphenol blue, 0.05 % xylene cyanol, 30 % glycerol in ddH_2O.

3.1.4 Synthetic oligonucleotides

Customized synthetic DNA oligonucleotides were purchased from MWG Biotech. A complete list of primers used for PCR can be found in the appendix.

3.1.5 Synthetic peptides

Peptides derived from the dynamin 1 and syndapin 1 were synthesized at the Charité, Berlin.

PxxP peptide: ^{773}RSPTSSPTPQRRAPAVPPARPG^{794}

AxxA peptide: ^{773}RSPTSSPTPQRRA**A**AV**A**PARPG^{794}

Syndapin 1-derived NPF peptide: ^{358}SDDESGNPFGGNEANGGANPFEDDA^{382}.

3.1.6 Bacterial strains

Strain	Description	Source
E. coli TOP 10	high-efficiency cloning and plasmid propagation	Invitrogen
E. coli ER2566	high-level expression of heterologous proteins	NEB
E. coli BL21 CodonPlus^{TM} (DE3)-RP	high-level expression of heterologous proteins; extra tRNA genes	Stratagene

3.1.7 Plasmids

Plasmid	Description	Tag (pos.)	Resistence	Source
pGEX-4T-1	prokaryotic expression vector	GST (N)	Amp^r	Amersham Pharmacia
pGEX-2T	prokaryotic expression vector	GST (N)	Amp^r	Amersham Pharmacia
pET-28a(+)	prokaryotic expression vector	His_6 (N)	Kan^r	Novagen
pEGFP-C1	eukaryotic expression vector	eGFP (N)	Kan^r/Neo^r	BD Biosciences Clontech
pmCherry-N1	eukaryotic expression vector	mCherry (C)	Kan^r/Neo^r	BD Biosciences Clontech
pmRFP-N1	eukaryotic expression vector	RFP (C)	Kan^r/Neo^r	

3.1.8 Constructs

Name of construct	Mutations & Truncations	Amino acids	Vector	Restriction sites
Syndapin 1-FL	---	1-441	pET-28a(+)	Nhe I/EcoR I
Syndapin 1-(1-337)	---	1-441	pET-28a(+)	Nhe I/EcoR I
Syndapin 1-(1-337)	K145E,K146E, K148E	1-337	pET-28a(+)	Nhe I/EcoR I
Syndapin 1	Q396R,E397R	1-441	pET-28a(+)	Nhe I/EcoR I
endophilin 1-(1-256)	---	1-256	pET-28a(+)	Nhe I/EcoR I
amphiphysin 1-(1-245)	---	1-245	pET-28a(+)	Nhe I/EcoR I
EHD1-(401-534)	---	401-534	pET-28a(+)	Nhe I/EcoR I
Dynamin 1-(509-864)	---	509-864	pET-28a(+)	Nhe I/EcoR I
GST	---	---	pGEX-2T	---
Syndapin 1-(340-441)	---	340-441	pGEX-2T	EcoR I/BamH I
Syndapin 1-(379-441)	---	379-441	pGEX-2T	EcoR I/BamH I
Syndapin 1-SH3 domain	E400R	379-441	pGEX-2T	EcoR I/BamH I
Syndapin 1-SH3 domain	P434L	379-441	pGEX-2T	EcoR I/BamH I
Syndapin 1-SH3 domain	D394R,E400R	379-441	pGEX-2T	EcoR I/BamH I
Syndapin 1-SH3 domain	Q396R,E397R	379-441	pGEX-2T	EcoR I/BamH I
Endophilin 1-SH3 domain	---	245-352	pGEX-4T-1	EcoR I/BamH I
Amphiphysin 1-SH3 domain	---	546-695	pGEX-4T-1	EcoR I/BamH I
Syndapin 1-FL	---	1-441	pEGFP-C1	EcoR I/BamH I
Syndapin 1	I122F,M123F	1-441	pEGFP-C1	EcoR I/BamH I
Syndapin 1	K127E,K130E	1-441	pEGFP-C1	EcoR I/BamH I
Syndapin 1-(1-304)	---	1-337	pEGFP-C1	EcoR I/BamH I
Syndapin 1-(1-304)	I122F,M123F	1-337	pEGFP-C1	EcoR I/BamH I
Syndapin 1-(1-304)	I122T,M123Q	1-337	pEGFP-C1	EcoR I/BamH I
Syndapin 1-(1-304)	K127E,K130E	1-337	pEGFP-C1	EcoR I/BamH I
Syndapin 1-(1-304)	K145E,K146E, K148E	1-337	pEGFP-C1	EcoR I/BamH I
Syndapin 1-SH3 domain	---	379-441	pmCherry-N1	Hind III/Kpn I
Syndapin 1-SH3 domain	D394R,E400R	379-441	pmCherry-N1	Hind III/Kpn I
Syndapin 1-SH3 domain	Q396R,E397R	379-441	pmCherry-N1	Hind III/Kpn I
Dynamin 1	---	1-864	pmRFP-N1	
Dynamin 1	K44A	1-864	pmRFP-N1	

3.1.9 Mammalian cell lines

COS-7: African green monkey kidney cells fibroblasts

3.1.10 Buffers, medium and solutions

Molecular biology

Ampicillin stock: 50 mg/ml in ddH_2O sterile filtered

Kanamycin stock:10 mg/ml in ddH_2O sterile filtered

LB medium: 1 % (w/v) yeast extract, 0.5 % (w/v) trypton, 0.5 % (w/v) NaCl pH 7.2

2xYT medium: 1.6 % (w/v) trypton, 1 % (w/v) yeast extract, 0.5 % (w/v) NaCl pH 7.4

Ethidium bromide stock solution: 10 mg/ml in ddH_2O

10 x TBE (Tris-Borate-EDTA): 108 g Tris base**,** 55 g boric acid**,** 9.3 g Na_4EDTA

5x M9 stock: 30 g Na_2HPO_4，15 g KH_2PO_4, 5 g NH_4Cl and 2.5 g NaCl in 1L ddH_2O (autoclaved)

1L M9 culture medium: 200 ml 5x M9 stock
700ml ddH_2O (autoclaved)
1ml 1M $MgSO_4$
100ml 40% (w/v) glucose stock (sterile filtered)
100µl 0.5% (w/v) thiamine vitamin (sterile filtered)

Biochemistry

4x SDS-PAGE Separating Gel Buffer: 0.4 % SDS, 1.5 M Tris pH 8.8

4x SDS-PAGE Stacking Gel Buffer: 0.4 % SDS, 0.5 M Tris pH 6.8

Coomassie Stain (1L):1 g Coomassie G250, 100 ml Acetic acid, 250 ml Methanol

Coomassie Destain (1L): 100 ml Acetic acid, 250 ml Methanol

10x SDS Running Buffer: 246 mM Tris, 1.92 M Glycine,1 % SDS

Sample buffer: 200 mM Tris-HCl, 4 % SDS, 16 % glycerol, 0.01 % Bromophenol blue, pH 6.8

2x Bradford Reagent: 70 mg CoomassieG250, 100 ml 85 % H3PO4, 50 ml Ethanol

in 500 ml, filtered

PMSF stock solution: 100 mM in DMSO

Cell Biology

Cos7 cell medium: Dulbecco's modified Eagle's medium (DMEM) (1g/L Glucose) supplemented with 10% heat inactivated (30 min at 56°C) fetal calf serum, and antibiotics (50 units/ml Penicillin, 50 µg/ml Streptomycin)

3.1.11 Devices and equipment

Autoclaves	Systec model V-65	Systec, Wettenberg
Centrifuges	tuttnauer Systec model 5075 ELV	Systec, Wettenberg
	Beckman Avanti J-26XP Rotors: JS-5.3, JA-25.50	Beckman Coulter, Krefeld
	Eppendorf model 5417-R	Eppendorf, Hamburg
	Eppendorf model 5702R	Eppendorf, Hamburg
Gel dryer	Model 583	BioRad, Munich
Incubators	Microbiological organisms Memmert	Memmert , Schwabach
	Heraeus for tissue culture	ThermoElectron,Langenselbold
Microscopes	Axiovert 200M Fluorescence	Carl Zeiss
	Philips EM 208	Philips, Eindhoven
pH meter	SevenEasy (electrode InLab 410)	Mettler-Toledo, Giessen
Sonification	Microtip System Sonoplus	Bandelin, Berlin
PCR	T3 Thermocycler	Biometra
Protein purification	ÄKTA prime His-Trap column	Amersham Bioscience
	ÄKTA FPLC UPC-900 Column: HiLoad_16/60_Superdex_200_Prep_grade	Amersham Phamacia Biotech

3.1.12 Software and internet resources

Premier 5.0	- primer design
Volocity Software (Improvision)	- microscopy analysis
Adobe 9.0 Professional	-Adobe Systems, San Jose, CA, USA

Adobe Photoshop CS	-Adobe Systems
Microsoft Office Applications	-Microsoft
PDB (Protein Data Bank)	-Research Collaboratory for Structural Bioinformatics (RCSB) www.rcsb.org/pdb
ExPASy (Expert Protein Analysis System)	- www.expasy.org - alignments, protein parameters - DNA-protein translation tool
NCBI (Ntl. Center for Biotech. Information)	- www.ncbi.nlm.nih.gov - BLAST, literature - DNA and protein sequences
CCP4 program Suite	- crystal structure determination
Pymol	- crystal structure analysis

3.2 Molecular biology

3.2.1 Polymerase chain reaction (PCR)

The PCR was not only used to amplify DNA fragments from existing plasmids or cDNA for subsequent cloning, but also for PCR-based site directed mutagenesis (overlap extension PCR). Routinely, PCR was also used to screen *E. coli* colonies after transformation with newly generated plasmid constructs (Colony PCR). A standard PCR was performed in a final volume of 50 µl containing the following constituents: template DNA (0.1-1 µg), 1 x reaction buffer, 200 µM dNTPs, 1 µM of each primer, and 1 U of Vent-polymerase (NEB). For colony PCRs, the final volume was 20 µl and Taq polymerase was used instead (0.25 U per reaction). The following is standard PCR recipe and program for amplification.

ddH2O	37 µl
10×Thermal buffer	5 µl
Template (100 ng/µl)	1 µl
dNTP mixture (5 mM/each)	4 µl
forward primer (10 pmol/µl)	1 µl
reverse primer (10 pmol/µl)	1 µl
Vent polymerase	+ 1 µl
Total	50 µl

step	time/ min	temperature/ °C		Process
1	5	95	1 cycle	Initial denaturation
2	1	95		Denaturation
3	1	55-65 (55)*		Annealing
4	1-5**	72	30 cycles steps 2-4	Elongation
5	10	72	1 cycle	final elongation

* for Colony PCRs using vector-specific primers

** depending on the length of the amplicon (approx. 1 min per 1000 bp)

3.2.2 Overlap extension PCR

The overlap extension PCR was applied to insert specific point mutations. An internal mutagenic primer pair was designed totally or partially overlapping and including base substitutions resulting in the desired mutation. Each of these primers was used in a separate reaction together with an outer flanking primer designed to one end of the DNA region of interest. The two halfs generated by these PCRs were then used in one PCR as partly overlapping templates together with the two outer flanking primers to amplify the final amplicon containing the desired mutation.

3.2.3 Agarose gel electrophoresis and gel extraction

Agarose gels were used to separate PCR amplicons, restricted inserts and vectors. They were prepared in a concentration of 0.7, 1, 1.5 or 2 % agarose (w/v) in 1x TBE buffer. DNA solutions were mixed with 6x loading dye prior to loading onto the gel. PCR products or digested vectors were loaded on agarose gels and run at 100 V. Subsequently, the DNA was stained in an ethidium bromide (EtBr) containing water bath. The stained DNA was visualised by UV illumination of the gel. DNA bands of the desired size were cut and the DNA was extracted according to manufacture's kit instruction.

3.2.4 DNA restriction digest and dephosphorylation of vector DNA

1-5 µg plasmid DNA or isolated PCR products were digested in a final volume of 50 µl containing NEBuffer (10x stock), BSA (10x stock), and 10 U (or 50 U for 5 µg plasmid) of restriction enzymes. The reaction mixtures were incubated at 37°C for 2 h or overnight. Digested PCR amplicons were purified using a Cycle Pure Column (PeqLab). Inserts and vectors were extracted from preparative agarose gels.

In order to prevent re-ligation of the vector backbone, linearized plasmid DNA was 5'-dephosphorylated before ligation. 0.5 units calf intestine phosphatase (NEB) were used for 1 µg of vector DNA in any NEB buffer directly after the restriction enzyme digest. The dephosphorylation reaction was performed at 37°C for 10 min. Afterwards, the DNA was purified using the E.Z.N.A. Cycle Pure kit (PeqLab).

3.2.5 Ligation of DNA inserts into linearized vectors

For ligation, vector and insert DNA were combined in a 1:3 molar ratio in a total volume of 20 µl including reaction buffer and 1 U T4-DNA ligase. Samples were incubated at room temperature for 1 h or at 4°C overnight. Then, the ligation mix was applied for the transformation of chemically competent *E. coli* TOP10 cells

3.2.6 Preparation of chemically competent *E. coli* cells

To prepare chemically competent *E. coli* TOP10, or BL21, or ER2566 straints, one fresh colony from an overnight agar plate was inoculated into 5 ml LB medium for overnight culture at 37°C. This overnight culture (1ml) was inoculated into 50 ml LB medium grown at 37°C until the OD_{600} reached 0.4 (2 x 10^8 cells/ml). Cells were centrifuged at 2500 xg and 4°C for 10 min. The supernatant was discarded and the pellert were resuspended in 10 ml of 0.1 M $CaCl_2$ solution and incubated on ice for at least 15 to 30 min up to 3 h. After another centrifugation (10 min, 2500x g, 4°C), cells were resuspended in 2 ml of 0.1 M $CaCl_2$ solution. 50 % glycerol solution was adjusted to a final concentration of 10 %. 100 µl straint was aliquoted into 1.5 ml eppendorf tube and then frozen in liquid nitrogen and stored at -80°C until use.

3.2.7 Transformation of chemically competent *E. coli* cells

For transformation, 100 µl aliquots of competent *E. coli* cells (TOP10, or BL21, or ER2566) were thawed on ice. 5 µl of a ligation reaction solution (50~100ng DNA) was added. After 30 min incubation on ice, cells were heat shocked in a water bath at 42°C for 90 sec and immediately put on ice for at least 2 min. Bacteria were incubated 900 µl LB at 37°C for 1 h to allow for the gene expression of the resistance. Then cells were plated on selective LB agar plates supplemented with appropriate antibiotics. Plates were incubated at 37°C overnight (16~20 h).

3.2.8 Colony PCR

Colony PCRs were used to screen grown bacteria colonies with the integration of the correct DNA insert. For this purpose, eight colonies for each sample were selected and inoculated into 100 µl LB medium in the presence of appropriate antibiotics in a 96-well plate. The plate was then shaken at 37°C for 2 h. The following protocol was used to prepare a single PCR screen reaction mixture:

ddH2O	16 µl
10×dream Tap buffer	2 µl
E.coli culture	1 µl
dNTP mixture (5 mM/each)	0.5 µl
forward primer (10 pmol/µl)	0.2 µl
reverse primer (10 pmol/µl)	0.2 µl
Tap polymerase	+ 0.06 µl
Total	20 µl

The master solution was prepared and then aliquoted. For PCR, a standard programme was run in a thermocycler as described above. The PCR products were analyzed by agarose gel electrophoresis.

3.2.9 Plasmid DNA mini and midi preparation

After agarose gel electrophoresis and EB staining, positive clones were selected and inoculated into small-scale LB medium for overnight culture at 37°C. Mini preparations of plasmid DNA were performed from 5 ml *E. coli* overnight cultures using the *Wizard Plus* DNA mini preparation kit (Promega) according to the manufacture's instructions. To prepare larger, higher quality DNA amounts (e.g. for transfection of mammalian cells) 100-150 ml overnight cultures were applied to the QIAGEN Plasmid Midi Kit with a Qiagen-tip 100 according to the manufacture's instructions.

3.2.10 DNA sequencing

1 µg of purified plasmid DNA (mini-prep) was sent to MWG Biotech for sequencing. Obtained sequences were analyzed using the alignment tool available under http://multalin.toulouse.inra.fr/multalin/multalin.html

3.2.11 Glycerol stocks

For long-term storage of *E. coli* clones containing a desired construct, 700 µl overnight culture was mixed with 700 µl 50 % (w/v) sterile glycerol and stored at -80°C.

3.3 Biochemistry

3.3.1 Overexpression of recombinant proteins in *E. coli*

Lysis buffer: 50 mM HEPES (pH 7.4)
200 mM NaCl
10 mM imidazole (for His_{x6}-tag fusion protein)

Solid amino acid supplements:

L-Lysine	100 mg/L
L-Phenylalanine	100 mg/L
L-Threonine	100 mg/L
L-Isoleucine	50 mg/L
L-Leucine	50 mg/L
L-Valine	50 mg/L
L-SelenoMetionine	50 mg/L

His_{x6}-Dynamin 1-(509-864) lysis buffer:

50 mM Tris-HCl (pH 8.5)
500 mM NaCl
10% glycerol
10 mM imidazole

Strains *E. coli* BL21 and ER2566 cells carrying the desired expression vector were used to express proteins of interest. Overnight cultures were usually diluted 1:20 in 2xYT-medium supplemented with appropriate antibiotics and incubated in a shaker at 37°C until the OD_{600} reached 0.6 to 0.8. Protein expression was induced by adding 0.5 mM (final concentration) Isopropyl-β-D-thiogalactopyranoside (IPTG) and expressed overnight (about 10 h) at 28°C. If needed, the expression temperature was lowered to 18°C to increase the solubility of the recombinant proteins. After overexpression, the bacteria were pelleted by centrifugation at 5300 rpm for 15 min at 4°C. After removal of the medium, the cell pellets of 1 liter culture were resuspended in 40 to 100 ml ice-cold lysis buffer (depending on the expected yield) and stored at -20°C.

His_6-Selenomethionine-substituted syndapin 1-(1-337) (abbreviated as SeMet-synd 1-337 later on) was prepared as described (Van Duyne et al., 1993). Briefly, overnight cultures (1 ml LB medium) were gently centrigued at 1300 xg at room temperature for 1~2 min, gently resuspended pellet in 1 ml M9 culture medium, inoculated to 250 ml M9 culture medium, and grown at 37°C until OD_{600} reached 0.3 (growth is really slow-from 1/2 to 1/5 of the usual growth rate for the strain in rich medium). Solid amino acid supplements were added to the culture. After 15 min for inhibition of methionine synthesis to start, the cloned protein expression was induced by 0.5 mM IPTG. Growth continued for a further 6 h and then the bacterial was harvested as usual.

3.3.2 Affinity-purification of recombinant GST

Washing buffer: 50 mM HEPES (pH 7.4)
200 mM NaCl

For recombinant GST fusion proteins, affinity purification was applied. Bacterial pellets resuspended in lysis buffer were supplemented with 1 mM PMSF, 100 units of Benzonase endonuclease (Sigma) and a "tip of a spatula" lysozyme. The mixture was incubated on ice for 10 min and sonicated for 2x 60 s with 70 % power and 50 % duty cycle. Subsequently, 1 % Triton X-100 (or 2 % CHAPS detergent in some cases) was added, incubated for 20 min, centrifuged for 15 min at 24,000rpm at 4°C. The supernatant was added to the pre-washed GST binding resin (Novagen), incubated for 2 h at a rotating wheel at 4°C, washed 3 times (centrifugation 4000 rpm for 2 min) by washing buffer. Afterwards, beads containing GST fusion proteins were pelleted by centrifuguation and resuspended in 1 ml washing buffer for further GST-pulldown assay experiments.

3.3.3 Affinity-purification of recombinant His_{x6}-fusion proteins

Washing buffer: 50 mM HEPES (pH 7.4)
200 mM NaCl
10 mM imidazole

Elution buffer: 50 mM HEPES (pH 7.4)
200 mM NaCl
300 mM imidazole

Running buffer: 50 mM HEPES (pH 7.4)
200 mM NaCl

As the same as purification of GST fusion proteins, bacterial pellets resuspended in lysis buffer were supplemented with 1 mM PMSF, 100 units of Benzonase endonuclease (Sigma) and a "tip of a spatula" lysozyme. The mixture was incubated on ice for 10 min and sonicated for 2x 60 s with 70 % power and 50 % duty cycle. Subsequently, 1 % Triton X-100 (or 2 % CHAPS in some cases) was added, incubated for 20 min, centrifuged for 15 min at 24,000rpm at 4°C and ultrafiltered by 0.45 µm filterer (Amicon® Ultra). The supernatant was loaded to a Ni-NTA column (Novagen) with the flow rate at 1 ml/min and extensively washed by washing buffer. The binding proteins were eluted by elution buffer. The elution fractions were concentrated and incubated with thrombin (Sigma) (1 U/mg) and 2.5 mM $CaCl_2$ (Sigma) at 4℃ overnight, and then loaded onto a Sephadex 200 size-exclusion column for further purification using 50 mM HEPES (pH7.4), 200 mM NaCl as running buffer. The purity was confirmed by SDS-PAGE. All purified samples were concentrated using centrifugal filter tubes (Millipore and Amicon Bioseparations) and were aliquoted into 100 µl and stored at -80℃ for further studies.

3.3.4 Protein quantification - Bradford assay

1 µl for His_{x6} fusion proteins or 2 µl for GST fusion proteins were diluted in water to a final volume of 500 µl and mixed with 500 µl of 2 x Bradford reagent. The absorption at 595 nm was determined after incubation for 10 min at room temperature. 1 x Bradford reagent (500 µl 2 x Bradford reagent diluted 1:1 in water) was used as a blank. The protein content was calculated from a reference curve determined with BSA as a standard.

3.3.5 *In vitro* binding Assays

Binding buffer:

20 mM HEPES-Na(pH7.4)
50 mM NaCl
0.1% Triton X-100

For direct binding assays, immobilized GST fusion proteins (20 µg) were incubated in a total volume of 500 µl binding buffer for 2 h at 4℃ with recombinant His_6-tagged proteins (60 or 80 µg) in presence or absence of peptides (100 µM).

10-15 µl GST binding resin was added if the beads volume was too low. For salt sensitive experiment, the concentration of NaCl was 50 mM, 100 mM, 200 mM and 400 mM. Samples were washed extensively using binding buffer. Complexes were analyzed by SDS-PAGE and staining with Coomassie blue.

3.3.6 SDS polyacrylamide gel electrophoresis (SDS-PAGE)

To separate proteins according to their size, SDS polyacrylamide gels were casted with varying concentrations: 9-12 % acrylamide for the separating gel, and 3 % for the stacking gel. Protein samples for electrophoresis were mixed with sample buffer, denatured at 95°C for 3 min and loaded onto the gel. Electrophoresis was performed in 1 x SDS-PAGE running buffer with a constant 20 mA per gel. Afterwards, the gels were stained with Commassie blue followed by a destaining procedure to detect the protein bands and analyze the complex formation. For salt sensitive experiments, Protein band intensities were quantified by Image J.

3.4 Cell Biology

3.4.1 Mammalian cell culture

Freezing medium:

10% DMSO
90% fetal calf serum (FCS)

COS-7 cells were used as model mammalian cell line for immunofluorescence and transferrin uptake experiments in this study. Cells were cultured in Dulbecco's modified Eagle's medium (D-MEM) containing glutamate, sodium pyruvate, pyridoxine and glucose (1 g/l). Medium were supplemented with 10 % heat inactivated (30 min, 56°C) fetal calf serum (FCS) and antibiotics (50 units/ml penicillin, 50 µg/ml streptomycin). Cells were passaged twice a week using trypsin/EDTA solution for detachment, plated at 1:5-1:20 dilutions onto culture dishes, and incubated at 37°C, 5 % carbon dioxide, and 95 % humidity. For Long-Term Storage of Cell Lines, the cells were disattached from a 10 cm tissue culture dish by treatment with 2 ml trypsin/EDTA (GibcoBRL, Eggenstein). Trypsin/EDTA was inactivated by the addition of 8 ml serum containing medium. Cells were centrifuged at 200 x g for 3 minutes and resuspended the pellet in 3 ml

freezing medium. 1 ml aliquots were frozen at -80°C and transferred to liquid nitrogen from1 day to half a year after freezing.

3.4.2 Transfection of mammalian cells with plasmid DNA

For transfection of cell lines with plasmid constructs, Lipofectamine™ 2000 (Invitrogen) was used as reagent to transfect mammalian cells with plasmid DNA, essentially according to manufacturer's instructions with minor variations. The liposome-based transfection method was applied on cells having a confluency of about -50 % in this study. For 6-well plates, 2 µg DNA and 4 µl Lipofectamine per well were diluted into 2x 100 µl Optimem, respectively. Plasmid DNA and Lipofectamine were mixed in Optimem in separate polystyrol tubes and incubated for 5 min at room temperature, and then both mixtures were combined. After 25 min incubation the solution was added to the cells for transfection and incubated for 2 h at 37°C before changing the medium with appropriate antibiotics. Cells were analyzed after 10-15 h transfection.

3.4.3 Live cell confocal imaging experiment

We used live cell confocal imaging assay to study the membrane tubulation ability of syndapin or syndapin F-BAR alone. Cos7 cells expressing low levels of fluorescent proteins were imaged after 10-15 h post-transfection with Lipofectamine 2000 using a Zeiss Axiovert 200M-based PerkinElmer Life Science UltraView ERS dual spinning disc system. Compared with conventional optical microscopy, spinning disc confocal microscopy has several advantages, including widefield, laser scanning confocal microscopy and acquisition of images at very high frame rates with minimum illumination of samples. Particularly, the spinning disc confocal microscopy is able to apply high speed 3D imaging of living systems. The microscopy with a closet was prewarmed at 37°C with humidity and 5 % carbon dioxide. The coverslip with cells was mounted to a metal champer with 1ml prewarmed 1x HBSS buffer supplemented with 5% FCS, 1 mM Ca^{2+} and 1 mM Mg^{2+}. Data were processed using Volocity software (Improvision). For quantification, at least 20 transfected cells were chosen for each experiment. The numbers of tubules were manually determined, and the average number of tubules per cell was calculated. Cells of interest from at least three different independent experiments

were collected and used for quantification.

3.4.4 Electron microscopy analysis of Cos7 cells

Cos7 cells grown on the glass coverslips were fixed with 2% glutaraldehyde in PBS and postfixed with aqueous 1% osmium tetroxide solution, dehydrated and finally flat embedded in Epon as described elsewhere (Mundigl et al., 1993). Upon resin polymerization, glass was removed using liquid nitrogen and hot water. 50 nm sections were cut paralel to the coverslip, stained with 1% aqueous uranyl acetate and lead citrate and examined in a Philips EM 208 electron microscope. Images were taken at 20,000x magnification and negatives scanned at 1200 dpi. The diameter of membrane tubules was calculated by Image Tool software. More than 10 membrane tubules were selected for each image..

3.4.5 Transferrin uptake assay

Normally, the fluorescence-labeled transferrin (Tf) internalization is used as a read out for endocytosis. Here we used transferrin uptake assay to determine the origin of membrane tubules which were generated by overexpression of syndapin F-BAR in Cos 7 cells. Transfected Cos7 cells were serum-starved for 2h using DMEM medium without anything. Alexa Fluor^{568}-Tf (Molecular Probes) was diluted into serum free medium with a final concentration of 25 μg/ml and centrifuged at 14,000 rpm for 5 min. The starved cells grown on the coverslip were transferred upside-down onto a droplet of transferring solution (~50 μl) and incubated for 10 min or 30 mim at 37°C in a prewarmed humidity chamber. The humidity chamber was immediately placed on ice after incubation. The cells was transferred back to 6-well plates and washed three times with ice-cold 1x PBS buffer. The cells were immediately used for living cell confocal image analysis. The live cell imaging was processed as described in 3.4.3.

3.5 Protein crystallography

3.5.1 Crystallizaiton

Two of the most commonly methods - hanging drop and sitting drop for protein crystallization are used in this study. Initially, a droplet (2 μl) containing 1 μl purified

protein and 1 µl precipitant in different buffers were added onto 96-well crystallization plate and equilibrated with a larger (100 µl) reservoir containing similar buffers and precipitants in higher concentrations. As water vaporizes from the drop and transfers to the reservoir, the precipitant concentration increases to a level optimal for crystallization. Crystals were grown at 291K by the sitting-drop vapor diffusion method using Hampton Screen kit I & kit II, Hampton PEG/ION screen and Emerald Wizard I & II as a starting point. For protein-protein complex, Hampton screen Protein Complex Kit was used for the initialing screening. All of the above products use the sparse matrix method, which is based on the successful conditions reported before. The 96-well crystallization plates were inspected every day at first week and then every week. All changes were recorded in special forms. The conditions with crystals were optimized by changing are protein concentration, temperature, buffer, pH, precipitant, salt and additives (Hampton Research additive screen kits). 2 µl or 4 µl protein samples were used for crystal optimization to obtain a single and well-diffracted crystal. The hanging drop method was used for crystallization opitimiztion. 12 well-plates were used once crystallization conditions were screened. The reservoir was filled with 1 ml of precipitant solution with buffer (called reservoir solution). The crystallization drop was mixed with 2 µl or 4 µl protein samples and 2 µl or 4 µl reservoir solution and was placed on a siliconised glass plate and placed over the reservoir. Usually, 4 smaller drops are able to be placed on a siliconised glass plate, which normally can be used for optimizing the different protein concentration in the same condition. As usual, the crystallization drops were inspected every day at first week and then every week. All conditions and changes are recored in special forms.

Normally, the protein sample concentration is more than 5 mg/ml for crystallization trial. In this study, Syndapin 1 full-length protein was concentrated to 2.5-15 mg/ml in 50 mM HEPES-NaOH (pH 7.4), 200 mM NaCl sample buffer; Syndapin 1 was mixed with EHD1-(401-534) at a molar ratio of 1:2 and concentrated to 25 mg/ml in 50 mM HEPES-NaOH (pH 7.4), 200 mM NaCl sample buffer; SeMet-syndapin 1 (1-337) was concentrated to 10 mg/ml in 50 mM HEPES-NaOH (pH 7.4), 200 mM NaCl sample buffer.

More than 20 conditions using PEG 3350 as the precipitant appeared crystals of full-length syndapin 1, but they were very thin and flat even after optimization. These crystals were diffracted to the very low resolution (about 17 Å). One condition was targeted and opitimized: 8% PEG 4000 and 0.1 M sodium acetate (pH 4.6). This condtion gave good crystals at three-dimension, even though the size of crystal was small. The single and big crystals were obtained when decreasing the concentration of PEG 4000 to 3-5% and increasing the pH of sodium acetate buffer up to 5.0-5.5. However, the best crystals were obtained with the additive glycyl-glycyl-glycine (10 mM final concentration) or $NiCl_2$ (10 mM final concentration) which were selected from Hampton Addtive Screen Kit.

Crystals of Syndapin 1/EHD1-(401-534) complex formed after one month under the following conditions: (1) 10% PEG 4000, 0.2 M sodium acetate and 0.1 M sodium citrate (pH 5.5) and (2) 15% PEG 6000 and 0.1 M sodium citrate (pH 5.3). These crystals were ready to be diffracted without any opitimization. However, it turned out to be the degraded syndpain 1-F-BAR domain.

Crystal of SeMet-syndapin 1 (1-337) formed under the following conditions: (1) 5% or 10% PEG 6000 and 0.1 M Citric acid pH 4.0 or pH 5.0, (2) 0.2 M Tri-potassium citrate and 20% PEG 3350, (3) 0.1 M Sodium acetate (pH 5.0) and 20 % MPD (2-methylpentan-2,4-diol) and (4) 5% iso-propanol and 2.0 M ammounium sulfate. However, the crystals from condition (2), (3) and (4) were always very small even after optimization. The quality of crystals was increased after optimizing condition (1). The condition was 4-6% PEG 6000 and 0.1 M citric acid (pH 5.1-5.4). The replacement precipitant PEG 6000 with PEG 3350 also improved the crystals. The best diffraction data were from crystals under the condtion 10% PEG 3350 and 0.1 M sodium citrate (pH 5.5).

3.5.2 X-ray data collection and processing

All the diffraction experiments were carried out at low temperature (100K). The crystals need to be freezed during data collection, which normally minimizes the effects of radiation damage at high brilliance tightly focused X-ray beams available at synchrontron beamlines and prolongs the lifes of crystal in the X-ray beam. To prevent crystals from damage and the formation of so-called ice-ring during the

diffraciton, cryo-protectants (such as Glycerol, MPD, glucose, PEG…) were used together with the reservoir solution. F-BAR, Ful 1, and SeMet-F-BAR crystals were cryo-protected by shortly soaking in their reservoir solution plus 20% glycerol and 15% polyethylene glycol 3350, then frozen directly in the cold N2 stream, which is called “flash cooling”; the Ful-2 crystal was cryo-protected by steadily increasing the polyethylene glycol 4000 concentration in the reservoir solution until approaching 40% and frozen in liquid N2. All X-ray diffraction data were collected at Berlin BESSY synchrotron (beamline 14.1) (Table 1). The crystal structure of F-BAR degraded from Syndapin 1/EHD1-(401-534) complex was determined to a resolution of 2.45 Å in the space group C2221. Full length syndapin 1 has two forms which were diffracted to a maximal resolution of 3.4 and 2.6 Å in the same space group C2221. For SeMet-F-BAR, three data sets (peak, inflection and remote) were collected as shown in Table 1. These data sets were used to solve phase problem of syndapin.

All the X-ray diffraction data were collected on CCD detectors. The diffraction data were measured using the rotation method by oscillating a small angle of crystal sample (0.3° was normally used in this work). The exposure time depends on the quality of crystals. Normally, increasing the exposure time improves the diffraction resolution. But it cannot use high exposure time, because it also increases backgroup noise.

Data from native syndapin 1 crystals were processed with XDS (Kabsch, 1993); data from the selenomethionine syndapin 1 crystal were indexed and integrated with Mosflm (Leslie, 2006) and Scala (1994). Data were analyzed and merged with XPREP (Bruker, Madison, WI). The data statistics are summarized in Table 1 (in Results Section).

3.5.3 Structure determination

The phase problem occurs when making a physical measurement in X-ray crystallography. Although the diffraction data of a crystal contains the structure factors magnitudes, the information of its phase has been lost during the diffraction process. In order to reconstruct the electron density map, the phase problem has to be solved. Various approaches have been developed over the years. They are direct

methods, Patterson function, molecular replacement (MR), multiple isomorphous replacement (MIR) and multiple anomalous dispersion (MAD).

Molecular replacement method is normally used to solve the phase problem when a homologue protein or homology domain has been previously determined. Normally, they should share at least 30% sequence identity and have less than 1 Å root mean squar deviation (r.m.s.d). Although the crystal structure of several BAR domains has been determined. Low sequence identity and the different BAR domain curvature, molecular replacement was not able to solve the phase problem of syndapin. MAD method by soaking crystals or co-crystallizing with heavy atom (like Mercury (II) acetate, Mercury (II) chloride, Uranyl nitrate and $NiCl_2$) was also used to solve the phase problem of syndapin. However, owing to low quality of data set, it failed to give a reasonable structural solution.

Multi-wavelength anomalous dispersion (also called Multi-wavelength anomalous diffraction) is another technique used in X-ray crystallography to solve the phase problem of biological macromolecules. The phase problem became possible to be solved if the structure contains more than one atom (including one atom) that causes significant anomalous scattering. The most common way is to replace methionine residues with selenomethionine in a protein by using selective medium during protein expression as described in section 3.3.1. The selenium atoms have a strong anomalous signal at different wavelengths X-rays generated at a synchrotron. By collecting data at several wavelengths near the absorption edge of the selenium atom in the crystal, phase information can be obtained. The structure of F-BAR domain was solved by multiwavelength anomalous dispersion method assisted by the selenomethionine-derived crystal. The selenium substructure was solved by SHELXD (Schneider and Sheldrick, 2002). Then, the phases were calculated, improved and extended to 2.9Å resolution by SHELXE (Sheldrick, 2008). Initial helical fragments were built automatically by Arp_Warp (Morris et al., 2004). Phases were further improved via NCS averaging implemented in DM and extended to 2.5Å using the native data. Subsequently, model building and refinement were carried out alternately. The full-length syndapin 1 structures were solved by molecular replacement using Phaser (McCoy et al., 2007). The refined F-BAR dimer/monomer

and the SH3 domain of 2DRK were used as searching models.

3.5.4 Model building and refinement

The model was gradually built and adjusted by hand using Xtalview (McRee, 1999), by fitting the model into the electron density map with the consideration of chemical geometry. Omit maps were used intensively to confirm the constructed parts. The selenium atoms were used to trace the polypeptide chain. Side chains lacking defined electron density were left on their geometric positions, provided the main chain was traced into well-defined electron density. Atomic positions, individual B factors, group TLS parameters, an overall anisotropic scaling factor and a bulk solvent model were refined using refmac5 (Murshudov et al., 1997) with tight geometric and B factor restraints to maximize the amplitude based likelihood function. TLS groups were either assigned by TLSMD web server (Painter and Merritt, 2006) or each chain arbitrarily assigned as one group. Rfree was used to monitor all refinement cycles.

Other CCP4 programs were heavily used in the crystallographic calculations (1994).The geometry of the final models was validated by PROCHECK (Laskowski et al., 1993). Analysis of the domain interfaces was performed with PISA web server (Krissinel and Henrick, 2007). Structure figures were made with Pymol (DeLano Scientific, Palo Alto, CA). Coordinates and structure factors were deposited in the Protein Data Bank with accession number 2x3v for the structure of the F-BAR domain, 2x3w and 2x3x for the structures of full-length syndapin 1.

3.6 Tubulation assay *in vitro*

3.6.1 Liposome preparation

To prepare 1 mg/ml liposome sample for electrom microscopy analysis of protein-lipid tubes, a stock solution of 1,2-Dioleoyl-sn-Glycero-3-[Phospho-L-Serine] (PS; Avanti Polar Lipids cat. # 840035) was mixed (w/v) with 100µl of chloroform and 30µl of methanol in a glass vials, dried in glass tubes using Ar gas using slow-flow Nitrogen (0.1 units) to produce a film on the glass and incubated in a vacuum desiccator overnight. The mixture of lipid was rehydrated in PBS (pH 7.2) at

room temperature for 5 minutes and gently agitated occasionally. Liposomes were extruded through 0.4 μm polycarbonate filters using a mini lipid extruder (Avanti Polar Lipids). The liposome was push 3-11 times through the filter and deposited into a buffer-rinsed glass vial.

3.6.2 Electron microscopy analysis of protein-lipid tubes

Proteins were added at a concentration of 0.1 mg/ ml to liposomes and the protein-lipid solution was incubated for 90 min at room temperature. For the EM analysis carbon-coated copper mesh grids (200 mesh, EMS) were put on droplets of protein-lipid solution for 1 min before negative staining in 1% uranyl acetate. Protein-lipid tube structures were observed and photographed at 80 kV in a Tecnai 12 electron microscope. NIH Image J software was used to quantify the length of protein-lipid tubes. Two-sided Student's t-test was used to compare the means.

3.6.3 Liposome sedimentation assay

Proteins were spun down separately before mixing with liposomes to remove aggregates prior to mixing with lipids. Protein-lipid samples (prepared as described above) were centrifuged at 200,000 x*g* for 1 h at room temperature in an ultracentrifuge (Beckman) or in an Airfuge® ultracentrifuge (Beckman) at top speed for 60 min at room temperature. Supernatant was removed and mixed 1:1 in sample buffer (200 mM Tris-HCl, 4 % SDS, 16 % glycerol, 0.01 % Bromophenol blue, pH 6.8). Pellets were resuspended in 2x sample buffer. Samples were boiled, analyzed by SDS-PAGE and stained with Coomassie blue. Protein band intensities were quantified using Adobe Photoshop CS3 software.

4 Results

4.1 Syndapin 1-F-BAR but not full-length syndapin 1 forms membrane tubules in living cells

As mentioned before, syndapin 1 is comprised of an N-terminal F-BAR linked to a C-terminal dynamin-binding SH3 domain via a long flexible tether containing two NPF motifs (Figure 4-1A). Similar to other BAR family proteins, such as endophilin, amphiphysin, CIP4 and FBP17, the N-terminal F-BAR domain of syndapins is required for self-association and for the stabilization of curved membrane domains (Halbach et al., 2007; Itoh et al., 2005; Kessels and Qualmann, 2006). As shown in Figure 1-11, numerous membrane tubules were generated upon overexpression of BAR/F-BAR domain or BAR/F-BAR domain containing proteins in Cos 7 cells. To analyze its potential membrane-tubulating activity full-length mouse syndapin 1 fused to eGFP was expressed in Cos7 cells and imaged by live cell spinning disc confocal microscopy. Surprisingly, syndapin 1-eGFP displayed a largely cytoplasmic distribution with some enrichment at peripheral plasmalemmal ruffles but no syndapin 1-coated membrane tubules or vesicles were observed (Figure 4-1B and D). By contrast, expression of syndapin 1-F-BAR-eGFP, a truncation mutant lacking the C-terminal linker-SH3 domain, produced numerous membrane tubules from internal mostly perinuclear membranes (Figure 4-1C and E) with an average diameter of about 73 ± 10 nm (Figure 4-1E) which was determined by analysis of Cos7 cells overexpressing syndapin 1-F-BAR-eGFP using electron microscopy. To determine the origin of these membrane tubules, the fluorescence-labeled transferrin (Tf) internalization assay was used. Interestingly, most of these tubules were accessible to internalized transferrin-Alexa568 (Figure 4-2), suggesting that they were of endosomal origin. Besides membrane tubules, overexpression of syndapin 1-F-BAR-eGFP also induced membrane protrusions (Figure 4-3). These were not seen in cells overexpressing full-length syndapin (Figure 4-1B).

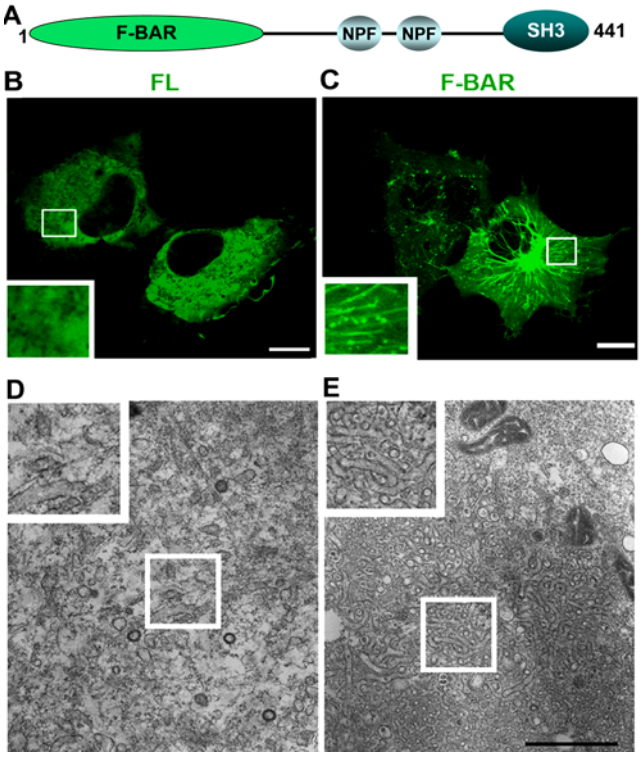

Figure 4-1 Syndapin 1-F-BAR but not full-length syndapin 1 forms membrane tubules in living cells. (A) Schematic representation of the domain organization of syndapin 1. **(B, C)** Expression of full-length eGFP-syndapin 1 did not cause membrane tubulation where membrane tubules generated by expression of eGFP-syndapin 1 F-BAR domain. Scale bars, 10 µm. **(D, E)** Representative electron micrographs of Cos7 cells expressing full-length eGFP-syndapin 1 **(D)** or eGFP-syndapin 1 F-BAR **(E)**. Note the presence of numerous F-BAR-induced membrane tubules with an average diameter of about 73 ± 10 nm in **D**. (Scale bar, 0.5 µm). The diameter of membrane tubules was calculated by Image Tool software. More than 10 membrane tubules were selected for each image. The experiment **D** & **E** were carried out by Dr. Dmytro Puchkov.

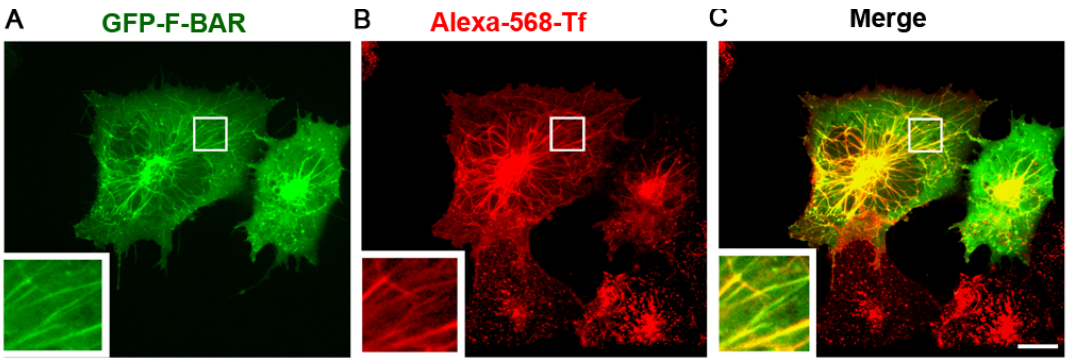

Figure 4-2 eGFP-syndapin 1-F-BAR induced membrane tubules contain internalized transferrin. (A-C) eGFP-syndapin 1-F-BAR-expressing Cos7 cells **(A)** were allowed to internalize Alexa568-labeled transferrin (Tf) for 10 min at 37°C. Internalized Alexa568-Tf **(B)** co-localized with F-BAR-induced eGFP-positive tubules **(C)**. Representative images are shown.

Scale bar, 10μm.

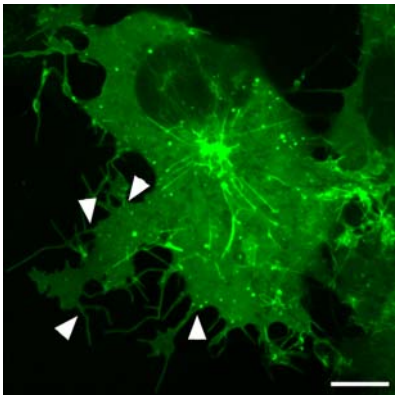

Figure 4-3 Membrane protrusions were formed by overexpression of syndapin 1-F-BAR in living Cos7 cells. Membrane protrusions in two Cos7 cells are indicated by arrow. Scale bars, 10 μm**.**

All these data show that syndapin 1 harbors a potent membrane tubulating activity within its F-BAR domain that is suppressed in the full-length protein. The reason could be posttranslational modification, or the fusion of GFP tag. As shown in Figure 1-18, syndapin not only can interact with other proteins but also can be homo-oligomerized, so the membrane tubulating activity of syndapin could be also inhibited by self-association or interaction with other proteins. Given that syndapin contains phosphorylation sites for protein kinase C and casein kinase 2 (Plomann et al., 1998), the membrane tubulating activity of syndapin could be also regulated by phosphorylation/dephosphorylation. The crystal structure of syndapin may provide some clues to explain the reason why the membrane tubulating actvitity of syndapin is blocked.

4.2 Protein expression and purification

In order to investigate the molecular basis of syndapin 1 F-BAR domain mediated membrane tubulation, we aimed at solve the crystal structure of syndapin 1-F-BAR and full-length syndapin 1. For this purpose, syndapin 1 full-length and syndapin 1-(1-337) cDNAs were inserted into the pET28 (+) vector which carries a His_{x6}-tag for affinity purification and a thrombin cleavage sites after the His_{x6}-tag. As described in Material and Methods section, plasmids encoding syndapin 1 full-length and syndapin 1-(1-337) cDNAs were transformed into *E. coli* BL21 competent cells. Expression of His_{x6}-tag fusion proteins were induced by IPTG at 28°C, overnight. As

shown in Figure 4-4, soluble syndapin 1 or syndapin 1-(1-337) was detected in the supernatant. The supernatant was loaded onto a Ni-NTA column and extensively washed with buffer containing 15mM imidazole. After elution, fractions were concentrated and applied to a gel filtration column for further purification. Peak fractions for syndapin 1 and SeMet-synd 1(1-337) are shown in Figure 4-5. The purity was analysed by SDS-PAGE. Routinely, 10 mg protein was recovered after gel flitration purification from 1 L expressed bacterial culture.

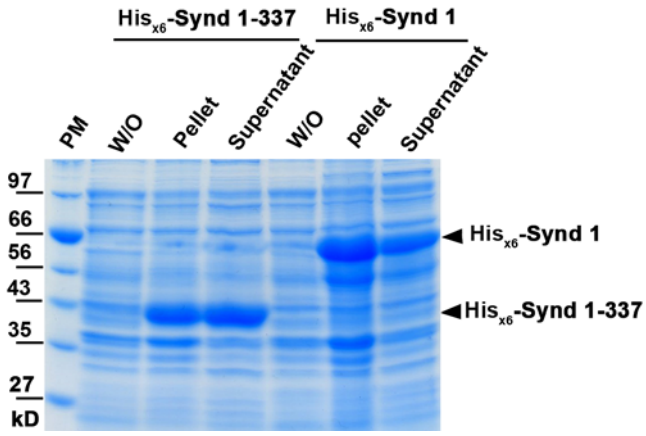

Figure 4-4 Expression of His$_{x6}$-syndapin 1 and syndapin 1-(1-337). PM: protein marker; W/O: without IPTG induction. 50 µl overnight culture was spun down and lysed, 20µl lysed sample was taken and centrifuged. Both supernatant and pellet were supplied with 20µl 2x SDS-PAGE loading buffer, respectively. 100 µl overnight cluture (W/O) was used as contol. Molecular weight is indicated by protein marker bands. Expressed His$_{x6}$-tagged fusion proteins are indicated. Synd 1-337 is syndapin 1-(1-337).

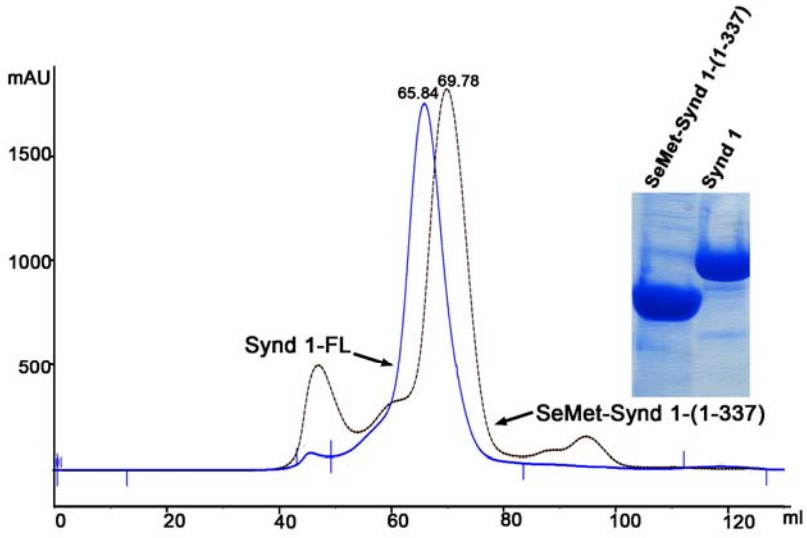

Figure 4-5 Protein purification by gel filtration. Concentrated Synd 1 or SeMet-Synd 1-(1-337)

purified by Ni-NTA column was loaded onto a Sephadex 200 size-exclusion column. The peak elution volume for Synd 1-FL (blue curve) or SeMet-Synd 1-(1-337) (brown curve) was indicated. The purity was analysed by SDS-PAGE Gel (Insert). Synd 1 is full-length syndapin 1, while SeMet-Synd 1 is selenomethionine-syndapin 1.

4.3 Protein crystallization and structure determination

More details are described in Material and Methods section for crystallization of syndapin 1, syndapin/EHD1(401-534) complex and SeMet-Syndapin 1-F-BAR. Crystals of syndapin 1 full-length were obtained from the solution by mixing 2µl protein solution with an equal volume of reservoir solution containing 100 mM Na-acetate (pH 5.0), 3-5% (w/v) polyethylene glycol 4000 and 10 mM glycyl-glycyl-glycine (from additive screen) (Figure 4-6A). In an attempt to crystallize a syndapin/EHD1(401-534) complex, Syndapin 1 was mixed with EHD1 at a molar ratio of 1:2. Crystals appeared after one month in drops consisting of 2 µl of the protein complex solution and 2 µl reservoir solution containing 100 mM sodium citrate (pH 5.5), 10% (w/v) Polyethylene Glycol 4000 and 200 mM Na-acetate (pH 5.0). Unexpectedly, the crystals only contained the F-BAR domain of syndapin 1 due to protein degradation, which has the same space group with similar parameters of the cell unit as SeMet-F-BAR (F-BAR, Table 1). The degraed band (labelled crystal) was shown in Figure 4-7. SeMet-syndapin 1-(1-337) crystals were obtained from crystallization drops containing 2 µl SeMet-syndapin -(1-337) mixed with 2 µl reservoir solution 100 mM sodium citrate (pH 5.5), 10% (w/v) polyethylene glycol-3350 (SeMet-F-BAR, Table 1). The crystal structure of F-BAR was determined to a resolution of 2.45 Å in the space group C2221 (a=85.06 Å, b=153.49 Å, c=212.29 Å) (Figure 4-6B). Full length syndapin 1 has two forms which were diffracted to a maximal resolution of 3.4 and 2.6 Å in the space group C2221 (Ful-1: a=83.08 Å, b=154.54 Å, c=255.81 Å; Ful-2: a=88.28 Å, b=154.61 Å, c=191.74 Å), respectively (Table 1). Crystal structures were solved using the multiwavelength anomalous diffraction (MAD) method (Table 1). The data for MAD was colletcted on a crystal grown from selenomethionine-derivatized protein. SeMet-F-BAR has the same space group as F-BAR with cell dimension a=85.4 Å, b=153.5 Å, c=215.3 Å. After SHELXD processing, the phaser density map was obtained and positions of selenomethionine were indicated in Figure 4-8. The SeMet-F-BAR model was built according to amino acid sequence and fit into the

electron density map. The full-length syndapin 1 structures were solved by molecular replacement using the crystal structure of SeMet-F-BAR as a searching model. Coordinates and structure factors were deposited in the Protein Data Bank with accession number 2x3v for the structure of the F-BAR domain, 2x3w and 2x3x for the structures of full-length syndapin 1, respectively.

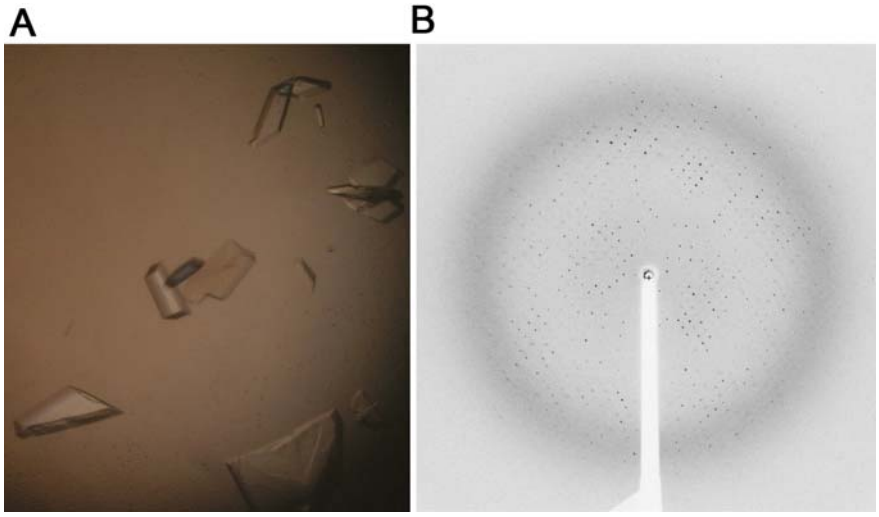

Figure 4-6 Representation of syndapin 1 full-length crystals and diffraction map of syndapin 1-F-BAR. (A) Crystal of full-length syndapin 1. **(B)** Diffraction map of syndapin 1-F-BAR.

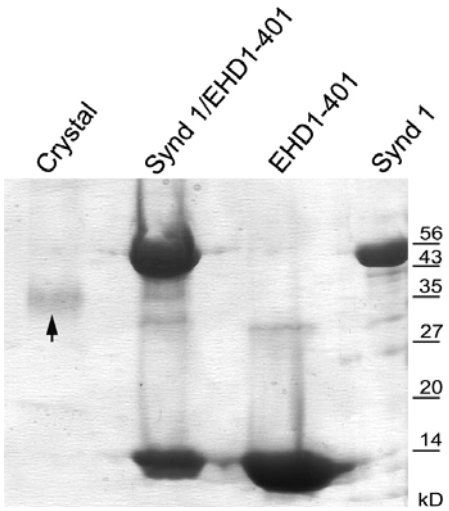

Figure 4-7 Syndapin 1 was degraded as an attempt to crystallize Synd 1/EHD1-401 complex. The crystals were washed three times with reservoir solution (50µl) and dissolved in 1x SDS-PAGE sample buffer. Synd 1: purified syndapin 1; EHD1-401: purified EHD 1-(401- 534); Synd 1/EHD 1-401: syndapin 1/EHD 1-(401-534) mixture. The molecular weight is indicated. The arrow indicates the band of crystals of the degraded syndapin 1 from the mixture of syndapin 1/EHD 1-(401-534). Samples were analyzed by SDS-PAGE and staining with Coomassie blue.

Table 1 Data Collection, Phasing, and Refinement Statistics

Crystals	F-BAR[1]	Ful-1	Ful-2	SeMet-F-BAR		
				peak	inflection	remote
X-ray diffraction data						
X-ray source	BL14.1/BESSY, BERLIN					
Wavelength (Å)	0.9780	0.9184	0.9184	0.9797	0.9799	0.9184
Space group	C2221	C2221	C2221	C2221		
Resolution limits (Å)	76.75-2.45 (2.55-2.45)	73.17-3.35 (3.45-3.35)	34.35-2.64 (2.75-2.64)	74.80-2.90 (3.00-2.90)		
Unique reflections	50261	23772	38766	31367	31299	31148
Completeness (%)	97.2 (81.8)	98.3 (99.1)	99.7 (99.1)	99.0 (98.9)	98.4 (96.7)	97.2 (96.5)
Mean I/σ(I)	16.35 (1.84)	14.97 (2.62)	10.81 (2.88)	12.22 (2.94)	12.90 (2.84)	13.34 (2.96)
multiplicity	6.69 (3.96)	6.11 (6.16)	7.17 (7.03)	5.96 (5.92)	5.92 (5.73)	5.61 (5.41)
R_{int}(%)[2]	8.13 (83.90)	12.26 (85.94)	12.85 (68.88)	14.28 (52.16)	13.15 (57.88)	12.05 (51.79)
R_{sigma}(%)[3]	4.52 (66.0)	6.07 (35.50)	6.60 (32.30)	6.93 (39.34)	6.55 (40.96)	6.36 (39.84)
Refinement						
Resolution range (Å)	5-2.45	73.13-3.35	34.36-2.64			
R_{work}/R_{free} (%)[4]	21.2/26.0	22.1/27.7	22.1/27.4			
modeled chain:residues	A: 14-304 B: 13-304 C: 14-304	A:14-304 B:13-169,188-304 C:14-304 D[5]:385-440 E[5]:385-440	A:14-304 B:13-302 C:14-165, 193-301 D[5]:385-440			
non-H atoms(protein/water)	7261/156	8006/0	7449/62			
r.m.s. deviations: Bonds (Å)/ angles(°)	0.007/0.929	0.007/0.972	0.006/0.850			
Ramachandran analysis Favored/allowed/outliers (%)	96.5/3.5/0	90.2/9.8/0	92.8/7.2/0			

1. F-BAR domain crystallized from degraded full-length syndapin.

2. $R_{int} = \Sigma||F_o|^2 - |F_o|^2 \text{ (mean)}|/\Sigma|F_o|^2$. $|F_o|^2$ are intensities of reflections in unmerged data. $|F_o|^2$ (Mean) is the mean intensity for symmetric mates, including Friedel pairs.

3. $R_{sigma} = \Sigma[\sigma(|F_o|^2)]/\Sigma[|F_o|^2]$. $|F_o|^2$ are intensities of reflections in the unique data.

4. $R = \Sigma||F_o| - |F_c||/\Sigma|F_o|$. $|F_o|$ are the amplitudes of the structure factors. R_{work} is the *R* value for reflections used in refinement, while R_{free} is the *R* value for 5% of the reflections which are selected in thin shells and not included in refinement.

5. D or E refers to SH3 domain, which should be assigned with the same ID of its relevant F-BAR domain, *i.e.* A, B or C. However, lacking electron density for the 80aa linker region between the F-BAR and SH3 domains made either assignment uncertain, so different chain IDs were assigned.

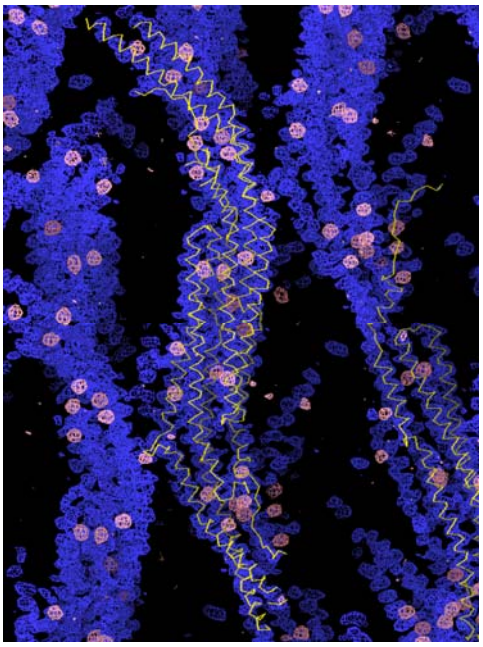

Figure 4-8 Electron density map of SeMet-F-BAR after SHELXD processing. The electron density map is colorated in blue. Positions of Selenomethionine are indicated in light-pink density. The main chain model is fitted into the electron density map with orange color.

4.4 Overall crystal structure of syndapin I F-BAR

Three F-BAR monomers sit in one crystal asymmetric unit: Two monomers dimerize into an elongated "S" shape with local twofold symmetry (Figure 4-9), while the third forms a dimer with its crystal symmetry-related mate. Each monomer consists of four long helices, α1 to α4, and a short C-terminal helix α5 following an extended proline-rich coil (Figure 4-9A and D). The head-to-head dimerization of F-BAR domains results in a six-helical bundle consisting of α1, α2, and the N-terminal part of α4 from each monomer and a buried solvent-accessible area of about 4,600 $Å^2$, indicating a stable dimer in solution. A coiled-coil consisting of α3 and the C-terminal part of α4 of each monomer bends to the same side and thus gives the dimer a crescent shape. A striking feature is the charge distribution on the dimer surface: On the concave face, lysines (e.g., K127, K130, K145, K146, K148, K205, and K208) form a continuous positively charged belt (Figure 4-9F) which is necessary for membrane binding, whereas the convex and side surfaces are

negatively charged. The characteristics in scaffold organization and charge distribution are shared with other BAR proteins.

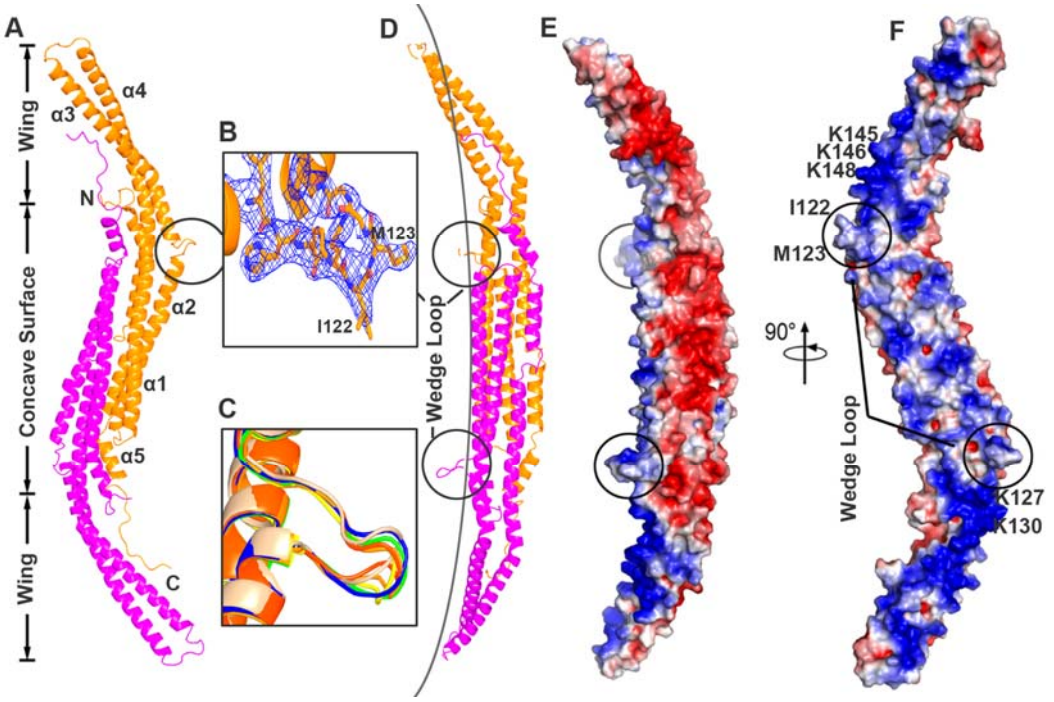

Figure 4-9 Structure of the syndapin 1 F-BAR domain. (A) Secondary-structure representation of the syndapin 1 F-BAR domain. Protein coloration: orange, monomer A; magenta, monomer B. N- and C-terminal ends, the secondary-structure assignment (α1:22–71, α2:74–118, α3:127–177, α4:181–275, and α5:277–289), and the wedge loop protruding from the long helical region are labeled only on chain A. **(B)** σA-weighted |fo|−|fc| omit map (contoured at 2σ level) around the wedge loop. **(C)** Superposition of 7 monomer structures (using different colors) indicates the rigidity of the wedge loop. **(D)** F-BAR structure is viewed from the other side. **(E, F)** The protein surface is colored according to electric potential: red (negative) through white (neutral) to blue (positive). Residues mutated in the functional study are labeled. The wedge loop is indicated by a black circle

4.5 Distinct features of the F-BAR domain of syndapin

Compared with other determined crystal structures of F-BAR domain, an interesting feature in syndapin is that a wedge loop consisting of ^{119}HKQIMGGF^{126}, with hydrophobic residues (I122-M123) at the tip (Figure 4-9B, C, D and E), protrudes about 12 Å from the area joining α2 and α3. These two helices compose an uninterrupted long helix in other BAR proteins. This wedge loop distinguishes syndapin 1 from known N-BAR and F-BAR proteins. Superposing monomers available from different crystal-packing environments reveals the rigidity of the

wedge loop (Figure 4-9C), namely the overall shape and the relative orientation to the helical bundle. Two wedges, with a tip-to-tip distance of about 83 Å in the dimer, are located on the borders of the positively charged concave face and are adjacent to positively charged, conserved residues (e.g., K127 and K130). This suggests a concerted function of the wedge loop with the charged surface in membrane bending. The importance of the wedge loop and the adjacent charged surface for the membrane-tubulating activity of eGFP-F-BAR was confirmed by expression of site-directed mutants in Cos7 cells. Replacing the hydrophobic amino acids I122 and M123 within the wedge loop (Figure 4-9B) by hydrophilic residues (I122T/M123Q) completely eliminated tubule formation in cells (Figure 4-10B and E), although this mutation did not alter membrane phospholipid binding. Interestingly, if residues I122 and M123 were mutated to a bulkier hydrophobic phenylalanine, the number of tubules per cell was significantly increased (Figure 4-10A and E). Additionally, the replacement of either of two basic patches (K127E/K130E or K145E/K146E/K148E) within the positively charged belt on F-BAR eliminated membrane tubulation (Figure 4-10C and D). These data are in agreement with the structural analysis and confirm the critical role of the positively charged belt and the amphipathic wedge loop in driving syndapin 1 F-BAR-mediated membrane bending.

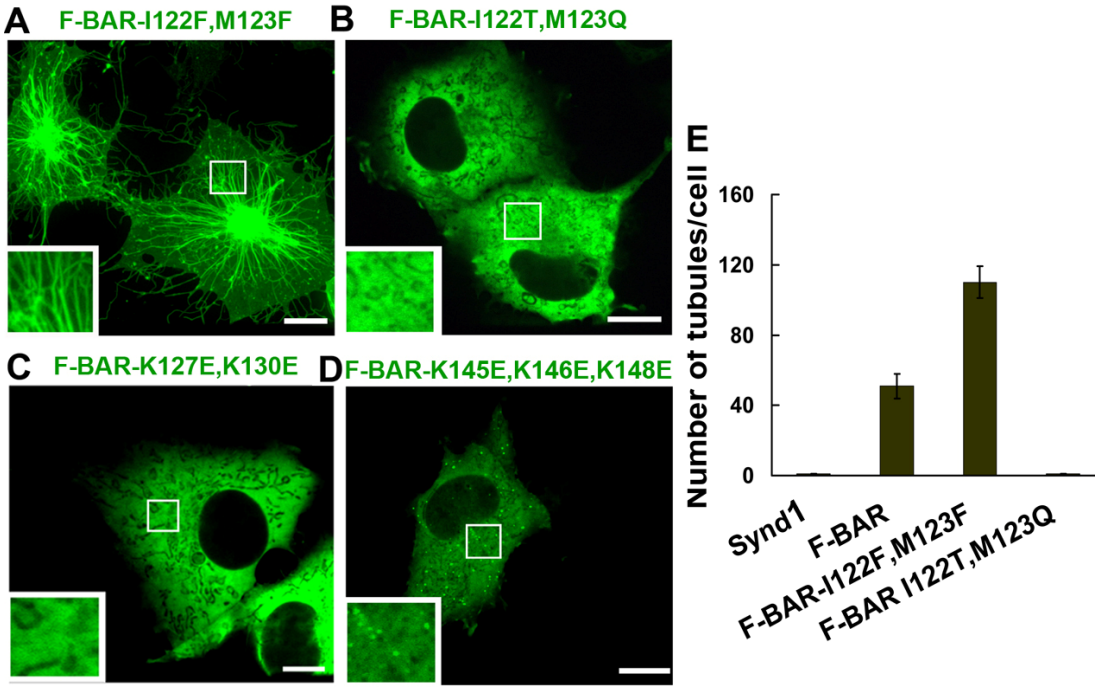

Figure 4-10 The wedge loop and positively charged residues are important for the membrane tubulating activity of syndapin 1-F-BAR domain. (A-D) Live-cell spinning-disk

confocal micrography of Cos7 cells expressing eGFP-syndapin 1-F-BAR mutants. **(A)** Membrane tubules induced by expression of eGFP-syndapin 1 F-BAR -I122F/M123F. Mutational inactivation of the amphipathic wedge loop I122T/M123Q **(B)** or the basic belt (K127E/K130E) **(C)** and (K145E/K146E/K148E) **(D)** eliminated the tubulating activity. Representative images from at least three independent experiments are shown. Scale bars, 10 µm. **(E)** Quantification of the number of eGFP-positive tubules in Cos7 cells expressing syndapin 1 variants. Given are the mean number of tubules (±SE) per cell (n = 3 for each syndapin 1 variant) averaged for at least 20 cells.

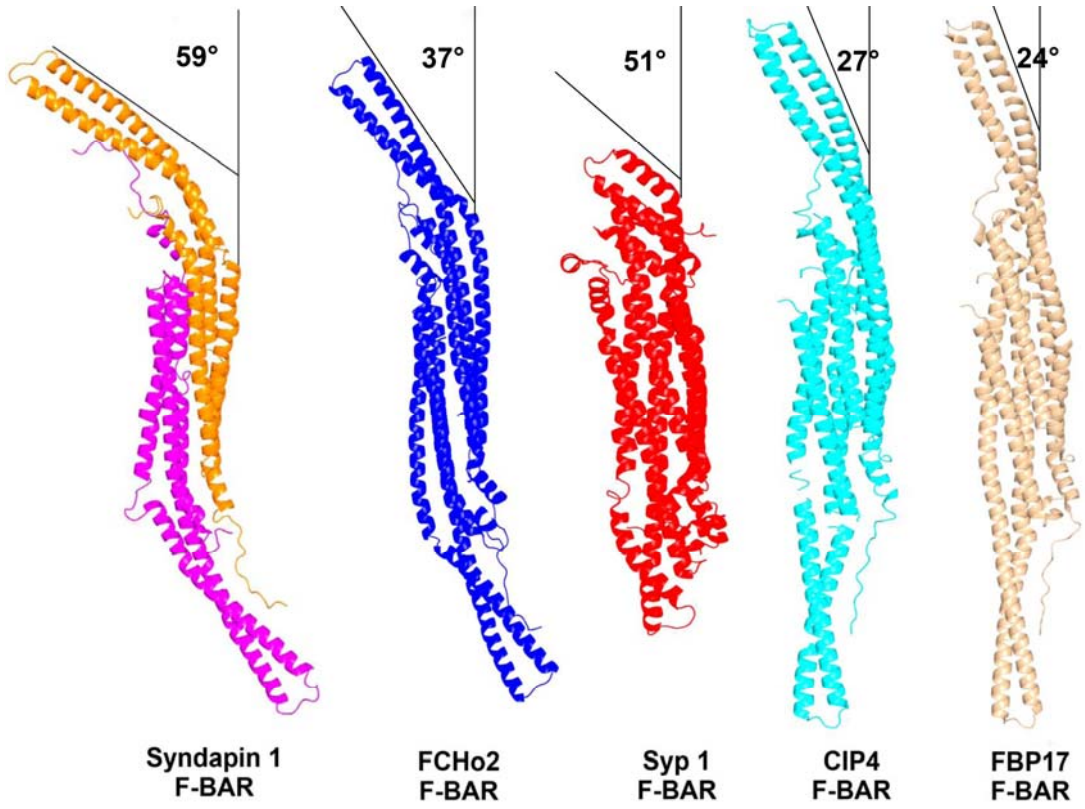

Figure 4-11 Comparison of F-BAR domains. The structures of F-BAR domain dimers from syndapin 1, FCHO2, Syp 1, CIP4, and FBP17 are shown. Protein coloration: Syndapin 1 F-BAR as Figure 4-7; FCHO2 F-BAR: blue; Syp 1 F-BAR: red; CIP4 F-BAR: cyan; FBP17 F-BAR: tint. The degree of "wing" bending was quantified by determining the angle between the long axis of the central 6-helix bundle (concave surface) and the long axis of the helical "wing" region. The degree for each F-BAR domain is indicated.

Another striking feature of syndapin 1-F-BAR is a highly kinked lateral "wing" relative to the central dimerization region in syndapin. F-BAR domains of CIP4 and FBP17 are rather straight and FCHO2 F-BAR has an only moderately kinked "wing" (Figure 4-11) (Frost et al., 2008; Henne et al., 2007; Shimada et al., 2007). Although

the F-BAR domain of Syp1 displays high curvature of the wing region, this “wing” region is very short. The “wing” region of syndapin 1-F-BAR is bent away from its central body in a ~59° angle which generates a pronounced twisted S-shape in the dimeric molecule (Figure 4-11). The concave surface of syndapin 1-F-BAR is less curved. To interact and satisfy membrane binding, the extreme degree of lateral wing kinking may help syndapins to bind and stabilize membranes with higher curvature or vesicular structure.

4.6 Crystal structure of full-length syndapin 1 reveals an F-BAR-SH3 clamp

Our own cell-based experiments (Figure 4-1) together with recent data using purified syndapin incubated with liposomes (Wang et al., 2009a) suggested that the membrane-tubulating activity of the F-BAR domain is autoinihibited by the SH3 domain. However, the molecular basis for this behavior is still unknown. To unravel the structural basis of autoinhibition, we solved the structure of full-length syndapin 1 by protein x-ray crystallography (Figure 4-12). We obtained two distinct crystal forms of full-length syndapin 1 (Ful-1, Ful-2) with different unit cell dimensions (Table 1), as confirmed by SDS/PAGE and mass spectrometry. Both Ful-1 and Ful-2 crystals contain one dimer and one monomer of the F-BAR domain in the asymmetric unit, similar to the crystals of the isolated F-BAR domain. In addition, we found extra electron density to fit SH3 domains (385–440). These SH3 domains adopt a conventional β-barrel fold, with the prototype C-terminal β-strand retrograding to an extended coil (Figure 4-12A and B). The RT-src loop and the N-src loop flank the putative PxxP-binding groove with conserved residues such as P434, W420, and Y393 in syndapin 1 lying at the bottom. In none of the full-length molecules was the linker connecting the F-BAR and SH3 domains visible, suggesting a high degree of flexibility in this region, in agreement with secondary-structure predictions. Surprisingly, electron density was found for only two SH3 domains in Ful-1 and a single SH3 domain in Ful-2, indicating that physiological interactions can be interrupted by crystal-packing forces. Due to the long invisible linker, it was not possible to assign the SH3 domains to one of the F-BAR domains.

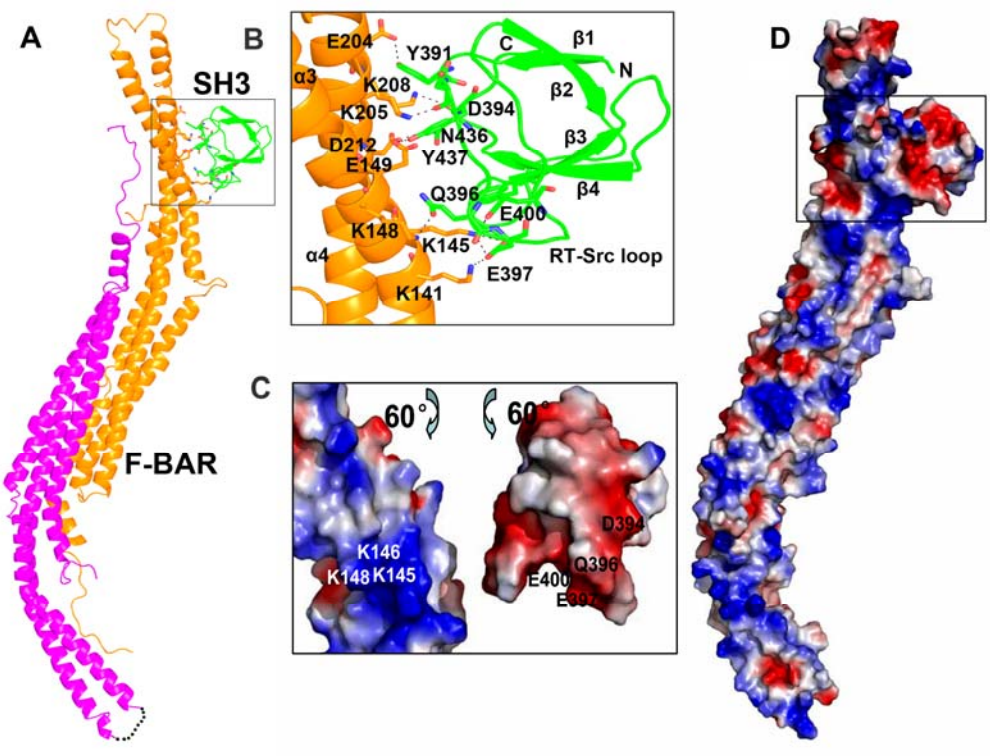

Figure 4-12 Structure of full-length syndapin 1. (A) Secondary-structure representation of syndapin 1. Protein coloration: orange, monomer A; magenta, monomer B; green, the SH3 domain. The SH3 domain may be associated with either chain A or chain B of the F-BAR domain, but the lacking electron density for the tether disallows a definite chain assignment. A second SH3 domain found in the asymmetric unit which interacts with the F-BAR domain in an irrelevant manner is not shown in the model. N and C termini, the secondary-structure assignment, and the wedge loop protruding from the long helical region are labeled only on monomer A. The undetermined loop in F-BAR is indicated by a dashed line. **(B)** Close-up view of the interface of the SH3 and F-BAR domains. β-Strands of the SH3 domain are labeled. Residues involved in the interaction are shown as a stick model. Polar contacts are presented as black dashed lines. **(C, D)** The protein surface is colored according to the electrostatic potential: red (negative) through white (neutral) to blue (positive). The lower panel shows an open-up view of the surface charge distribution between F-BAR and SH3. Residues mutated in functional studies are labeled.

To identify possible physiological interactions between the F-BAR and SH3 domains, the packing of the SH3 domains against the F-BAR domain in the crystal was analyzed. Previous low-resolution data suggested that the SH3 domains of endophilin (Wang et al., 2008) and syndapin (Wang et al., 2009a) are placed at or near their respective BAR domains, although the precise position could not be determined. Such an interaction was also found in our crystals (Ful-1), where the

SH3 domain with its putative PxxP-binding groove contacts the positively charged concave face at the tip of the F-BAR domain (Figure 4-12A and B), with a small buried solvent-accessible area of 460 $Å^2$. Interestingly, the charge distribution in the SH3 domain is also uneven: negatively charged at the side of the peptide-binding groove and positively charged at the opposite side. Thus, a clear charge complement exists within and near the interface (Figure 4-12C and D). Residues at the interface are mainly located in α3 and α4 of the F-BAR domain and the RT-src loop of the SH3 domain. They form an extended hydrogen-bonding and/or salt-bridge network (Figure 4-12B and Table 2), which is the major contributor to the interaction. In particular, K141, K145, and K148 from α3 of the F-BAR domain intensively interact with Q396, E397, and E400 in the RT-src loop of the SH3 domain. Indeed, ^{145}KKMK^{148} is a common basic motif found in several F-BAR and BAR domain proteins such as amphiphysin and endophilin (Figue 4-13). The interface also contains a small hydrophobic patch formed by aromatic side chains in the peptide-binding groove of the SH3 domain and by aliphatic side chains of the F-BAR domain. The F-BAR/SH3 interaction is mainly mediated by hydrogen bonds/salt bridges (Table 2), implying that the interaction is salt- and pH-sensitive. The small buried area indicates that the SH3 binds weakly to the F-BAR domain, which is consistent with the observation that SH3 domains generally associate with their binding partners with relatively low affinities (Jia et al., 2005). However, "complex" formation between the F-BAR and SH3 domains would be significant in solution due to the high local concentration of the two domains within the dimer.

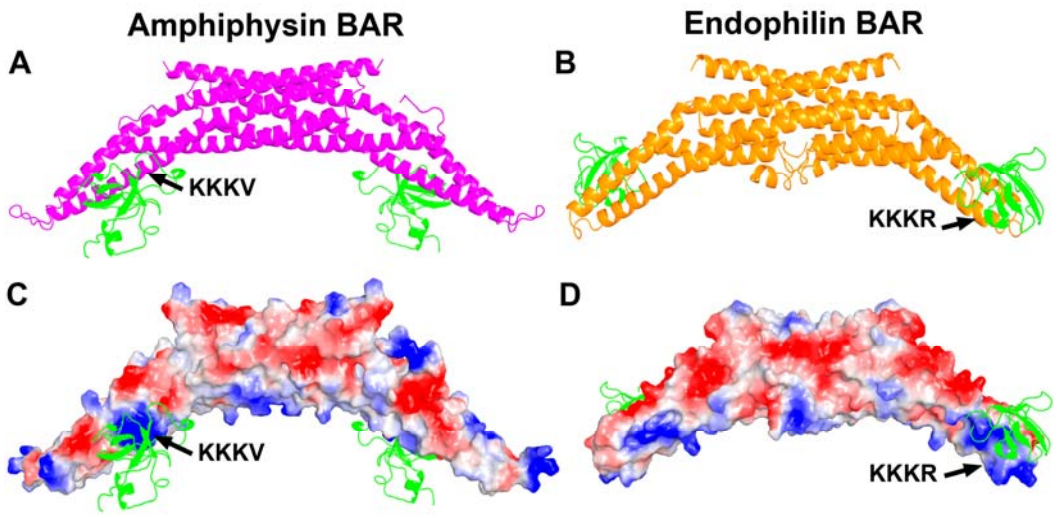

Figure 4-13 Structure models for endophilin and amphiphysin. (A) Secondary structural

representation of the amphiphysin 1 BAR domain, magenta; SH3 domain, green. The position of the KKKV motif is indicated. **(B)** Secondary structural representation of the endophilin 1 BAR domain, orange; SH3 domain, green. The position of the KKKR motif is indicated. **(C)** Surface charge of the BAR domain of amphiphysin 1. **(D)** Surface charge of the BAR domains of endophilin 1. Modeling was done by local structural alignment for the basic stretches common in F-BAR and BAR domains. As for amphiphysin 1, the BAR domain of PDB code 1URU was positioned by superposing the ^{132}KKKV^{135} motif onto ^{145}KKMK^{148} of the syndapin 1 F-BAR domain; the SH3 domain of PDB code 1BB9 was superposed to the syndapin 1 SH3 domain. As for endophilin 1, the BAR domain of PDB code 1X03 was positioned by superposing the ^{171}KKKR^{174} motif onto ^{145}KKMK^{148} of the syndapin F-BAR domain; the SH3 domain of PDB code 3C0C was superposed to the syndapin 1 SH3 domain

Table 2 Hydrogen bonds/salt bridges between SH3 and F-BAR domains

SH3 domain (Chain D)	Distance(Å)	F-BAR domain (Chain A)
Y391 [OH]	2.92	E204 [OE2]
D392 [O]	2.52	K205 [NZ]
Q396 [OE1]	2.94	K148 [NZ]
E397 [OE1]	2.88	K145 [NZ]
E397 [OE2]	2.93	K145 [NZ]
E397 [OE2]	3.14	K141 [NZ]
E400 [OE2]	2.79	K145 [NZ]
E400 [OE1]	3.52	K145 [NZ]
D436 [O]	2.88	K208 [NZ]
N436 [ND2]	3.09	D212 [OD1]
Y437 [OH]	3.09	E149 [OE1]

The interaction between the SH3 and F-BAR domains of syndapin 1 was confirmed by direct binding experiments using GST-linker-SH3 or GST-SH3 and His_6-F-BAR (Figure 4-14A). Replacement of K145, K146, and K148 from α3 of the F-BAR with glutamates completely abolished association with GST-SH3 (Figure 4-15A). Conversely, mutation of the charged/hydrophilic residues D394R/E400R or Q396R/E397R within the RT loop of the SH3 domain also significantly impaired association with the F-BAR domain (Figure 4-15B), thereby confirming the crystallographically determined interface. To test whether association between the SH3 and F-BAR domains affects membrane tubulation in cells, we cotransfected both domains *in trans* into Cos7 cells and analyzed these by live-cell spinning-disk confocal microscopy (Figure 4-16). Indeed, coexpression of wild-type (WT)

mCherry-tagged SH3 strongly impaired the ability of eGFP-F-BAR to generate membrane tubules, whereas SH3s carrying point mutations that interfere with F-BAR association were much less potent (Figure 4-16). All SH3-mCherry chimeras were expressed at identical levels (Figure 4-16K). Hence, the F-BAR and SH3 domains of syndapin 1 interact both in vitro and in living cells.

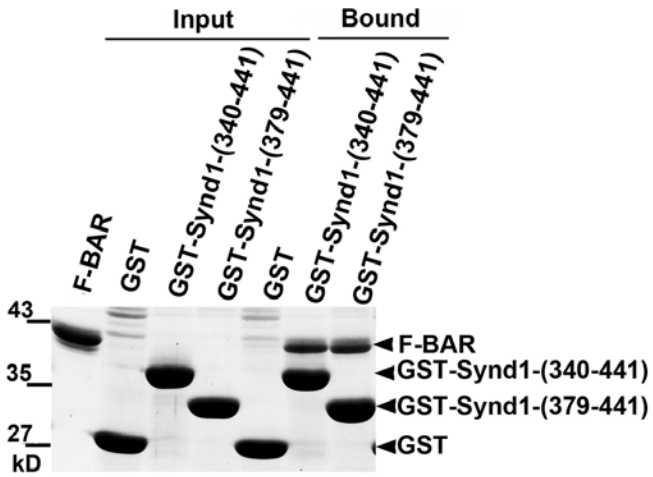

Figure 4-14 Syndapin 1 F-BAR binds to its SH3 domain. GST-syndapin 1 SH3 (379-441) or GST-syndapin 1-ΔF-BAR (340-441) bind to their F-BAR domain *in vitro*, whereas GST does not. Samples were analyzed by SDS-PAGE and staining with Coomassie blue. Input, 15 % of the total amount of purified F-BAR used for the binding assay.

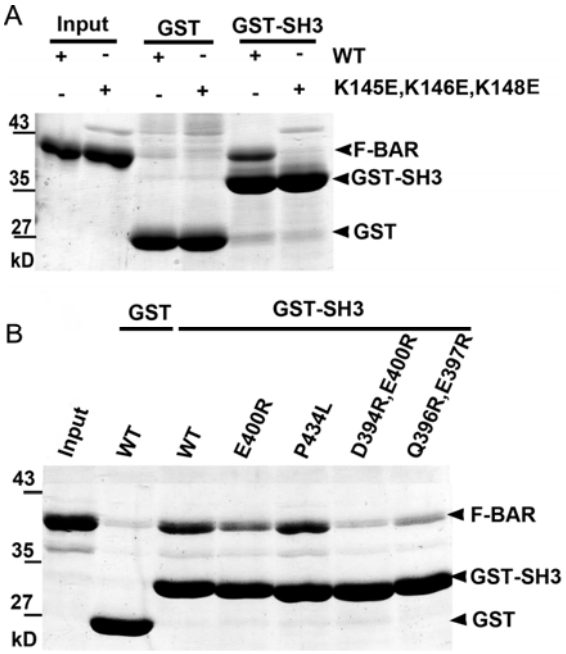

Figure 4-15 Biochemical characterization of F-BAR-SH3 interface. (A) Mutation of a basic patch on the F-BAR domain (K145E,K146E,K148E) eliminates the binding to SH3 domain. **(B)** Mutations within the SH3 domain (E400R,D394R,E400R) and (Q396R,E397R) selectively

impair binding to the F-BAR domain. By contrast, mutation of the proline-rich motif binding site on SH3 (P434L) does not affect F-BAR association. Binding assays were done as described in materials and methods. Samples were analyzed by SDS-PAGE and staining with Coomassie blue. Input, 15 % **(A)** or 10% **(B)** of the total amount of purified F-BAR used for the binding assay.

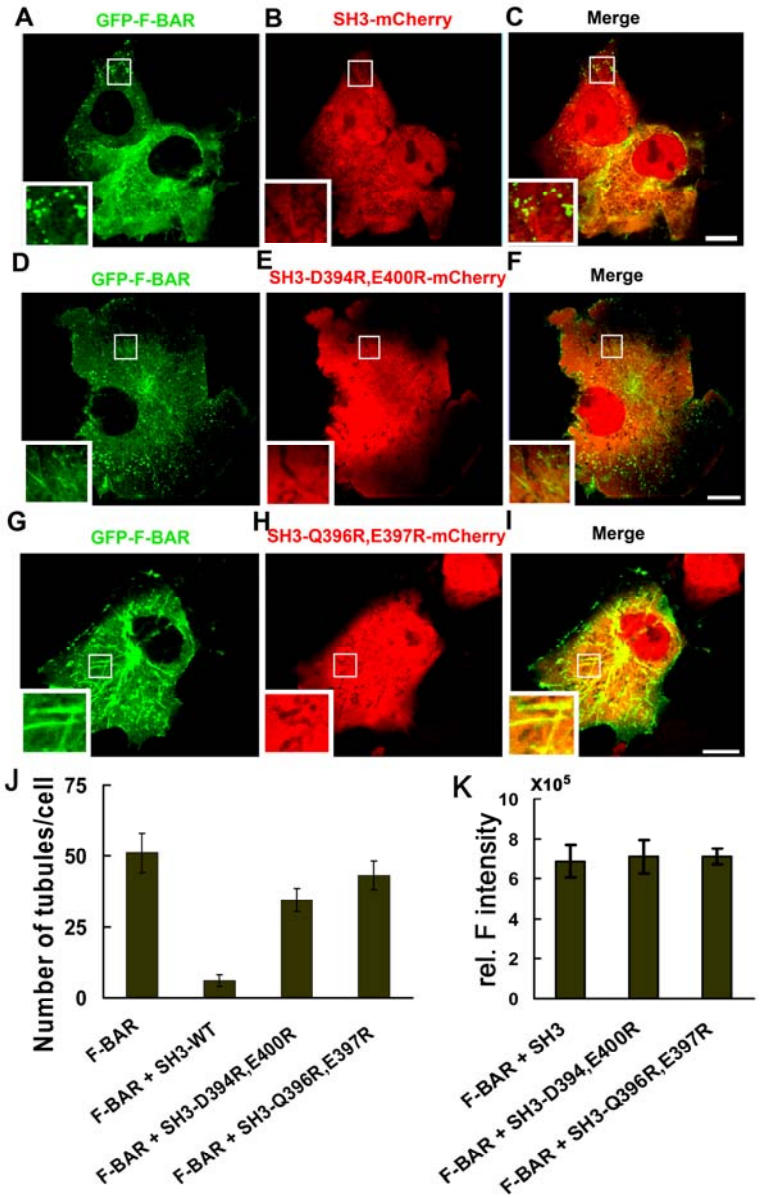

Figure 4-16 Co-expression of SH3-mCherry impairs syndapin 1-F-BAR-mediated tubule formation in living cells. Cos7 cells co-expressing eGFP-syndapin 1-F-BAR and SH3-mCherry or various mutants thereof were analyzed by live cell spinning disc confocal microscopy. Representative still images from at least three independent experiments are shown. F-BAR-mediated membrane tubulation is blocked by coexpressed SH3 wild-type **(A-C)** but not by F-BAR binding-defective D394R/E400R **(D-F)** or Q396R/E397R mutants **(G-I)** Scale bar, 10µm. **(J)** Quantification of the number of tubules in Cos7 cells when co-expressing GFP-Syndapin 1-F-BAR with mCheery-SH3 WT and mutants. Given are the mean number of

tubules (±SE) per cell (*n* = 3 for each syndapin 1 variant) averaged for at least 20 cells. **(K)** SH3-mCherry fusion proteins are expressed at similar levels. Bars represent the mean SH3-mCherry fluorescence intensity per μm^2 (mean ± SD; n = 10).

Given that the F-BAR/SH3 interaction is mainly mediated by hydrogen bonds/salt bridges revealed by the crystal structure of full-length syndapin 1, the salt concentration should affect the syndapin 1 intramolecular interaction (it could also be intermolecular interaction). To answer this question, different salt concentrations were used *in vitro* binding experiments. The amount of F-BAR protein bound to the SH3 domain dramatically decreased when the salt concentration was increased from 50mM to 400mM NaCl (Figure 4-17A and C). At 200mM NaCl, the amount of protein bound to SH3 was hardly detectable. Since SH3 domains normally recognize the proline-rich motifs, we wanted to test whether the interaction between the SH3 domain and proline-rich proteins is also affected by salt. To test this, we performed affinity-chromatography experiments using purified dynamin 1-PRD, a fragment of dynamin 1 containing the GED and PH domain as well as a proline-rich segment at their C-terminus. As shown in Figure 4-17, dynamin 1-PRD bound to SH3 even at 400mM NaCl (Figure 4-17B and C), implying that the association with dynamin 1 or proteins with PRD domains may unlock the syndapin 1 F-BAR from the SH3 clamp. Under physiological conditions, the intracellular concentration of NaCl is about 150mM, suggesting that the syndapin 1 intramolecular interaction is weak, but potentially biologically significant.

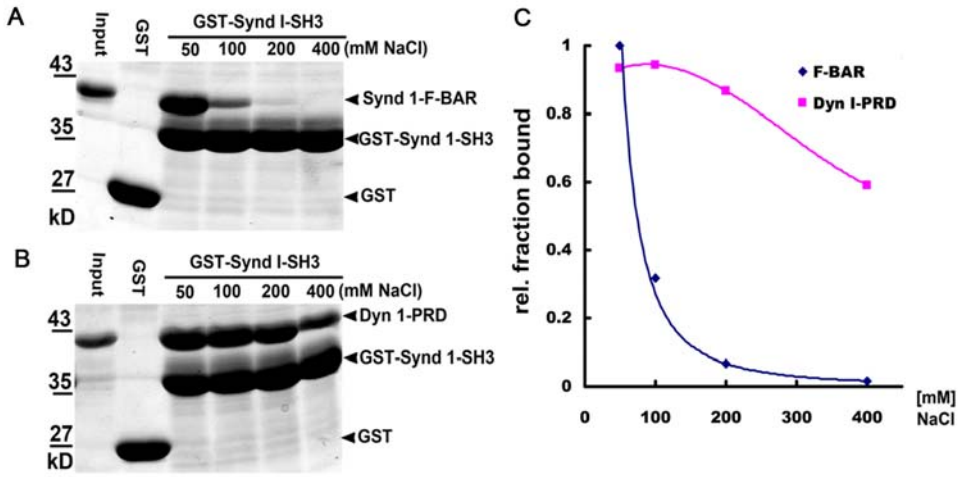

Figure 4-17 Complex formation between syndapin 1 F-BAR and SH3 is salt-sensitive. GST-syndapin 1 SH3 (379–441) or GST (as a negative control) were incubated with purified

F-BAR **(A)** or the proline-rich domain of dynamin 1 (PRD) **(B)** in the presence of the indicated concentrations of NaCl. The relative fraction of bound PRD or F-BAR is plotted as a function of salt concentration **(C)**. The amount of either protein specifically bound to GST-SH3 in the presence of 50 mM NaCl was set to 1.

To further assess the specificity of SH3-BAR/F-BAR domain interactions, we analyzed the behavior of the endocytic N-BAR-SH3 domain proteins endophilin 1 and amphiphysin 1. Molecular modeling suggests the existence of a basic patch on the N-BAR domains of endophilin 1 and amphiphysin 1 (Figure 4-13) that could serve as a docking site for SH3 domains, in agreement with recent low-resolution small-angle X-ray scattering data (Wang et al., 2008). To address this possibility, we performed affinity-chromatography experiments using endophilin 1 SH3 or amphiphysin 1 SH3 fused to GST and purified recombinant BAR domains. Both endophilin 1 SH3 (Figure 4-18A) and amphiphysin 1 SH3 (Figure 4-18B) bound to their corresponding BAR domains. Interactions between BAR and SH3 domains were also specific to some degree. When offered to different endocytic SH3 domains, syndapin 1 F-BAR preferentially associated with its own SH3 domain, whereas weaker interactions were observed between syndapin 1 F-BAR and amphiphysin 1 SH3 and endophilin 1 SH3 (Figure 4-18C).

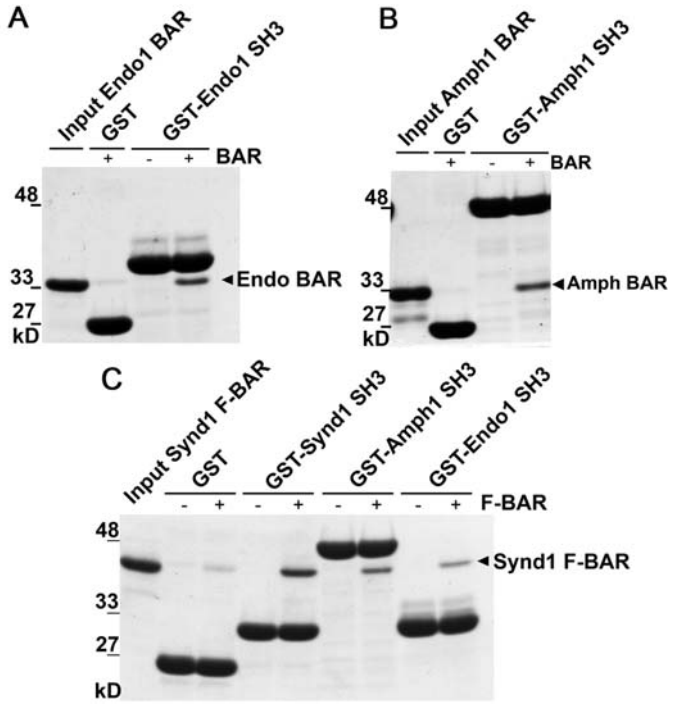

Figure 4-18 The interaction between BAR domain and SH3 domain. *In vitro* binding assays, GST or GST-SH3 fusion proteins were immobilized on glutathione beads and incubated with

purified His_6-tagged endophilin 1-BAR **(A)**, amphiphysin 1-BAR **(B)**, or syndapin 1-F-BAR **(C)** domains. Input, 5 % (A, B) or 3.5 % (C) of the total amount of purified BAR domains used for the assay. Samples were analyzed by SDS-PAGE and staining with Coomassie blue. This experiment was performed by Dr. Arndt Pechstein.

Collectively, the experiments described above suggest that the membrane-tubulating activity of syndapin 1 is under regulatory control by its SH3 domain. The fact that the SH3 contacts the F-BAR domain via its putative PxxP-binding groove further suggests a role for proline-rich SH3 ligands such as dynamin 1 or N-WASP in regulating F-BAR-mediated membrane tubulation. We further explored this putative functional partnership between syndapin 1 and dynamin 1 directly.

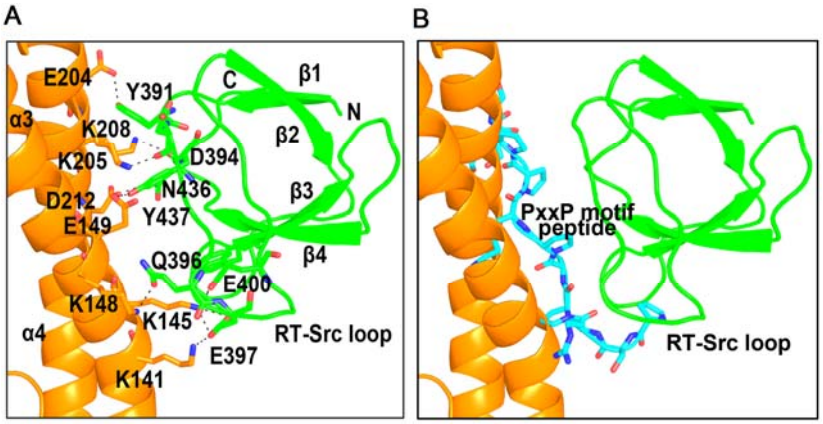

Figure 4-19 The PxxP motif peptide and syndapin 1 F-BAR partially overlapping binding sites on syndapin 1-SH3. (A) Close-up view of the interface of the SH3 and F-BAR domains as shown in Figure 4-12B. (B) A proline-rich peptide (blue) is modeled by hand to the putative PxxP-binding groove in the syndapin 1 SH3 domain, corresponding to the peptide position in the SH3-peptide complex structures PDB ID codes 1W70 and 2DRK.

4.7 Association of syndapin 1 with dynamin 1 unlocks its latent membrane tubulating activity

The crystallographic data suggest that dynamin may compete with the F-BAR domain to unlock the syndapin 1 F-BAR-SH3 clamp. Actually, an overlapping surface on the RT loop of SH3 domain is found when superimposing syndapin 1-SH3 domain with SH3-peptide complex structures (PDB ID codes 1W70 and 2DRK) (Figure 4-19). To comfirm our structure analysis, purified dynamin 1-PRD was applied to wild-type syndapin 1-SH3 domain or mutants. As a control, mutant P434L in the SH3 domain indeed eliminates the association with dynamin but not

syndapin 1-F-BAR (Figure 4-15B and 4-20A). Mutations E400R and D394R/E400R not only impair SH3 association with syndapin 1-F-BAR but also with the proline-rich domain (PRD) of dynamin 1 (Figure 4-15B and 4-20A). By contrast, SH3 Q396R/E397R maintains the ability to bind to dynamin 1-PRD, although it fails to associate with the F-BAR (Figure 4-15B and 4-20A). Hence, dynamin 1 and F-BAR use an overlapping, yet, partially distinct interaction surface on the RT loop of the syndapin 1 SH3 domain for binding. This conclusion is further substantiated by peptide competition in direct binding assays. F-BAR domain binding to GST-SH3 is potently inhibited by a dynamin 1-derived proline-rich peptide (PxxP) (Anggono et al., 2006), whereas mutant (AxxA) or unrelated control peptides are inactive (Figure 4-20B).

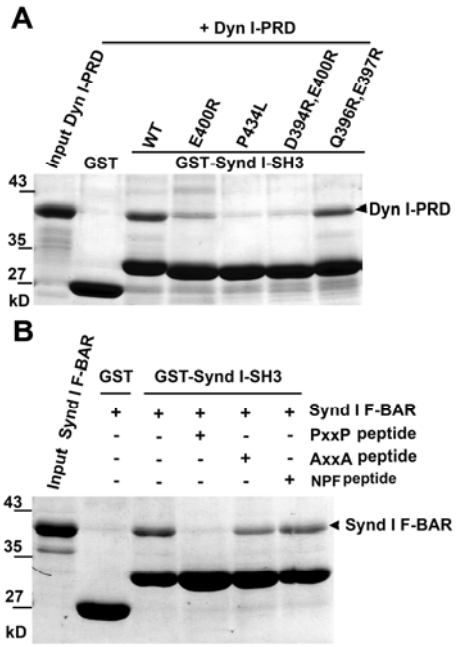

Figure 4-20 Association of syndapin 1-SH3 with dynamin 1 PRD domain or dynamin 1-derived peptide. (A) The proline-rich domain of dynamin 1 (Dyn I-PRD) and syndapin 1 F-BAR compete for partially overlapping binding sites on syndapin 1-SH3. GST pulldowns assays were performed as described in materials and methods. **(B)** A dynamin 1-derived syndapin 1-binding wild-type (PxxP) but not an inactive mutant (AxxA) peptide competes with F-BAR for binding to GST-SH3. A peptide derived from the syndapin 1 linker region (NPF) was taken as a further negative control. Samples were analyzed by SDS-PAGE and staining with Coomassie blue. Input, 15 % (A, B) of the total amount of purified F-BAR domain used in the assay.

If indeed association of SH3 with proline-rich ligands releases the F-BAR from the SH3 clamp, addition of a dynamin 1-derived PRD peptide should potently stimulate

syndapin 1-mediated membrane sculpting. We tested this idea using purified syndapin 1 incubated with liposomes *in vitro*. As expected from our cellular studies syndapin 1 avidly bound to liposomes (Figure 4-21E) but did not cause significant tubulation like syndapin F-BAR (Figure 4-21A, B and F). However, a potent syndapin 1-dependent membrane deformation activity was released upon addition of the dynamin 1 PRD peptide (Figure4-21C and F). The dynamin 1-PRD peptide did not alter liposomal membrane association of syndapin 1 (Figure 4-21E) nor did it cause membrane tubulation on its own. Similarly, breaking the F-BAR-SH3 clamp by mutation (Q396R/E397R) also unleashed the membrane sculpting activity of syndapin 1 on liposomes (Figure 4-21D and F). These results suggest syndapin 1 functionally cooperates with PRD ligands, most notably dynamin 1, in driving membrane deformation and fission.

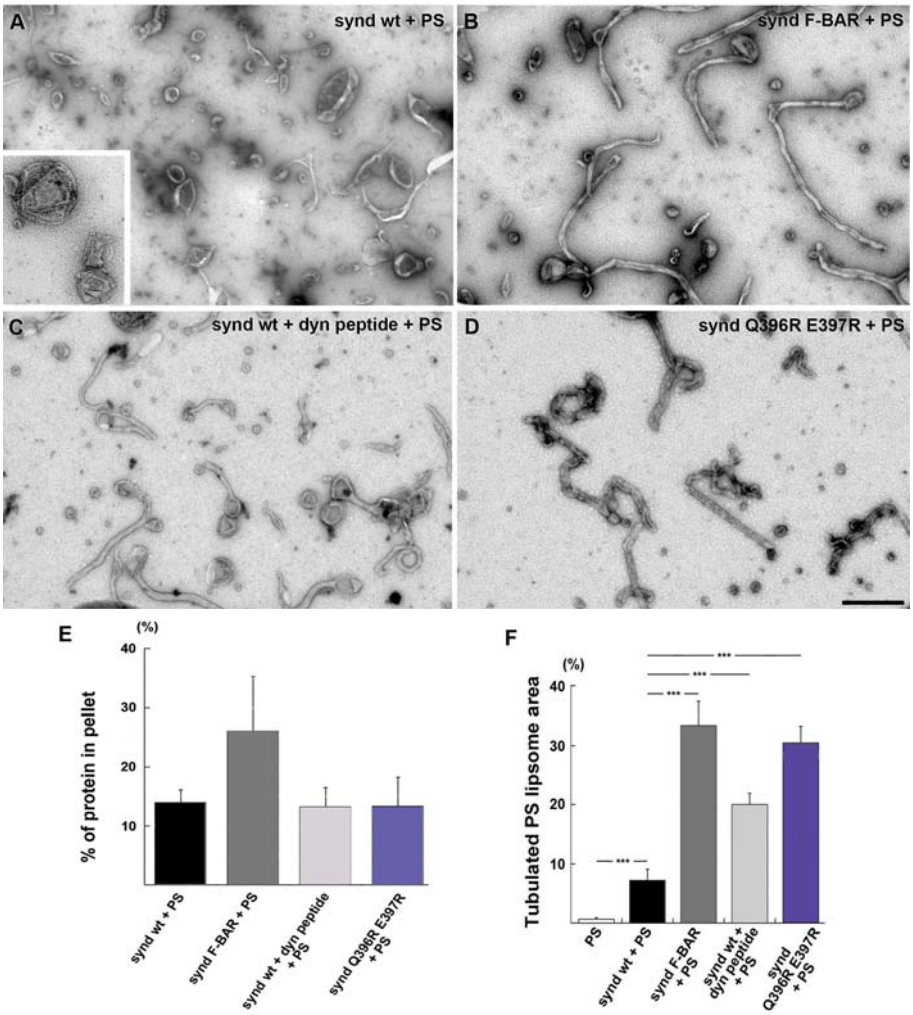

Figure 4-21 Syndapin 1-induced membrane tubulation reconstituted on liposomes *in vitro*. **(A-D)** Negative-stain EM. **(A)** TEM image of PS liposomes incubated with full-length (FL)

syndapin 1. Inset shows PS liposomes without the protein. (B-D) Representative micrographs of PS liposomes incubated with syndapin 1 F-BAR **(B)**, FL syndapin 1 with 170 µM dynamin peptide **(C)**, and FL syndapin 1 (Q396R/E397R) **(E)** Association of syndapin 1 variants with liposomal membranes. Purified full-length wild-type (WT) syndapin 1 was incubated with PS-containing liposomes in the presence or absence of the dynamin 1-derived PRD peptide. Similar experiments were carried out with mutant (Q396R/E397R) syndapin 1. Fractions of bound proteins was analyzed by a sedimentation assay (see methods). Note that addition of the peptide or mutation (Q396R/E397R) did not change the PS-containing liposome binding of syndapin 1 significantly (P>0,05, Students t-test; bars represent mean±SD; n=3). **(F)** Quantification of liposome tubulation in the experiments illustrated above. Note the significant increase in tubulation efficiency (P<0.001, Students t-test) of FL syndapin 1 after addition of the dynamin peptide and or upon mutation of its SH3-domain. Scale bar, 500 nm. This experiment was performed by Anna Sundborger from Karolinska Institutet, Stockholm, Sweden.

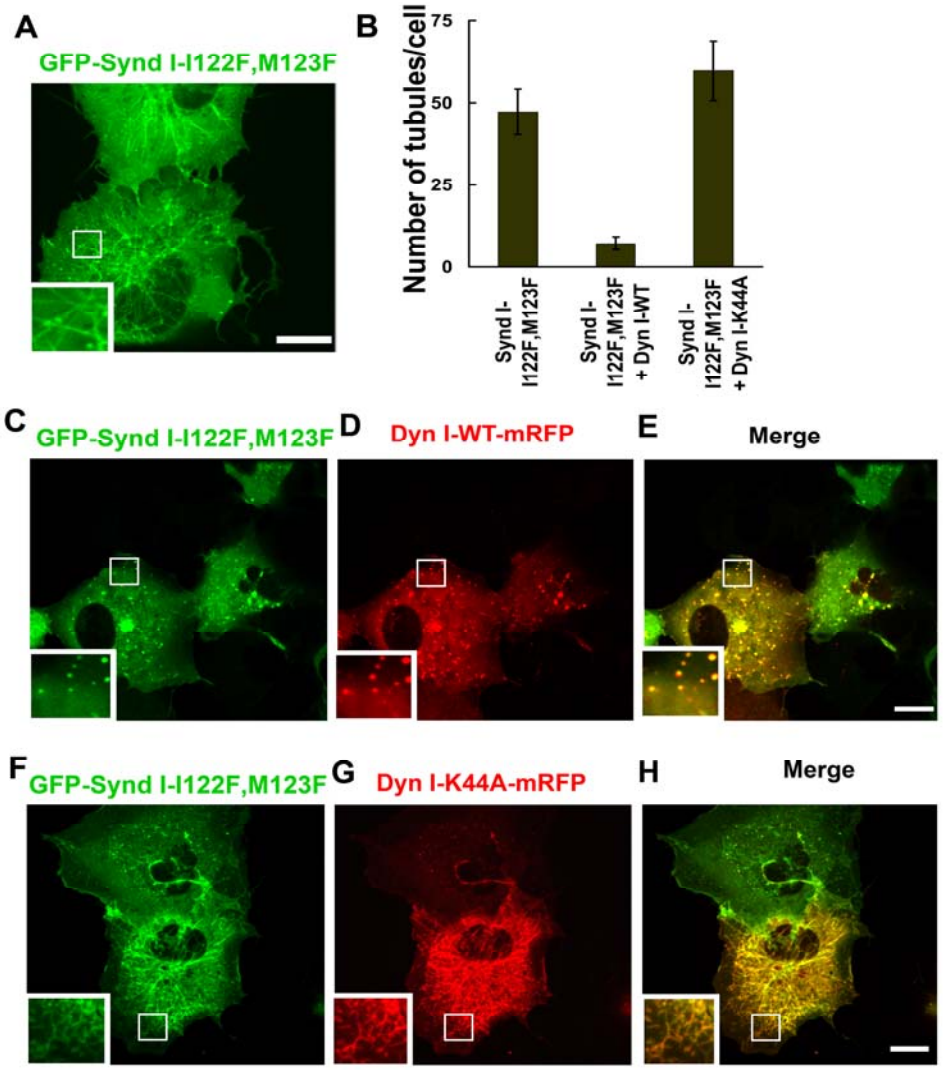

Figure 4-22 Syndapin 1 (I122F/M123F)-induced membrane tubules are consumed by

co-expressed dynamin 1-mRFP. (A) eGFP-syndapin 1-I122F/M123F along generates tubules in living Cos7 cells. **(B)** Quantification of the average number of tubules seen in Cos7 cells co-expressing eGFP-syndapin 1-I122F/M123F and either dynamin 1-WT (Dyn 1-WT-mRFP) or its K44A mutant (Dyn 1-K44A-mRFP). Given are the mean number of tubules (± S.E.) per cell (n=3 each) averaged for at least 20 cells; **(B-G)** Still images of cells co-expressing Dyn 1-WT-mRFP (B-D) or Dyn 1-K44A-mRFP (E-G) with eGFP-syndapin 1-I122F/M123F. Data shown are representative of at least three independent experiments. Scale bar, 10µm.

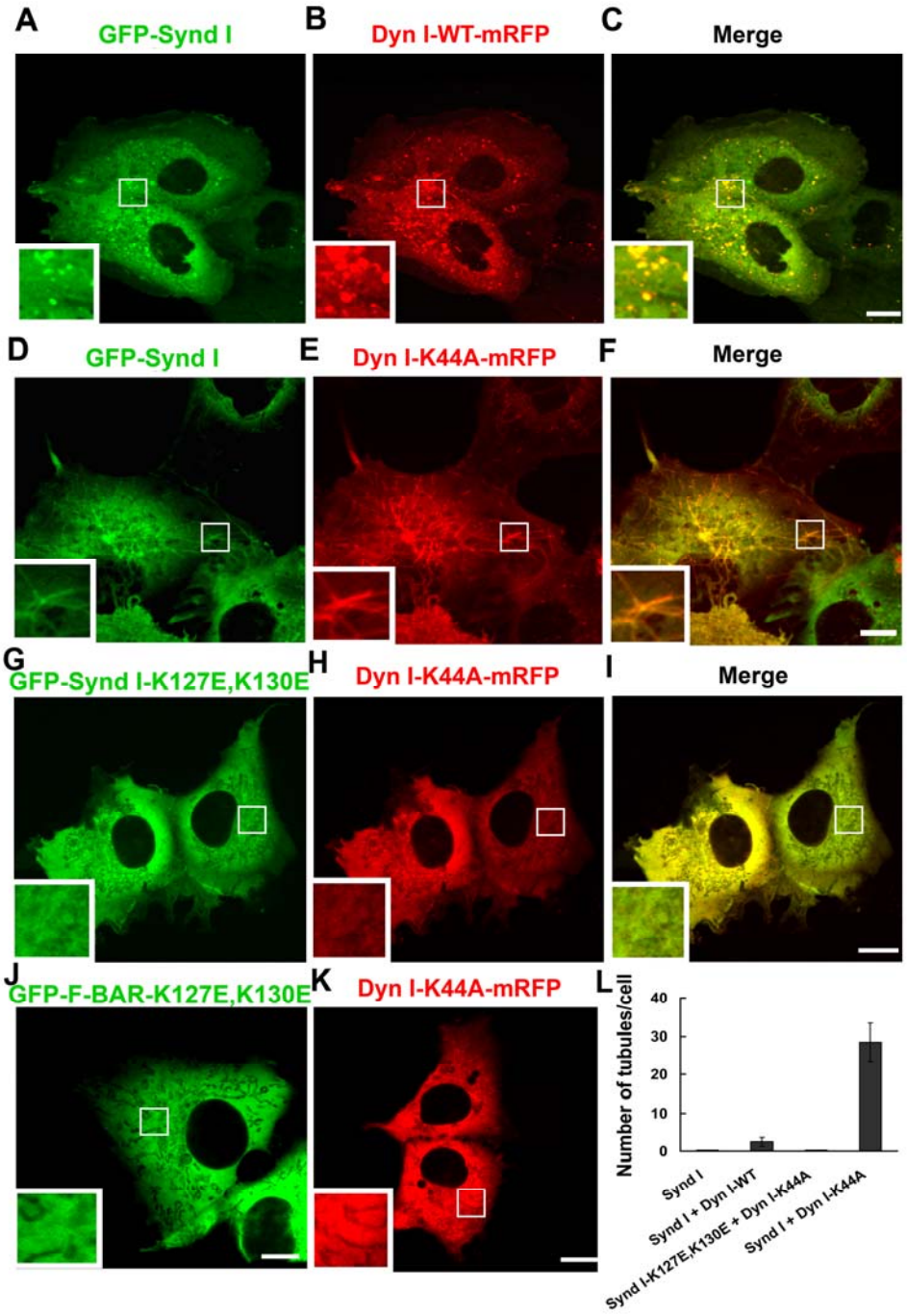

Figure 4-23 Co-expression of eGFP-syndapin 1 with dynamin 1 K44A causes numerous F-BAR-dependent membrane tubules in living cells. Cos7 cells co-expressing eGFP-syndapin

1 (eGFP-Synd 1) and mRFP-tagged dynamin 1 wild-type (Dyn 1-WT-mRFP) or K44A (Dyn 1-K44A-mRFP) were analyzed by live cell spinning disc confocal microscopy. (A-C) Cytoplasmic vesicles along with few short membrane tubules were detected in cells co-expressing eGFP-Synd 1 and Dyn 1-WT-mRFP. (D-F) Numerous membrane tubules were observed in cells co-expressing eGFP-Synd 1 and Dyn 1-K44A-mRFP. (G-I) Absence of membrane tubules from cells co-expressing mutant eGFP-Synd 1-K127E/K130E and Dyn 1-K44A-mRFP. (J) Cells expressing Dyn 1-K44A-mRFP alone do not form tubules. Representative still images from at least three independent experiments are shown. Scale bar, 10μm. (L) Quantification of eGFP-syndapin 1-induced membrane tubules in Cos7 cells co-expressing either mRFP or mRFP-tagged dynamin 1 variants (wild-type, WT, or GTPase-defective mutant K44A). Shown are the mean number of tubules (± S.E.) per cell (n=3 for each syndapin 1 variant) averaged for at least 20 cells.

To test such a hypothetical scenario, eGFP-syndapin 1 was co-expressed with either WT or GTP-locked (K44A) dynamin 1-mRFP. As a control, excessive tubulation occured in Cos7 cells when co-expressing dynamin 1 (K44A)-mRFP with the wedge loop mutant eGFP-syndapin 1 (I122F/M123F) which enhances tubulation even in syndapin full-length constructs (Figure 4-10A and Figure 4-22A-B and F-H), whereas membrane tubules are consumed by co-expression of dynamin 1-(WT)-mRFP (Figure 4-22B-E). Similarly, confocal live cell imaging revealed numerous syndapin 1- and dynamin 1-positive membrane tubules in cells co-expressing eGFP-syndapin 1 and dynamin 1 (K44A)-mRFP. Much fewer and shorter tubules were observed in dynamin 1 (WT)-mRFP transfected cells, which instead accumulated membrane-bound vesicles (Figure 4-23A-F and L). Membrane tubulation was not observed in cells co-expressing dynamin 1 (K44A)-mRFP together with eGFP-syndapin 1 (K127E/K130E) (Figure 4-23G-I and L), a variant carrying point mutations within the F-BAR domain that abrogate tubulation (Figure 4-10C), but do not impair association with either its SH3 domain or with dynamin 1. Tubules were absent from cells expressing dynamin 1 (K44A)-mRFP (Figure 4-23K) or eGFP-syndapin 1 alone (Figure 4-1B). Collectively, we conclude that dynamin 1 is able to release the F-BAR domain of syndapin 1 from SH3 domain-mediated autoinhibition, thereby uncovering its latent membrane-deforming activity. Thus, syndapin 1 and dynamin 1 appear to undergo a functional partnership in driving membrane remodelling during endocytosis.

5 Discussion

5.1 Crystallization of full-length syndapin 1

Similar to other BAR domain containing-proteins, syndapin 1 contains an N-terminal F-BAR domain and a C-terminal SH3 domain which are connected by an ~80aa long flexible linker. So far, several groups tried to obtain the crystal structure of full-length syndapin 1 as shown in Table 3, but failed. Instead structures of the degraded F-BAR domain were obtained. In this study, we obtained crystals of full-length syndapin 1 which were confirmed by SDS-PAGE and mass spectrometry. As shown in Table 3, HEPES or Tris-HCl buffer at ~ pH 7.4 was generally used as protein sample buffer while pH conditions were different in crystallization conditions. Our crystal structure of full-length syndapin 1 revealed that syndapin 1-SH3 domain binds to its F-BAR domain and froms an autoinhibitory comformation. The intramolecular interaction of syndapin 1 is pH- and salt-sensitive. Increasing the salt concentration dissociated the interaction of the SH3 domain and F-BAR domain. Likewise, high pH will also disrupt syndapins intramolecular interaction thus leading to the open conformation state. Other groups (Table 3) commonly used more than 150mM NaCl (at physiological conditions). According to our data, the F-BAR domain does not bind to the SH3 domain under these conditions. Although 200mM NaCl was also used as protein sample buffer in this study, this was diluted to 100mM NaCl when mixed with the salt-free reservoir solution at which the F-BAR domain of syndapin maintains association with the SH3 domain (Figure 4-17A). Additionally, pH 5.0 was used for crystallization in this study. A low pH may stabilize the interaction between the SH3 domain and the F-BAR and inhibit degradation.

The crystal structure of full-length syndapin 1 was successfully determined in this study and revealed a clamped conformation resulting from an interaction between its SH3 domain and its F-BAR domain. A somewhat puzzling observation was that the SH3 domains appear to bind different regions of F-BAR domains in the two crystal structures obtained. How can this be explained? First, the interaction between the SH3 and F-BAR domains is comparably weak. It relies on salt-sensitive electrostatic interactions. High salt concentrations in the crystallization assay may dissociate the

SH3 from the F-BAR domain. In addition, the syndapin 1 F-BAR domain can assemble into tubules, indicating a noticeable attraction between F-BAR domains. At high concentration of syndapin 1-F-BAR domain occurring in the crystallization drop, this intermolecular interaction between F-BAR domains may compete with the intra-molecular SH3/F-BAR interaction. Finally, SH3 domain positions can be deteriorated by crystal packing forces.

Table 3 Crystallization Conditions of Syndapins/Pacsins

PDB ID	Protein sample buffer		Crystal conditions			Reference
	Buffer	Salt	Precipitant	Salt	pH	
3LLL	20mM HEPES **pH7.4**	---	4–5% PEG-MME 550	1.6–1.7 M $(NH_4)_2SO_4$	0.1 M HEPES **pH 7.5**	(Plomann et al., 2010)
3I2W	10mM HEPES **pH 7.5**	0.2 M NaCl	17% PEG 3350,	0.1 M Na2HPO4		(Edeling et al., 2009)
3HAI	25mM Tris-HCl **pH7.4**	0.4 M NaCl	18% PEG3350 1% Tryptone	---	0.1 M HEPES **pH 7.0**	(Wang et al., 2009a)
3HAJ	25mM Tris-HCl **pH7.4**	0.4 M NaCl	20% PEG-MME 5000	---	0.1 M Bis-Tris **pH 6.5**	(Wang et al., 2009a)
2X3W	50mM HEPES **pH 7.4**	0.2 M NaCl	4% PEG4000	---	0.1 M NaAc **pH 5.0**	(Rao et al., 2010)
--	10mM HEPES **pH 7.5**	0.5 M NaCl	20% PEG 3350	---	0.2 m*M* $NH_4H_2PO_4$ **pH 7.9**	(Bai et al., 2010)

5.2 Formation of membrane tubules and protrusions in cells overexpressing syndapin 1-F-BAR domain

BAR domain superfamily proteins play a fundamental role in shaping membranes during diverse cellular processes (Frost et al., 2009) ranging from the formation of endocytic vesicles (Clayton et al., 2009; Peter et al., 2004; Qualmann and Kessels, 2002; Shupliakov et al., 1997; Wieffer et al., 2009) and T-tubules in muscle (Lee et al., 2002; Rikhy et al., 2002), to cell migration and morphogenesis (Ahuja et al., 2007; Dharmalingam et al., 2009; Edeling et al., 2009; Guerrier et al., 2009). Previous studies have allowed us a glimpse at the molecular mechanisms by which BAR/F-BAR domain proteins drive membrane sculpting (Frost et al., 2008; Peter et al., 2004) or sense and stabilize curved membrane domains (Bhatia et al., 2009;

Hatzakis et al., 2009). Here we studied the F-BAR containing-protein syndapin I which is mainly restricted to the (adult) brain and accumulates in synaptic compartments (Plomann et al., 1998; Qualmann et al., 1999). Similar to other BAR or F-BAR containing-proteins, the syndapin 1-F-BAR domain produces membrane tubules in living Cos7 cells and generates tubules when incubated with liposomes. Unlike other BAR or F-BAR contaning-proteins, which produce membrane tubules from the plasma membrane upon overexpression in cells (Itoh and De Camilli, 2006; Itoh et al., 2005; Lee et al., 2002), most of the membrane tubules generated by syndapin 1-F-BAR are of endosomal origin (Figure 4-2). Although syndapin 1 has been linked to vesicle formation at the plasma membrane via cooperation of its F-BAR and SH3 domains, it is possible that syndapin 1 also functions in endosomal compartments. Previous studies have shows that syndapin 1 directly interacts with EHD proteins, which function in the exit of receptors and other membrane proteins from the endosomal recycling compartment. This interaction involves syndapin's two NPF motifs residing in the linker between the F-BAR and SH3 domains (Braun et al., 2005). This suggests that syndapin 1 may play a role in endosomal recycling.

Compared with other BAR/F-BAR domains, the F-BAR domain of syndapin 1 has an additional "wedge loop" consisting of ^{119}HKQIMGGF^{126} with hydrophobic residues (I122-M123) at the tip. Mutation of I122T/M123Q blocks F-BAR's membrane tubulation ability while mutation I122F/M123F leading to the incorporation of a bulkier hydrophobic residue, significantly increases the membrane tubulation ability. This suggests that the wedge loop is necessary for membrane binding and probably for membrane insertion. Interestingly, mutation of I122F/M123F enables full length syndapin 1 to generate numerous membrane tubules in living cells, which does not occur in wild type syndapin 1. Some of these membrane tubules originated from the plasma membrane (Figure 4-22).

Strikingly, membrane protrusions (or filopodia) were also found after overexpression of syndapin 1-F-BAR in living Cos7 cells (Figure 4-3). This phenomenon was likewise observed in the case of the F-BAR containing-protein srGAP2. The membrane protrusions formed by the srGAP2 F-BAR domain negatively regulate neuronal migration and induce neurite outgrowth and branching (Guerrier et al., 2009). Interestingly, membrane protrusions are normally found in cells expressing

I-BAR containing proteins, like IRSp53, but not BAR/F-BAR family members. Filopodia are often found embedded in or protruding from the lamellipodial actin network (Small and Celis, 1978; Svitkina et al., 2003) and play an important role in neurite outgrowth, wound healing and cell migration, and function as precursors for dendritic spines in neurons (Mattila and Lappalainen, 2008). In neurons, growth cones contain a large number of filopodia to guide axons and dendrites to their proper targets (Mattila and Lappalainen, 2008). Syndapin 1 not only accumulates in the synaptic compartment but also localizes at neuronal growth cones (Braun et al., 2005). The fact that syndapin 1 has the ability to induce membrane protrusions or filopodia suggests that syndapin 1 plays a role in neurite outgrowth. Neurite number and dendrite branching were highly increased in neurons overexpressing syndapin 1 (Dharmalingam et al., 2009). Transfecting a syndapin mutant lacking the SH3 domain did not show increased number of neurites or dendrite branches (Dharmalingam et al., 2009). The crystal structure of full-length syndapin 1 reveals the autoinhibitory conformation. To carry out membrane targeting and then induce membrane deformation by its F-BAR domain, the autoinhibitory conformation of syndapin 1 has to be unlocked. Given that the influence of syndapin 1 on neuronal morphology depends on N-WASP (Dharmalingam et al., 2009), the interaction with N-WASP may also unlock the autoinhibitory conformation of syndapin, similar to dynamin 1. Interestingly, knockdown of syndapin 1 leads to aberrant axon branching and impaired axon development (Dharmalingam et al., 2009). How syndapin 1 regulates neuronal morphology and neuron development remains to be understood in detail.

How does syndapin 1 F-BAR domain induce the formation of filopodia? Generally, the formation of filopodia is dependent on proteins that regulate actin polymerization at the barbed end of actin filaments and on actin factors (Gupton and Gertler, 2007). One may ask whether the syndapin 1-F-BAR domain relies on the same mechanism used by I-BAR domains to induce filopodia formation (Figure 1-14) (Lim et al., 2008; Mattila et al., 2007; Saarikangas et al., 2009). Unlike the BAR/F-BAR domain, the dimerization of the I-BAR domain generates negative curvature and induces the formation of dynamic membrane protrusions opposite to those seen in syndapin 1 F-BAR expressing cells. Filopodia formation by I-BAR domains depends on the inherent negative curvature of the I-BAR domain and on phopholipid-binding

residues on the convex side of the I-BAR homodimers (Lim et al., 2008; Mattila and Lappalainen, 2008; Mattila et al., 2007; Saarikangas et al., 2009). Additionally, Eps8 functions as an regulatory protein for I-BAR domain containing-proteins to regulate filopodia formation by blocking addition of actin at the barbed ends of actin filaments (Figure 1-14C,D) (Disanza et al., 2004; Higgs, 2004). By contrast, F-BAR domains induce and stabilize positive membrane curvature, impying that the mechanism of filopodia formation by the F-BAR domain must be different from that used by the I-BAR domain. Another F-BAR family protein PSTPIP 2 is able to directly associate with F-actin and induce filopodia formation (Chitu et al., 2005), suggesting that syndapin 1 may use a similar mechanism to induce filopodia formation.

Collectively, our data suggests that syndapin 1-F-BAR can generate both positive curvature (membrane tubules in this study) and membrane protrusions. Whereas the positive curvature generated by syndapin 1 is used for vesicle formation in case of other BAR containing proteins, the ability to generate membrane protrusions regulates neuronal morphology and development. Syndapin-induced neuronal arborization is N-WASP- and Cdc42-dependent. Deletion of syndapin 1 impaires axon development and especially phenocopies the aberrant axon branching observed upon N-WASP or Arp2/3 complex deficiency (Dharmalingam et al., 2009), suggesting that N-WASP and Cdc42 are linked to syndapin 1-induced filopodia formation. However, additional work is required to understand how syndapin may direct membrane protrusions of opposite curvature in living cells and perhaps *in vitro*.

5.3 Dynamins unlock the autoinhibitory conformation of BAR domain containing-proteins

Unlike syndapin 1-F-BAR, syndapin 1 does not induce membrane tubulation in living Cos7 cells. The crystal structure of full-length syndapin 1 reveals that its F-BAR domain is autoinhibited by its SH3 domain. The interaction between the F-BAR domain and the SH3 domain is mainly mediated by hydrogen bonds and salt bridges. Do BAR-SH3 proteins, such as endophilin and amphiphysin, have a similar autoinhibited conformation? Based on the crystal structures of their BAR domains,

endophilin and amphiphysin contain motifs ("KKKV" in amphiphysin BAR domain and "KKKR" in endophilin BAR domain) similar to the basic stretch found in syndapin 1-F-BAR domain ("KKMK" motif) (Figure 4-13). Mutagenesis data confirm the importance of these residues for binding to syndapin 1 SH3 domain in *in vitro* binding assays (Figure 4-15). Previous low-resolution data have shown that the SH3 domain of endophilin is localized at or near its respective BAR domain (Wang et al., 2008). Our data confirm that both amphiphysin and endophilin SH3 domains can each bind to their own BAR domains (Figure 4-18). Interestingly, other groups have shown that both endophilin and amphiphysin were able to form autoinhibitory conformations, involving their SH3 domains and a proline-rich motif localized between BAR and SH3 domains (Chen et al., 2003; Farsad et al., 2003; Yoshida et al., 2004). More experiments are needed to determine whether endophilin and /or amphiphysin are autoinhibited in a manner similar to that seen for syndapin and how release form such autoinhibition migh be regulated

Strikely, mutating residues involved in the binding of the SH3 domain rescue the membrane tubulation ability of syndapin 1 in liposome tubulation assays (Figue 4-21D). However, the binding affinity between the two domains appears comparably weak. Owing to the charge surface of the F-BAR domain, which makes the F-BAR domain couple to sensor chip CM5, it is difficult to obtain the KD value using Surface Plasmon Resonance (SPR) technique. A weak intramolecular interaction most likely is physiologically important, because the interaction between the SH3 domain and its physiological binding partners dynamin 1 and N-WASP is weak as well, yet, is required to release syndapin from the locked conformation. Indeed, we have shown that the SH3 clamp on F-BAR is released by complex formation between the syndapin 1-SH3 domain and its physiological binding partner dynamin 1 (Anggono et al., 2006; Clayton et al., 2009; Qualmann and Kessels, 2002), suggesting a further mechanistic link between F-BAR domain mediated membrane deformation and the fission process. Our peptide competition and *in vitro* liposome tubulation assays show that a dynamin 1-derived peptide is able to release F-BAR/SH3 from autoinhibition. Syndapin 1, similar to other BAR-SH3 domain proteins, has been postulated to aid membrane recruitment of dynamin 1 within stimulated nerve terminals (Anggono et al., 2006). Although association of the syndapin 1-F-BAR and SH3 domains suppresses its membrane deforming activity,

phospholipid binding remains largely unaffected.

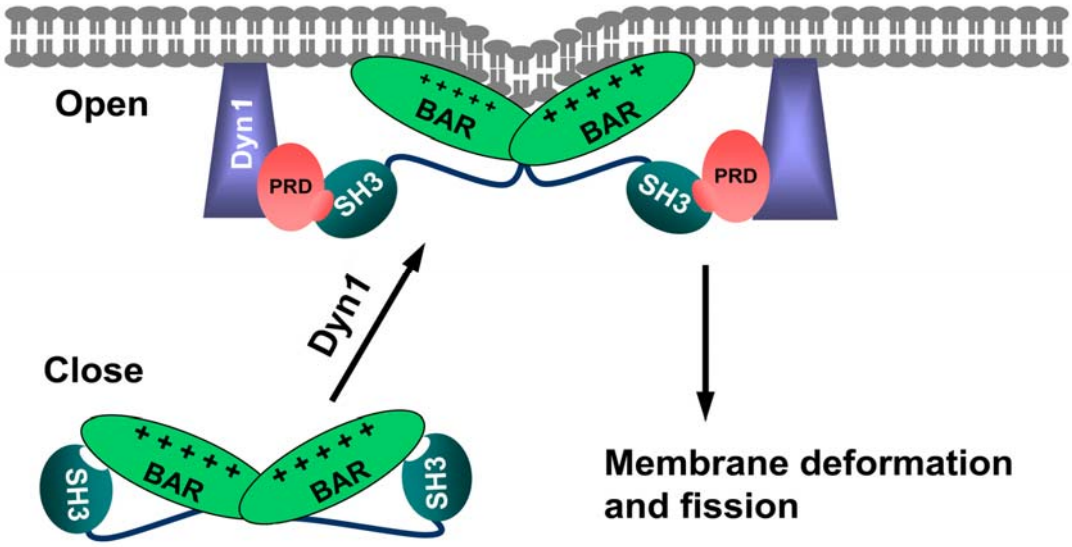

Figure 5-1 Hypothetical model for the cooperative role of BAR-SH3 domain-containing proteins and dynamin 1 in membrane deformation and fission. The positive charge surface of BAR/F-BAR domain is indicated by "+". The autoinhibition of BAR domain containing-proteins is shown in the "close" state, whereas the "open" state is released by the PxxP motif containing-protein dynamin 1. The recruitment of BAR domain to plasma membrane together with dynamin generates membrane deformation and fission.

In a hypothetical scenario, syndapin 1 dimers (or more general BAR domain containing-proteins with a C-terminal SH3 domain) undergo labile association with membranes. The capture of dynamin 1 via PRD-SH3 interactions drives several changes. By displacing the SH3 domain from the F-BAR domain dynamin 1 facilitates a conformational change within syndapin 1 to the open conformation, thereby releasing the F-BAR domain from geometrical constraints (Figure 5-1). Self-assembly of dynamin 1 in turn possibly stabilizes syndapin 1 in its membrane-bound state. Reorganization of syndapin 1-F-BAR into a helically arranged lattice, as recently shown for the structurally related proteins CIP4 and FBP17 (Frost et al., 2008), then serves as a trigger for membrane sculpting, a process further aided by dynamin 1 co-assembly (Sweitzer and Hinshaw, 1998; Takei et al., 1999) (Figure 5-1). Such locally deformed bilayers are then subject to dynamin GTPase-driven fission. It is possible that syndapin 1 directly contributes to this, e.g. by insertion of the amphipathic wedge loop into one leaflet of the deformed membrane and by stimulating dynamin's GTPase activity. Similar regulatory

principles may apply to the role of amphiphysin (Shupliakov et al., 1997) and endophilin (Koh et al., 2004; Ringstad et al., 1999) during the fissioning of late stage clathrin-coated pits by dynamin during endocytosis or SV recycling, although additional experimental data are required to test this. Such a model is consistent not only with the data presented here but also with earlier studies (Farsad and De Camilli, 2003). Furthermore, a molecularly distinct autoinhibitory mechanism involving the BAR and GAP domains has recently been proposed for members of the GRAF family (GRAF: GTPase regulator associated with focal adhesion kinase) (Eberth et al., 2009). GRAF, a tumour-suppressor gene of acute myelogenous leukaemia and myelodysplastic syndrome shares an N-terminal BAR domain, followed by a PH domain and a RhoGAP-related domain (Borkhardt et al., 2000; Eberth et al., 2009). It was shown that the N-terminal BAR domain directly associates with the corresponding GAP domain thereby blocking its activity (Eberth et al., 2009).

SH3-mediated control of BAR/F-BAR domain function may not only be of relevance to endocytic vesicle formation but could be of more general importance. Syndapin family members also are crucial regulators of notochord development (Edeling et al., 2009) and neuromorphogenesis by linking membrane sculpting to N-WASP-dependent actin polymerization (Dharmalingam et al., 2009). We predict that N-WASP binding to syndapin 1-SH3 (Kessels and Qualmann, 2002) will cause conformational changes similar to those elicited by association of dynamin. Interestingly, during neuromorphogenesis syndapin 1 may release N-WASP from autoinhibition (Dharmalingam et al., 2009). In fact, both the SH3 domain and the F-BAR domain of syndapin 1 are required for regulating neuronal morphology and development (Dharmalingam et al., 2009).. Hence, syndapin 1 action during actin-dependent remodelling of the neuronal plasma membrane and bulk endocytosis (Clayton et al., 2009) may follow similar regulatory principles.

5.4 The role of syndapin 1 and dynamin 1 in bulk endocytosis of SV membranes

In nerve terminals, only a limited supply of synaptic vesicles is available. These synaptic vesicles have to be quickly and reliably recycled to maintain neurotransmitter release, which is particularly important during elevated neuronal activity. However, the dominant recycling pathway, clathrin-mediated endocytosis,

has a limited capacity. Likewise, owing to the size of a synapse, the region of plasma membrane used for vesicle formation is limited. Bulk endocytosis is an alternative pathway which provides a fast and high capacity retrieval of synaptic vesicles by invaginating large regions of plasma membrane (hereafter referred to as "endosome-like structures") from which synaptic vesicles can bud. Activity-dependent bulk endocytosis has been postulated to provide additional synaptic vesicles to maintain the reserve pool (Cheung et al., 2010). Studies of dynamin 1-knockout neurons show that dynamin 1 is specifically required for synaptic vesicle recycling during intense neuronal activity (Ferguson et al., 2007). Activity-dependent bulk endocytosis but not clathrin-mediated endocytosis is blocked if the interaction between dynamin 1 and syndapin 1 is perturbed (Clayton et al., 2009). Interestingly, only the interaction between syndapin 1 and dynamin 1 is specifically regulated by dynamin 1 dephosphorylation which occurs during intense neuronal activity (Anggono et al., 2006; Cousin and Robinson, 2001; Cousin et al., 2001), implying that syndapin 1 and dynamin 1 function together in bulk endocytosis. In this study, we have shown that the autoinhibition of syndapin 1 can be unlocked by dynamin 1, but the precise function of syndapin 1 and dynamin 1 for bulk endocytosis still remains to be determined in detail.

It has been observed that in lamprey reticulospinal synapses perturbation of syndapin function by antibody under intense stimulation conditions massively increases membranous cisternae decorated by CCPs and invaginations around release sites, but not of coated pits at the plasma membrane (Andersson et al., 2008). These data suggest that syndapin 1 may stabilize the plasma membrane to facilitate bulk endocytosis during elevated neuronal activity, but not to generate endosome-like structures. Interestingly, when the purified syndapin F-BAR is incubated with liposomes, it not only generates tubular structures but also abundant small vesicles (d=35±5 nm) which often appear to be connected and clustered together, similar to beads on a string (Wang et al., 2009a), The tubular structures are of two classes: those with shallow curvature (d=53±18 nm) and others, which appear as striated (d=98±34 nm) tubules of high curvature with a mean diameter of 17±3 nm (Wang et al., 2009a). Collectively, these data imply that syndapin 1 is able to shape and bind to both low and high curvature membranes. Why is syndapin able to stabilize high membrane curvature? Based on our crystal structure, the F-BAR domain of syndapin

1 has two distinct features (i) an amphipathic "wedge loop" consisting of ^{119}HKQIMGGF^{126} with hydrophobic residues (I122-M123) which are necessary for F-BAR's membrane tubulation ability and (ii) a highly kinked lateral "wing" region. This special lateral "wing" region and the insertion of the amphipathtic wedge loop into the plasma membrane may lower the energy threshold for syndapin to stabilize high membrane curvature. Given that syndapin can generate and bind both low and high membrane curvature, the question how syndapin utilizes these features to facilitate bulk endocytosis awaits further elucidation.

6 Conclusion and Outlook

Syndapin 1, a synaptically enriched protein, is comprised of an N-terminal F-BAR linked to a C-terminal dynamin-binding SH3 domain via a long flexible tether containing two NPF motifs. It has to be been linked to bulk endocytosis pathway together with another synaptically enriched protein dynamin 1. Bulk endocytosis has been postulated to provide a fast and high capacity retrieval of synaptic vesicles by invaginating large regions of plasma membrane from which synaptic vesicles can bud. In this study, we solved the crystal structures of syndapin 1-F-BAR and full-length syndapin 1. These crystal structures show that the syndapin 1 F-BAR domain, in contrast to other BAR/F-BAR domains, contains a wedge loop consisting of ^{119}HKQIMGGF^{126} with hydrophobic residues (I122-M123) at the tip. This wedge loop is required for syndapin´s membrane-deforming activity. Additionally, a highly kinked lateral "wing" region in syndapin is observed in the crystal structure of syndapin 1. It suggests that syndapin 1 may utilize these features to facilitate bulk endocytosis by invaginating large regions of plasma membrane. Mutation of these regions may block the activity of syndapin in bulk endocytosis. However, the precise mechanism still remains to be understood.

Similar to other BAR/F-BAR domains, the F-BAR domain of syndapin also generated membrane tubules in living cells and tubulated liposomes *in vitro*. Interestingly, membrane protrusions were detected when overexpressing the syndapin F-BAR domain in living cells. Similar to other F-BAR domain containing-proteins, such as srGAP via induction of filopodia-like membrane protrusions, syndapin 1 may regulate neuronal morphogenesis. Recent studies have linked syndapin 1 to neuronal morphogenesis together with its binding partner N-WASP. Syndapin 1 appears to release N-WASP from autoinhibition. But how syndapin 1 regulates neuronal morphogenesis still awaits further elucidation.

We show that the membrane-deforming activity of syndapin 1 is autoinhibited by its SH3 domain. Crystallographic analysis reveals an interaction surface composed of a basic patch on the F-BAR domain that interacts with a corresponding acidic surface on the PRD-binding RT loop of the SH3 domian. Such charge complementarity is also used for binding by PxxP motifs within SH3 domain ligands including dynamin

1. Release from the clamped conformation is driven by association of syndapin 1-SH3 with the proline-rich domain of dynamin 1, thereby unlocking its potent membrane deforming-activity. *In vitro*, we show that BAR-SH3 proteins, endophilin and amphipysin also form intramolecular interaction. We hypothesize that this mechanism might be commonly used to regulate BAR/F-BAR domain-mediated membrane sculpting and to potentially couple this process to dynamin-mediated fission. The crystal structures of full-length BAR-SH3 proteins, such as endophilin and amphiphysin, may provide more evidence to support this model. It will be also interesting to test whether other proteins with proline-rich regions, such as N-WASP, display a similar ability as dynamin 1 to unlock the autoinhibitory conformation of BAR-SH3 proteins.

In summary, we predict that SH3-domain mediated autoregulation of the membrane-deforming activity of BAR/F-BAR domains is of crucial importance for the function of syndapin 1 and perhaps other BAR domain proteins.

7 Bibliography

(1994). The CCP4 suite: programs for protein crystallography. Acta Crystallogr D Biol Crystallogr *50*, 760-763.

Abou-Kheir, W., Isaac, B., Yamaguchi, H., and Cox, D. (2008). Membrane targeting of WAVE2 is not sufficient for WAVE2-dependent actin polymerization: a role for IRSp53 in mediating the interaction between Rac and WAVE2. J Cell Sci *121*, 379-390.

Ago, T., Kuribayashi, F., Hiroaki, H., Takeya, R., Ito, T., Kohda, D., and Sumimoto, H. (2003). Phosphorylation of p47phox directs phox homology domain from SH3 domain toward phosphoinositides, leading to phagocyte NADPH oxidase activation. Proc Natl Acad Sci U S A *100*, 4474-4479.

Ahmed, S., Goh, W. I., and Bu, W. (2010). I-BAR domains, IRSp53 and filopodium formation. Semin Cell Dev Biol *21*, 350-356.

Ahuja, R., Pinyol, R., Reichenbach, N., Custer, L., Klingensmith, J., Kessels, M. M., and Qualmann, B. (2007). Cordon-bleu is an actin nucleation factor and controls neuronal morphology. Cell *131*, 337-350.

Allan, V., and Vale, R. (1994). Movement of membrane tubules along microtubules in vitro: evidence for specialised sites of motor attachment. J Cell Sci *107 (Pt 7)*, 1885-1897.

Andersson, F., Jakobsson, J., Low, P., Shupliakov, O., and Brodin, L. (2008). Perturbation of syndapin/PACSIN impairs synaptic vesicle recycling evoked by intense stimulation. J Neurosci *28*, 3925-3933.

Anggono, V., and Robinson, P. J. (2007). Syndapin I and endophilin I bind overlapping proline-rich regions of dynamin I: role in synaptic vesicle endocytosis. J Neurochem *102*, 931-943.

Anggono, V., Smillie, K. J., Graham, M. E., Valova, V. A., Cousin, M. A., and Robinson, P. J. (2006). Syndapin I is the phosphorylation-regulated dynamin I partner in synaptic vesicle endocytosis. Nat Neurosci *9*, 752-760.

Antonny, B., Gounon, P., Schekman, R., and Orci, L. (2003). Self-assembly of minimal COPII cages. EMBO Rep *4*, 419-424.

Ayton, G. S., Lyman, E., Krishna, V., Swenson, R. D., Mim, C., Unger, V. M., and Voth, G. A. (2009). New insights into BAR domain-induced membrane remodeling. Biophys J *97*, 1616-1625.

Bai, X., Meng, G., Li, G., Luo, M., and Zheng, X. (2010). Crystallization and preliminary X-ray crystallographic analysis of human PACSIN 1 protein. Acta Crystallogr Sect F Struct Biol Cryst Commun *66*, 73-75.

Bhatia, V. K., Hatzakis, N. S., and Stamou, D. (2010). A unifying mechanism

accounts for sensing of membrane curvature by BAR domains, amphipathic helices and membrane-anchored proteins. Semin Cell Dev Biol *21*, 381-390.

Bhatia, V. K., Madsen, K. L., Bolinger, P. Y., Kunding, A., Hedegard, P., Gether, U., and Stamou, D. (2009). Amphipathic motifs in BAR domains are essential for membrane curvature sensing. EMBO J *28*, 3303-3314.

Bi, X., Corpina, R. A., and Goldberg, J. (2002). Structure of the Sec23/24-Sar1 pre-budding complex of the COPII vesicle coat. Nature *419*, 271-277.

Bi, X., Mancias, J. D., and Goldberg, J. (2007). Insights into COPII coat nucleation from the structure of Sec23.Sar1 complexed with the active fragment of Sec31. Dev Cell *13*, 635-645.

Bielli, A., Haney, C. J., Gabreski, G., Watkins, S. C., Bannykh, S. I., and Aridor, M. (2005). Regulation of Sar1 NH2 terminus by GTP binding and hydrolysis promotes membrane deformation to control COPII vesicle fission. J Cell Biol *171*, 919-924.

Boettner, D. R., D'Agostino, J. L., Torres, O. T., Daugherty-Clarke, K., Uygur, A., Reider, A., Wendland, B., Lemmon, S. K., and Goode, B. L. (2009). The F-BAR protein Syp1 negatively regulates WASp-Arp2/3 complex activity during endocytic patch formation. Curr Biol *19*, 1979-1987.

Borkhardt, A., Bojesen, S., Haas, O. A., Fuchs, U., Bartelheimer, D., Loncarevic, I. F., Bohle, R. M., Harbott, J., Repp, R., Jaeger, U., *et al.* (2000). The human GRAF gene is fused to MLL in a unique t(5;11)(q31;q23) and both alleles are disrupted in three cases of myelodysplastic syndrome/acute myeloid leukemia with a deletion 5q. Proc Natl Acad Sci U S A *97*, 9168-9173.

Braun, A., Pinyol, R., Dahlhaus, R., Koch, D., Fonarev, P., Grant, B. D., Kessels, M. M., and Qualmann, B. (2005). EHD proteins associate with syndapin I and II and such interactions play a crucial role in endosomal recycling. Mol Biol Cell *16*, 3642-3658.

Bretscher, M. S. (1996). Getting membrane flow and the cytoskeleton to cooperate in moving cells. Cell *87*, 601-606.

Brodin, L., Low, P., and Shupliakov, O. (2000). Sequential steps in clathrin-mediated synaptic vesicle endocytosis. Curr Opin Neurobiol *10*, 312-320.

Brown, W. J., Chambers, K., and Doody, A. (2003). Phospholipase A2 (PLA2) enzymes in membrane trafficking: mediators of membrane shape and function. Traffic *4*, 214-221.

Bu, W., Chou, A. M., Lim, K. B., Sudhaharan, T., and Ahmed, S. (2009). The Toca-1-N-WASP complex links filopodial formation to endocytosis. J Biol Chem *284*, 11622-11636.

Burgoyne, R. D., Fisher, R. J., and Graham, M. E. (2001). Regulation of kiss-and-run exocytosis. Trends Cell Biol *11*, 404-405.

Campellone, K. G., and Welch, M. D. (2010). A nucleator arms race: cellular control

of actin assembly. Nat Rev Mol Cell Biol *11*, 237-251.

Campelo, F., McMahon, H. T., and Kozlov, M. M. (2008). The hydrophobic insertion mechanism of membrane curvature generation by proteins. Biophys J *95*, 2325-2339.

Caplan, S., Naslavsky, N., Hartnell, L. M., Lodge, R., Polishchuk, R. S., Donaldson, J. G., and Bonifacino, J. S. (2002). A tubular EHD1-containing compartment involved in the recycling of major histocompatibility complex class I molecules to the plasma membrane. Embo J *21*, 2557-2567.

Carlton, J., Bujny, M., Peter, B. J., Oorschot, V. M., Rutherford, A., Mellor, H., Klumperman, J., McMahon, H. T., and Cullen, P. J. (2004). Sorting nexin-1 mediates tubular endosome-to-TGN transport through coincidence sensing of high- curvature membranes and 3-phosphoinositides. Curr Biol *14*, 1791-1800.

Carlton, J. G., Bujny, M. V., Peter, B. J., Oorschot, V. M., Rutherford, A., Arkell, R. S., Klumperman, J., McMahon, H. T., and Cullen, P. J. (2005). Sorting nexin-2 is associated with tubular elements of the early endosome, but is not essential for retromer-mediated endosome-to-TGN transport. J Cell Sci *118*, 4527-4539.

Carroll, E. A., Gerrelli, D., Gasca, S., Berg, E., Beier, D. R., Copp, A. J., and Klingensmith, J. (2003). Cordon-bleu is a conserved gene involved in neural tube formation. Dev Biol *262*, 16-31.

Casal, E., Federici, L., Zhang, W., Fernandez-Recio, J., Priego, E. M., Miguel, R. N., DuHadaway, J. B., Prendergast, G. C., Luisi, B. F., and Laue, E. D. (2006). The crystal structure of the BAR domain from human Bin1/amphiphysin II and its implications for molecular recognition. Biochemistry *45*, 12917-12928.

Chang, L., Adams, R. D., and Saltiel, A. R. (2002). The TC10-interacting protein CIP4/2 is required for insulin-stimulated Glut4 translocation in 3T3L1 adipocytes. Proc Natl Acad Sci U S A *99*, 12835-12840.

Chao, C. C., Su, L. J., Sun, N. K., Ju, Y. T., Lih, J. C., and Lin-Chao, S. (2003). Involvement of Gas7 in nerve growth factor-independent and dependent cell processes in PC12 cells. J Neurosci Res *74*, 248-254.

Chen, H., Fre, S., Slepnev, V. I., Capua, M. R., Takei, K., Butler, M. H., Di Fiore, P. P., and De Camilli, P. (1998). Epsin is an EH-domain-binding protein implicated in clathrin-mediated endocytosis. Nature *394*, 793-797.

Chen, Y., Deng, L., Maeno-Hikichi, Y., Lai, M., Chang, S., Chen, G., and Zhang, J. F. (2003). Formation of an endophilin-Ca2+ channel complex is critical for clathrin-mediated synaptic vesicle endocytosis. Cell *115*, 37-48.

Cheung, G., Jupp, O. J., and Cousin, M. A. (2010). Activity-dependent bulk endocytosis and clathrin-dependent endocytosis replenish specific synaptic vesicle pools in central nerve terminals. J Neurosci *30*, 8151-8161.

Chitu, V., Pixley, F. J., Macaluso, F., Larson, D. R., Condeelis, J., Yeung, Y. G., and Stanley, E. R. (2005). The PCH family member MAYP/PSTPIP2 directly regulates F-actin bundling and enhances filopodia formation and motility in macrophages. Mol

Biol Cell *16*, 2947-2959.

Clayton, E. L., Anggono, V., Smillie, K. J., Chau, N., Robinson, P. J., and Cousin, M. A. (2009). The phospho-dependent dynamin-syndapin interaction triggers activity-dependent bulk endocytosis of synaptic vesicles. J Neurosci *29*, 7706-7717.

Clayton, E. L., and Cousin, M. A. (2009a). The molecular physiology of activity-dependent bulk endocytosis of synaptic vesicles. J Neurochem *111*, 901-914.

Clayton, E. L., and Cousin, M. A. (2009b). Quantitative monitoring of activity-dependent bulk endocytosis of synaptic vesicle membrane by fluorescent dextran imaging. J Neurosci Methods *185*, 76-81.

Clayton, E. L., Evans, G. J., and Cousin, M. A. (2007). Activity-dependent control of bulk endocytosis by protein dephosphorylation in central nerve terminals. J Physiol *585*, 687-691.

Clayton, E. L., Evans, G. J., and Cousin, M. A. (2008). Bulk synaptic vesicle endocytosis is rapidly triggered during strong stimulation. J Neurosci *28*, 6627-6632.

Collins, C. A., and DiAntonio, A. (2004). Coordinating synaptic growth without being a nervous wreck. Neuron *41*, 489-491.

Cote, J. F., Chung, P. L., Theberge, J. F., Halle, M., Spencer, S., Lasky, L. A., and Tremblay, M. L. (2002). PSTPIP is a substrate of PTP-PEST and serves as a scaffold guiding PTP-PEST toward a specific dephosphorylation of WASP. J Biol Chem *277*, 2973-2986.

Cousin, H., Gaultier, A., Bleux, C., Darribere, T., and Alfandari, D. (2000). PACSIN2 is a regulator of the metalloprotease/disintegrin ADAM13. Dev Biol *227*, 197-210.

Cousin, M. A. (2009). Activity-dependent bulk synaptic vesicle endocytosis--a fast, high capacity membrane retrieval mechanism. Mol Neurobiol *39*, 185-189.

Cousin, M. A., and Robinson, P. J. (2001). The dephosphins: dephosphorylation by calcineurin triggers synaptic vesicle endocytosis. Trends Neurosci *24*, 659-665.

Cousin, M. A., Tan, T. C., and Robinson, P. J. (2001). Protein phosphorylation is required for endocytosis in nerve terminals: potential role for the dephosphins dynamin I and synaptojanin, but not AP180 or amphiphysin. J Neurochem *76*, 105-116.

Coyle, I. P., Koh, Y. H., Lee, W. C., Slind, J., Fergestad, T., Littleton, J. T., and Ganetzky, B. (2004). Nervous wreck, an SH3 adaptor protein that interacts with Wsp, regulates synaptic growth in Drosophila. Neuron *41*, 521-534.

Cremona, O., Di Paolo, G., Wenk, M. R., Luthi, A., Kim, W. T., Takei, K., Daniell, L., Nemoto, Y., Shears, S. B., Flavell, R. A., *et al.* (1999). Essential role of phosphoinositide metabolism in synaptic vesicle recycling. Cell *99*, 179-188.

Cui, H., Ayton, G. S., and Voth, G. A. (2009). Membrane binding by the endophilin N-BAR domain. Biophys J *97*, 2746-2753.

Da Costa, S. R., Sou, E., Xie, J., Yarber, F. A., Okamoto, C. T., Pidgeon, M., Kessels, M. M., Mircheff, A. K., Schechter, J. E., Qualmann, B., and Hamm-Alvarez, S. F. (2003). Impairing actin filament or syndapin functions promotes accumulation of clathrin-coated vesicles at the apical plasma membrane of acinar epithelial cells. Mol Biol Cell *14*, 4397-4413.

Dabora, S. L., and Sheetz, M. P. (1988). The microtubule-dependent formation of a tubulovesicular network with characteristics of the ER from cultured cell extracts. Cell *54*, 27-35.

Danino, D., and Hinshaw, J. E. (2001). Dynamin family of mechanoenzymes. Curr Opin Cell Biol *13*, 454-460.

Das, S., Sasaki, Y. F., Rothe, T., Premkumar, L. S., Takasu, M., Crandall, J. E., Dikkes, P., Conner, D. A., Rayudu, P. V., Cheung, W.*, et al.* (1998). Increased NMDA current and spine density in mice lacking the NMDA receptor subunit NR3A. Nature *393*, 377-381.

Daumke, O., Lundmark, R., Vallis, Y., Martens, S., Butler, P. J., and McMahon, H. T. (2007). Architectural and mechanistic insights into an EHD ATPase involved in membrane remodelling. Nature *449*, 923-927.

David, C., McPherson, P. S., Mundigl, O., and de Camilli, P. (1996). A role of amphiphysin in synaptic vesicle endocytosis suggested by its binding to dynamin in nerve terminals. Proc Natl Acad Sci U S A *93*, 331-335.

Dawson, J. C., Legg, J. A., and Machesky, L. M. (2006). Bar domain proteins: a role in tubulation, scission and actin assembly in clathrin-mediated endocytosis. Trends Cell Biol *16*, 493-498.

De Camilli, P., Takei, K., and McPherson, P. S. (1995). The function of dynamin in endocytosis. Curr Opin Neurobiol *5*, 559-565.

Demura, M., Takeda, Y., Yoneda, T., Furukawa, K., Usukura, M., Itoh, Y., and Mabuchi, H. (2002). Two novel types of contiguous gene deletion of the AVPR2 and ARHGAP4 genes in unrelated Japanese kindreds with nephrogenic diabetes insipidus. Hum Mutat *19*, 23-29.

Dharmalingam, E., Haeckel, A., Pinyol, R., Schwintzer, L., Koch, D., Kessels, M. M., and Qualmann, B. (2009). F-BAR proteins of the syndapin family shape the plasma membrane and are crucial for neuromorphogenesis. J Neurosci *29*, 13315-13327.

Dickman, D. K., Horne, J. A., Meinertzhagen, I. A., and Schwarz, T. L. (2005). A slowed classical pathway rather than kiss-and-run mediates endocytosis at synapses lacking synaptojanin and endophilin. Cell *123*, 521-533.

Diril, M. K., Wienisch, M., Jung, N., Klingauf, J., and Haucke, V. (2006). Stonin 2 is an AP-2-dependent endocytic sorting adaptor for synaptotagmin internalization and recycling. Dev Cell *10*, 233-244.

Disanza, A., Carlier, M. F., Stradal, T. E., Didry, D., Frittoli, E., Confalonieri, S., Croce, A., Wehland, J., Di Fiore, P. P., and Scita, G. (2004). Eps8 controls actin-based

motility by capping the barbed ends of actin filaments. Nat Cell Biol *6*, 1180-1188.

Disanza, A., Mantoani, S., Hertzog, M., Gerboth, S., Frittoli, E., Steffen, A., Berhoerster, K., Kreienkamp, H. J., Milanesi, F., Di Fiore, P. P., *et al.* (2006). Regulation of cell shape by Cdc42 is mediated by the synergic actin-bundling activity of the Eps8-IRSp53 complex. Nat Cell Biol *8*, 1337-1347.

Doherty, G. J., and McMahon, H. T. (2008). Mediation, modulation, and consequences of membrane-cytoskeleton interactions. Annu Rev Biophys *37*, 65-95.

Doherty, G. J., and McMahon, H. T. (2009). Mechanisms of endocytosis. Annu Rev Biochem *78*, 857-902.

Dreier, L., and Rapoport, T. A. (2000). In vitro formation of the endoplasmic reticulum occurs independently of microtubules by a controlled fusion reaction. J Cell Biol *148*, 883-898.

Drin, G., and Antonny, B. (2010). Amphipathic helices and membrane curvature. FEBS Lett *584*, 1840-1847.

Eberth, A., Lundmark, R., Gremer, L., Dvorsky, R., Koessmeier, K. T., McMahon, H. T., and Ahmadian, M. R. (2009). A BAR domain-mediated autoinhibitory mechanism for RhoGAPs of the GRAF family. Biochem J *417*, 371-377.

Ebinger, M., Senf, L., Wachowski, O., and Scheurlen, W. (2006). Expression of GAS7 in childhood CNS tumors. Pediatr Blood Cancer *46*, 325-328.

Edeling, M. A., Sanker, S., Shima, T., Umasankar, P. K., Honing, S., Kim, H. Y., Davidson, L. A., Watkins, S. C., Tsang, M., Owen, D. J., and Traub, L. M. (2009). Structural requirements for PACSIN/Syndapin operation during zebrafish embryonic notochord development. PLoS One *4*, e8150.

Engqvist-Goldstein, A. E., Zhang, C. X., Carreno, S., Barroso, C., Heuser, J. E., and Drubin, D. G. (2004). RNAi-mediated Hip1R silencing results in stable association between the endocytic machinery and the actin assembly machinery. Mol Biol Cell *15*, 1666-1679.

Epand, R. M., Shai, Y., Segrest, J. P., and Anantharamaiah, G. M. (1995). Mechanisms for the modulation of membrane bilayer properties by amphipathic helical peptides. Biopolymers *37*, 319-338.

Evergren, E., Gad, H., Walther, K., Sundborger, A., Tomilin, N., and Shupliakov, O. (2007). Intersectin is a negative regulator of dynamin recruitment to the synaptic endocytic zone in the central synapse. J Neurosci *27*, 379-390.

Fallon, L., Belanger, C. M., Corera, A. T., Kontogiannea, M., Regan-Klapisz, E., Moreau, F., Voortman, J., Haber, M., Rouleau, G., Thorarinsdottir, T., *et al.* (2006). A regulated interaction with the UIM protein Eps15 implicates parkin in EGF receptor trafficking and PI(3)K-Akt signalling. Nat Cell Biol *8*, 834-842.

Fan, L., Di Ciano-Oliveira, C., Weed, S. A., Craig, A. W., Greer, P. A., Rotstein, O. D., and Kapus, A. (2004). Actin depolymerization-induced tyrosine phosphorylation

of cortactin: the role of Fer kinase. Biochem J *380*, 581-591.

Farsad, K., and De Camilli, P. (2003). Mechanisms of membrane deformation. Curr Opin Cell Biol *15*, 372-381.

Farsad, K., Ringstad, N., Takei, K., Floyd, S. R., Rose, K., and De Camilli, P. (2001). Generation of high curvature membranes mediated by direct endophilin bilayer interactions. J Cell Biol *155*, 193-200.

Farsad, K., Slepnev, V., Ochoa, G., Daniell, L., Haucke, V., and De Camilli, P. (2003). A putative role for intramolecular regulatory mechanisms in the adaptor function of amphiphysin in endocytosis. Neuropharmacology *45*, 787-796.

Fath, S., Mancias, J. D., Bi, X., and Goldberg, J. (2007). Structure and organization of coat proteins in the COPII cage. Cell *129*, 1325-1336.

Feng, Y., Hartig, S. M., Bechill, J. E., Blanchard, E. G., Caudell, E., and Corey, S. J. (2010). The Cdc42-interacting protein-4 (CIP4) gene knock-out mouse reveals delayed and decreased endocytosis. J Biol Chem *285*, 4348-4354.

Ferguson, S. M., Brasnjo, G., Hayashi, M., Wolfel, M., Collesi, C., Giovedi, S., Raimondi, A., Gong, L. W., Ariel, P., Paradise, S., *et al.* (2007). A selective activity-dependent requirement for dynamin 1 in synaptic vesicle endocytosis. Science *316*, 570-574.

Ferguson, S. M., Raimondi, A., Paradise, S., Shen, H., Mesaki, K., Ferguson, A., Destaing, O., Ko, G., Takasaki, J., Cremona, O., *et al.* (2009). Coordinated actions of actin and BAR proteins upstream of dynamin at endocytic clathrin-coated pits. Dev Cell *17*, 811-822.

Fertuck, H. C., and Salpeter, M. M. (1974). Localization of acetylcholine receptor by 125I-labeled alpha-bungarotoxin binding at mouse motor endplates. Proc Natl Acad Sci U S A *71*, 1376-1378.

Fesce, R., Grohovaz, F., Valtorta, F., and Meldolesi, J. (1994). Neurotransmitter release: fusion or 'kiss-and-run'? Trends Cell Biol *4*, 1-4.

Ford, M. G., Mills, I. G., Peter, B. J., Vallis, Y., Praefcke, G. J., Evans, P. R., and McMahon, H. T. (2002). Curvature of clathrin-coated pits driven by epsin. Nature *419*, 361-366.

Ford, M. G., Pearse, B. M., Higgins, M. K., Vallis, Y., Owen, D. J., Gibson, A., Hopkins, C. R., Evans, P. R., and McMahon, H. T. (2001). Simultaneous binding of PtdIns(4,5)P2 and clathrin by AP180 in the nucleation of clathrin lattices on membranes. Science *291*, 1051-1055.

Fotin, A., Cheng, Y., Sliz, P., Grigorieff, N., Harrison, S. C., Kirchhausen, T., and Walz, T. (2004). Molecular model for a complete clathrin lattice from electron cryomicroscopy. Nature *432*, 573-579.

Fricke, R., Gohl, C., and Bogdan, S. (2010). The F-BAR protein family Actin' on the membrane. Commun Integr Biol *3*, 89-94.

Fricke, R., Gohl, C., Dharmalingam, E., Grevelhorster, A., Zahedi, B., Harden, N., Kessels, M., Qualmann, B., and Bogdan, S. (2009). Drosophila Cip4/Toca-1 integrates membrane trafficking and actin dynamics through WASP and SCAR/WAVE. Curr Biol *19*, 1429-1437.

Frost, A., Perera, R., Roux, A., Spasov, K., Destaing, O., Egelman, E. H., De Camilli, P., and Unger, V. M. (2008). Structural basis of membrane invagination by F-BAR domains. Cell *132*, 807-817.

Frost, A., Unger, V. M., and De Camilli, P. (2009). The BAR domain superfamily: membrane-molding macromolecules. Cell *137*, 191-196.

Fujiwara, T., Mammoto, A., Kim, Y., and Takai, Y. (2000). Rho small G-protein-dependent binding of mDia to an Src homology 3 domain-containing IRSp53/BAIAP2. Biochem Biophys Res Commun *271*, 626-629.

Funato, Y., Terabayashi, T., Suenaga, N., Seiki, M., Takenawa, T., and Miki, H. (2004). IRSp53/Eps8 complex is important for positive regulation of Rac and cancer cell motility/invasiveness. Cancer Res *64*, 5237-5244.

Gabernet-Castello, C., Dacks, J. B., and Field, M. C. (2009). The single ENTH-domain protein of trypanosomes; endocytic functions and evolutionary relationship with epsin. Traffic *10*, 894-911.

Gaidarov, I., Chen, Q., Falck, J. R., Reddy, K. K., and Keen, J. H. (1996). A functional phosphatidylinositol 3,4,5-trisphosphate/phosphoinositide binding domain in the clathrin adaptor AP-2 alpha subunit. Implications for the endocytic pathway. J Biol Chem *271*, 20922-20929.

Gaidarov, I., and Keen, J. H. (1999). Phosphoinositide-AP-2 interactions required for targeting to plasma membrane clathrin-coated pits. J Cell Biol *146*, 755-764.

Gallop, J. L., Jao, C. C., Kent, H. M., Butler, P. J., Evans, P. R., Langen, R., and McMahon, H. T. (2006). Mechanism of endophilin N-BAR domain-mediated membrane curvature. Embo J *25*, 2898-2910.

Gao, S., von der Malsburg, A., Paeschke, S., Behlke, J., Haller, O., Kochs, G., and Daumke, O. (2010a). Structural basis of oligomerization in the stalk region of dynamin-like MxA. Nature *465*, 502-506.

Gao, X., Lu, F., Zhou, L., Dang, S., Sun, L., Li, X., Wang, J., and Shi, Y. (2009). Structure and mechanism of an amino acid antiporter. Science *324*, 1565-1568.

Gao, X., Zhou, L., Jiao, X., Lu, F., Yan, C., Zeng, X., Wang, J., and Shi, Y. (2010b). Mechanism of substrate recognition and transport by an amino acid antiporter. Nature *463*, 828-832.

George, M., Ying, G., Rainey, M. A., Solomon, A., Parikh, P. T., Gao, Q., Band, V., and Band, H. (2007). Shared as well as distinct roles of EHD proteins revealed by biochemical and functional comparisons in mammalian cells and C. elegans. BMC Cell Biol *8*, 3.

Ghadimi, M. P., Sanzenbacher, R., Thiede, B., Wenzel, J., Jing, Q., Plomann, M., Borkhardt, A., Kabelitz, D., and Janssen, O. (2002). Identification of interaction partners of the cytosolic polyproline region of CD95 ligand (CD178). FEBS Lett *519*, 50-58.

Granseth, B., Odermatt, B., Royle, S. J., and Lagnado, L. (2007). Clathrin-mediated endocytosis: the physiological mechanism of vesicle retrieval at hippocampal synapses. J Physiol *585*, 681-686.

Grant, B., Zhang, Y., Paupard, M. C., Lin, S. X., Hall, D. H., and Hirsh, D. (2001). Evidence that RME-1, a conserved C. elegans EH-domain protein, functions in endocytic recycling. Nat Cell Biol *3*, 573-579.

Grant, B. D., and Caplan, S. (2008). Mechanisms of EHD/RME-1 protein function in endocytic transport. Traffic *9*, 2043-2052.

Greer, P. (2002). Closing in on the biological functions of Fps/Fes and Fer. Nat Rev Mol Cell Biol *3*, 278-289.

Guerrier, S., Coutinho-Budd, J., Sassa, T., Gresset, A., Jordan, N. V., Chen, K., Jin, W. L., Frost, A., and Polleux, F. (2009). The F-BAR domain of srGAP2 induces membrane protrusions required for neuronal migration and morphogenesis. Cell *138*, 990-1004.

Guipponi, M., Scott, H. S., Chen, H., Schebesta, A., Rossier, C., and Antonarakis, S. E. (1998). Two isoforms of a human intersectin (ITSN) protein are produced by brain-specific alternative splicing in a stop codon. Genomics *53*, 369-376.

Gupton, S. L., and Gertler, F. B. (2007). Filopodia: the fingers that do the walking. Sci STKE *2007*, re5.

Habermann, B. (2004). The BAR-domain family of proteins: a case of bending and binding? EMBO Rep *5*, 250-255.

Halbach, A., Morgelin, M., Baumgarten, M., Milbrandt, M., Paulsson, M., and Plomann, M. (2007). PACSIN 1 forms tetramers via its N-terminal F-BAR domain. Febs J *274*, 773-782.

Hanna, S. T., Pigeau, G. M., Galvanovskis, J., Clark, A., Rorsman, P., and MacDonald, P. E. (2009). Kiss-and-run exocytosis and fusion pores of secretory vesicles in human beta-cells. Pflugers Arch *457*, 1343-1350.

Hartig, S. M., Ishikura, S., Hicklen, R. S., Feng, Y., Blanchard, E. G., Voelker, K. A., Pichot, C. S., Grange, R. W., Raphael, R. M., Klip, A., and Corey, S. J. (2009). The F-BAR protein CIP4 promotes GLUT4 endocytosis through bidirectional interactions with N-WASp and Dynamin-2. J Cell Sci *122*, 2283-2291.

Hatzakis, N. S., Bhatia, V. K., Larsen, J., Madsen, K. L., Bolinger, P. Y., Kunding, A. H., Castillo, J., Gether, U., Hedegard, P., and Stamou, D. (2009). How curved membranes recruit amphipathic helices and protein anchoring motifs. Nat Chem Biol *5*, 835-841.

Heath, R. J., and Insall, R. H. (2008). F-BAR domains: multifunctional regulators of membrane curvature. J Cell Sci *121*, 1951-1954.

Henne, W. M., Boucrot, E., Meinecke, M., Evergren, E., Vallis, Y., Mittal, R., and McMahon, H. T. (2010). FCHo proteins are nucleators of clathrin-mediated endocytosis. Science *328*, 1281-1284.

Henne, W. M., Kent, H. M., Ford, M. G., Hegde, B. G., Daumke, O., Butler, P. J., Mittal, R., Langen, R., Evans, P. R., and McMahon, H. T. (2007). Structure and analysis of FCHo2 F-BAR domain: a dimerizing and membrane recruitment module that effects membrane curvature. Structure *15*, 839-852.

Higgs, H. N. (2004). There goes the neighbourhood: Eps8 joins the barbed-end crowd. Nat Cell Biol *6*, 1147-1149.

Higgs, H. N., and Pollard, T. D. (1999). Regulation of actin polymerization by Arp2/3 complex and WASp/Scar proteins. J Biol Chem *274*, 32531-32534.

Hilfiker, S., Pieribone, V. A., Czernik, A. J., Kao, H. T., Augustine, G. J., and Greengard, P. (1999). Synapsins as regulators of neurotransmitter release. Philos Trans R Soc Lond B Biol Sci *354*, 269-279.

Hinshaw, J. E. (2000). Dynamin and its role in membrane fission. Annu Rev Cell Dev Biol *16*, 483-519.

Hinshaw, J. E., and Schmid, S. L. (1995). Dynamin self-assembles into rings suggesting a mechanism for coated vesicle budding. Nature *374*, 190-192.

Ho, H. Y., Rohatgi, R., Lebensohn, A. M., Le, M., Li, J., Gygi, S. P., and Kirschner, M. W. (2004). Toca-1 mediates Cdc42-dependent actin nucleation by activating the N-WASP-WIP complex. Cell *118*, 203-216.

Honing, S., Ricotta, D., Krauss, M., Spate, K., Spolaore, B., Motley, A., Robinson, M., Robinson, C., Haucke, V., and Owen, D. J. (2005). Phosphatidylinositol-(4,5)-bisphosphate regulates sorting signal recognition by the clathrin-associated adaptor complex AP2. Mol Cell *18*, 519-531.

Howard, L., Nelson, K. K., Maciewicz, R. A., and Blobel, C. P. (1999). Interaction of the metalloprotease disintegrins MDC9 and MDC15 with two SH3 domain-containing proteins, endophilin I and SH3PX1. J Biol Chem *274*, 31693-31699.

Huang, M., Weissman, J. T., Beraud-Dufour, S., Luan, P., Wang, C., Chen, W., Aridor, M., Wilson, I. A., and Balch, W. E. (2001). Crystal structure of Sar1-GDP at 1.7 A resolution and the role of the NH2 terminus in ER export. J Cell Biol *155*, 937-948.

Hughson, F. M. (2010). Copy coats: COPI mimics clathrin and COPII. Cell *142*, 19-21.

Hui, E., Johnson, C. P., Yao, J., Dunning, F. M., and Chapman, E. R. (2009). Synaptotagmin-mediated bending of the target membrane is a critical step in Ca(2+)-regulated fusion. Cell *138*, 709-721.

Hussain, N. K., Jenna, S., Glogauer, M., Quinn, C. C., Wasiak, S., Guipponi, M., Antonarakis, S. E., Kay, B. K., Stossel, T. P., Lamarche-Vane, N., and McPherson, P. S. (2001). Endocytic protein intersectin-l regulates actin assembly via Cdc42 and N-WASP. Nat Cell Biol *3*, 927-932.

Hussain, N. K., Yamabhai, M., Bhakar, A. L., Metzler, M., Ferguson, S. S., Hayden, M. R., McPherson, P. S., and Kay, B. K. (2003). A role for epsin N-terminal homology/AP180 N-terminal homology (ENTH/ANTH) domains in tubulin binding. J Biol Chem *278*, 28823-28830.

Insall, R. H., and Machesky, L. M. (2004). Regulation of WASP: PIP2 Pipped by Toca-1? Cell *118*, 140-141.

Itoh, T., and De Camilli, P. (2006). BAR, F-BAR (EFC) and ENTH/ANTH domains in the regulation of membrane-cytosol interfaces and membrane curvature. Biochim Biophys Acta *1761*, 897-912.

Itoh, T., Erdmann, K. S., Roux, A., Habermann, B., Werner, H., and De Camilli, P. (2005). Dynamin and the actin cytoskeleton cooperatively regulate plasma membrane invagination by BAR and F-BAR proteins. Dev Cell *9*, 791-804.

Jackson, L. P., Kelly, B. T., McCoy, A. J., Gaffry, T., James, L. C., Collins, B. M., Honing, S., Evans, P. R., and Owen, D. J. (2010). A large-scale conformational change couples membrane recruitment to cargo binding in the AP2 clathrin adaptor complex. Cell *141*, 1220-1229.

Jakobsson, J., Gad, H., Andersson, F., Low, P., Shupliakov, O., and Brodin, L. (2008). Role of epsin 1 in synaptic vesicle endocytosis. Proc Natl Acad Sci U S A *105*, 6445-6450.

Janssen, O., Qian, J., Linkermann, A., and Kabelitz, D. (2003). CD95 ligand--death factor and costimulatory molecule? Cell Death Differ *10*, 1215-1225.

Jao, C. C., Hegde, B. G., Gallop, J. L., Hegde, P. B., McMahon, H. T., Haworth, I. S., and Langen, R. (2010). Roles of amphipathic helices and the bin/amphiphysin/rvs (BAR) domain of endophilin in membrane curvature generation. J Biol Chem *285*, 20164-20170.

Jia, C. Y., Nie, J., Wu, C., Li, C., and Li, S. S. (2005). Novel Src homology 3 domain-binding motifs identified from proteomic screen of a Pro-rich region. Mol Cell Proteomics *4*, 1155-1166.

Jung, N., and Haucke, V. (2007). Clathrin-mediated endocytosis at synapses. Traffic *8*, 1129-1136.

Kabsch, W. (1993). Automatic Processing of Rotation Diffraction Data from Crystals of Initially Unknown Symmetry and Cell Constants. J Appl Crystallogr *26*, 795-800.

Kamioka, Y., Fukuhara, S., Sawa, H., Nagashima, K., Masuda, M., Matsuda, M., and Mochizuki, N. (2004). A novel dynamin-associating molecule, formin-binding protein 17, induces tubular membrane invaginations and participates in endocytosis. J Biol Chem *279*, 40091-40099.

Karathanassis, D., Stahelin, R. V., Bravo, J., Perisic, O., Pacold, C. M., Cho, W., and Williams, R. L. (2002). Binding of the PX domain of p47(phox) to phosphatidylinositol 3,4-bisphosphate and phosphatidic acid is masked by an intramolecular interaction. Embo J *21*, 5057-5068.

Kelly, R. B. (1995). Endocytosis. Ringing necks with dynamin. Nature *374*, 116-117.

Kessels, M. M., and Qualmann, B. (2002). Syndapins integrate N-WASP in receptor-mediated endocytosis. Embo J *21*, 6083-6094.

Kessels, M. M., and Qualmann, B. (2004). The syndapin protein family: linking membrane trafficking with the cytoskeleton. J Cell Sci *117*, 3077-3086.

Kessels, M. M., and Qualmann, B. (2006). Syndapin oligomers interconnect the machineries for endocytic vesicle formation and actin polymerization. J Biol Chem *281*, 13285-13299.

Kim, S. H., Choi, H. J., Lee, K. W., Hong, N. H., Sung, B. H., Choi, K. Y., Kim, S. M., Chang, S., Eom, S. H., and Song, W. K. (2006). Interaction of SPIN90 with syndapin is implicated in clathrin-mediated endocytic pathway in fibroblasts. Genes Cells *11*, 1197-1211.

Kinuta, M., Yamada, H., Abe, T., Watanabe, M., Li, S. A., Kamitani, A., Yasuda, T., Matsukawa, T., Kumon, H., and Takei, K. (2002). Phosphatidylinositol 4,5-bisphosphate stimulates vesicle formation from liposomes by brain cytosol. Proc Natl Acad Sci U S A *99*, 2842-2847.

Klapisz, E., Sorokina, I., Lemeer, S., Pijnenburg, M., Verkleij, A. J., and van Bergen en Henegouwen, P. M. (2002). A ubiquitin-interacting motif (UIM) is essential for Eps15 and Eps15R ubiquitination. J Biol Chem *277*, 30746-30753.

Klopfenstein, D. R., Kappeler, F., and Hauri, H. P. (1998). A novel direct interaction of endoplasmic reticulum with microtubules. Embo J *17*, 6168-6177.

Kogata, N., Masuda, M., Kamioka, Y., Yamagishi, A., Endo, A., Okada, M., and Mochizuki, N. (2003). Identification of Fer tyrosine kinase localized on microtubules as a platelet endothelial cell adhesion molecule-1 phosphorylating kinase in vascular endothelial cells. Mol Biol Cell *14*, 3553-3564.

Koh, T. W., Verstreken, P., and Bellen, H. J. (2004). Dap160/intersectin acts as a stabilizing scaffold required for synaptic development and vesicle endocytosis. Neuron *43*, 193-205.

Kooijman, E. E., Chupin, V., Fuller, N. L., Kozlov, M. M., de Kruijff, B., Burger, K. N., and Rand, P. R. (2005). Spontaneous curvature of phosphatidic acid and lysophosphatidic acid. Biochemistry *44*, 2097-2102.

Krauss, M., and Haucke, V. (2007). Phosphoinositides: regulators of membrane traffic and protein function. FEBS Lett *581*, 2105-2111.

Krissinel, E., and Henrick, K. (2007). Inference of macromolecular assemblies from crystalline state. J Mol Biol *372*, 774-797.

Krugmann, S., Jordens, I., Gevaert, K., Driessens, M., Vandekerckhove, J., and Hall, A. (2001). Cdc42 induces filopodia by promoting the formation of an IRSp53:Mena complex. Curr Biol *11*, 1645-1655.

Kweon, D. H., Shin, Y. K., Shin, J. Y., Lee, J. H., Lee, J. B., Seo, J. H., and Kim, Y. S. (2006). Membrane topology of helix 0 of the Epsin N-terminal homology domain. Mol Cells *21*, 428-435.

Laskowski, R. A., Macarthur, M. W., Moss, D. S., and Thornton, J. M. (1993). Procheck - a Program to Check the Stereochemical Quality of Protein Structures. . J Appl Crystallogr *26*, 283-291.

Lazakovitch, E. M., She, B. R., Lien, C. L., Woo, W. M., Ju, Y. T., and Lin-Chao, S. (1999). The Gas7 gene encodes two protein isoforms differentially expressed within the brain. Genomics *61*, 298-306.

Le Roy, C., and Wrana, J. L. (2005). Clathrin- and non-clathrin-mediated endocytic regulation of cell signalling. Nat Rev Mol Cell Biol *6*, 112-126.

Lee, C., and Goldberg, J. (2010). Structure of coatomer cage proteins and the relationship among COPI, COPII, and clathrin vesicle coats. Cell *142*, 123-132.

Lee, E., Marcucci, M., Daniell, L., Pypaert, M., Weisz, O. A., Ochoa, G. C., Farsad, K., Wenk, M. R., and De Camilli, P. (2002). Amphiphysin 2 (Bin1) and T-tubule biogenesis in muscle. Science *297*, 1193-1196.

Lee, S. H. (2005). Interaction of nonreceptor tyrosine-kinase Fer and p120 catenin is involved in neuronal polarization. Mol Cells *20*, 256-262.

Lenz, M., Prost, J., and Joanny, J. F. (2008). Mechanochemical action of the dynamin protein. Phys Rev E Stat Nonlin Soft Matter Phys *78*, 011911.

Leslie, A. G. (2006). The integration of macromolecular diffraction data. Acta Crystallogr D Biol Crystallogr *62*, 48-57.

Leung, Y., Ally, S., and Goldberg, M. B. (2008). Bacterial actin assembly requires toca-1 to relieve N-wasp autoinhibition. Cell Host Microbe *3*, 39-47.

Lichte, B., Veh, R. W., Meyer, H. E., and Kilimann, M. W. (1992). Amphiphysin, a novel protein associated with synaptic vesicles. Embo J *11*, 2521-2530.

Lim, K. B., Bu, W., Goh, W. I., Koh, E., Ong, S. H., Pawson, T., Sudhaharan, T., and Ahmed, S. (2008). The Cdc42 effector IRSp53 generates filopodia by coupling membrane protrusion with actin dynamics. J Biol Chem *283*, 20454-20472.

Lin, S. X., Grant, B., Hirsh, D., and Maxfield, F. R. (2001). Rme-1 regulates the distribution and function of the endocytic recycling compartment in mammalian cells. Nat Cell Biol *3*, 567-572.

Lippincott-Schwartz, J., Yuan, L., Tipper, C., Amherdt, M., Orci, L., and Klausner, R. D. (1991). Brefeldin A's effects on endosomes, lysosomes, and the TGN suggest a general mechanism for regulating organelle structure and membrane traffic. Cell *67*,

601-616.

Liu, J. P., and Robinson, P. J. (1995). Dynamin and endocytosis. Endocr Rev *16*, 590-607.

Liu, Y., Kahn, R. A., and Prestegard, J. H. Dynamic structure of membrane-anchored Arf*GTP. Nat Struct Mol Biol *17*, 876-881.

Liu, Y., Kahn, R. A., and Prestegard, J. H. (2010). Dynamic structure of membrane-anchored Arf*GTP. Nat Struct Mol Biol *17*, 876-881.

Low, C., Weininger, U., Lee, H., Schweimer, K., Neundorf, I., Beck-Sickinger, A. G., Pastor, R. W., and Balbach, J. (2008). Structure and dynamics of helix-0 of the N-BAR domain in lipid micelles and bilayers. Biophys J *95*, 4315-4323.

Mackinnon, R. (2004). Structural biology. Voltage sensor meets lipid membrane. Science *306*, 1304-1305.

Mangiarini, L., Sathasivam, K., Seller, M., Cozens, B., Harper, A., Hetherington, C., Lawton, M., Trottier, Y., Lehrach, H., Davies, S. W., and Bates, G. P. (1996). Exon 1 of the HD gene with an expanded CAG repeat is sufficient to cause a progressive neurological phenotype in transgenic mice. Cell *87*, 493-506.

Maritzen, T., Podufall, J., and Haucke, V. (2010). Stonins--specialized adaptors for synaptic vesicle recycling and beyond? Traffic *11*, 8-15.

Marks, B., Stowell, M. H., Vallis, Y., Mills, I. G., Gibson, A., Hopkins, C. R., and McMahon, H. T. (2001). GTPase activity of dynamin and resulting conformation change are essential for endocytosis. Nature *410*, 231-235.

Masuda, M., and Mochizuki, N. (2010). Structural characteristics of BAR domain superfamily to sculpt the membrane. Semin Cell Dev Biol.

Masuda, M., Takeda, S., Sone, M., Ohki, T., Mori, H., Kamioka, Y., and Mochizuki, N. (2006). Endophilin BAR domain drives membrane curvature by two newly identified structure-based mechanisms. Embo J *25*, 2889-2897.

Mattila, P. K., and Lappalainen, P. (2008). Filopodia: molecular architecture and cellular functions. Nat Rev Mol Cell Biol *9*, 446-454.

Mattila, P. K., Pykalainen, A., Saarikangas, J., Paavilainen, V. O., Vihinen, H., Jokitalo, E., and Lappalainen, P. (2007). Missing-in-metastasis and IRSp53 deform PI(4,5)P2-rich membranes by an inverse BAR domain-like mechanism. J Cell Biol *176*, 953-964.

McCoy, J. A., Grosse-Kunstleve, R. W., Adams, P. D., Winn, M. D., Storoni, L. C., and Read, R. J. (2007). Phaser crystallographic software. J Appl Crystallogr *40*, 658-674.

McFadden, G. I., and Ralph, S. A. (2003). Dynamin: the endosymbiosis ring of power? Proc Natl Acad Sci U S A *100*, 3557-3559.

McMahon, H. T., and Gallop, J. L. (2005). Membrane curvature and mechanisms of dynamic cell membrane remodelling. Nature *438*, 590-596.

McPherson, P. S., de Heuvel, E., Phillie, J., Wang, W., Sengar, A., and Egan, S. (1998). EH domain-dependent interactions between Eps15 and clathrin-coated vesicle protein p95. Biochem Biophys Res Commun *244*, 701-705.

McRee, D. E. (1999). XtalView/Xfit--A versatile program for manipulating atomic coordinates and electron density. J Struct Biol *125*, 156-165.

Memon, A. R. (2004). The role of ADP-ribosylation factor and SAR1 in vesicular trafficking in plants. Biochim Biophys Acta *1664*, 9-30.

Merrifield, C. J. (2004). Seeing is believing: imaging actin dynamics at single sites of endocytosis. Trends Cell Biol *14*, 352-358.

Merrifield, C. J., Perrais, D., and Zenisek, D. (2005). Coupling between clathrin-coated-pit invagination, cortactin recruitment, and membrane scission observed in live cells. Cell *121*, 593-606.

Miki, H., and Takenawa, T. (2002). WAVE2 serves a functional partner of IRSp53 by regulating its interaction with Rac. Biochem Biophys Res Commun *293*, 93-99.

Miki, H., Yamaguchi, H., Suetsugu, S., and Takenawa, T. (2000). IRSp53 is an essential intermediate between Rac and WAVE in the regulation of membrane ruffling. Nature *408*, 732-735.

Millard, T. H., Bompard, G., Heung, M. Y., Dafforn, T. R., Scott, D. J., Machesky, L. M., and Futterer, K. (2005). Structural basis of filopodia formation induced by the IRSp53/MIM homology domain of human IRSp53. Embo J *24*, 240-250.

Mishra, S. K., Hawryluk, M. J., Brett, T. J., Keyel, P. A., Dupin, A. L., Jha, A., Heuser, J. E., Fremont, D. H., and Traub, L. M. (2004). Dual engagement regulation of protein interactions with the AP-2 adaptor alpha appendage. J Biol Chem *279*, 46191-46203.

Mizuno, N., Jao, C. C., Langen, R., and Steven, A. C. (2010). Multiple modes of endophilin-mediated conversion of lipid vesicles into coated tubes: implications for synaptic endocytosis. J Biol Chem *285*, 23351-23358.

Modregger, J., DiProspero, N. A., Charles, V., Tagle, D. A., and Plomann, M. (2002). PACSIN 1 interacts with huntingtin and is absent from synaptic varicosities in presymptomatic Huntington's disease brains. Hum Mol Genet *11*, 2547-2558.

Mori, S., Tanaka, M., Nanba, D., Nishiwaki, E., Ishiguro, H., Higashiyama, S., and Matsuura, N. (2003). PACSIN3 binds ADAM12/meltrin alpha and up-regulates ectodomain shedding of heparin-binding epidermal growth factor-like growth factor. J Biol Chem *278*, 46029-46034.

Morris, R. J., Zwart, P. H., Cohen, S., Fernandez, F. J., Kakaris, M., Kirillova, O., Vonrhein, C., Perrakis, A., and Lamzin, V. S. (2004). Breaking good resolutions with ARP/wARP. J Synchrotron Radiat *11*, 56-59.

Mundigl, O., Matteoli, M., Daniell, L., Thomas-Reetz, A., Metcalf, A., Jahn, R., and De Camilli, P. (1993). Synaptic vesicle proteins and early endosomes in cultured hippocampal neurons: differential effects of Brefeldin A in axon and dendrites. J Cell Biol *122*, 1207-1221.

Murray, M. J., Davidson, C. M., Hayward, N. M., and Brand, A. H. (2006). The Fes/Fer non-receptor tyrosine kinase cooperates with Src42A to regulate dorsal closure in Drosophila. Development *133*, 3063-3073.

Murshudov, G. N., Vagin, A. A., and Dodson, E. J. (1997). Refinement of macromolecular structures by the maximum-likelihood method. Acta Crystallogr D Biol Crystallogr *53*, 240-255.

Nakagawa, H., Miki, H., Nozumi, M., Takenawa, T., Miyamoto, S., Wehland, J., and Small, J. V. (2003). IRSp53 is colocalised with WAVE2 at the tips of protruding lamellipodia and filopodia independently of Mena. J Cell Sci *116*, 2577-2583.

Nikki, M., Merilainen, J., and Lehto, V. P. (2002). FAP52 regulates actin organization via binding to filamin. J Biol Chem *277*, 11432-11440.

Nossal, R. (2001). Energetics of clathrin basket assembly. Traffic *2*, 138-147.

O'Connor-Giles, K. M., Ho, L. L., and Ganetzky, B. (2008). Nervous wreck interacts with thickveins and the endocytic machinery to attenuate retrograde BMP signaling during synaptic growth. Neuron *58*, 507-518.

Painter, J., and Merritt, E. A. (2006). Controlled and automatic processing during mental rotation. J Appl Crystallogr *39*, 109-111.

Palade, G. E. (1953). Fine structure of blood capillaries. J Appl Physics *24*, 1424.

Palfrey, H. C., and Artalejo, C. R. (2003). Secretion: kiss and run caught on film. Curr Biol *13*, R397-399.

Pant, S., Sharma, M., Patel, K., Caplan, S., Carr, C. M., and Grant, B. D. (2009). AMPH-1/Amphiphysin/Bin1 functions with RME-1/Ehd1 in endocytic recycling. Nat Cell Biol *11*, 1399-1410.

Parton, R. G., and Simons, K. (2007). The multiple faces of caveolae. Nat Rev Mol Cell Biol *8*, 185-194.

Pechstein, A., Bacetic, J., Vahedi-Faridi, A., Gromova, K., Sundborger, A., Tomlin, N., Krainer, G., Vorontsova, O., Schafer, J. G., Owe, S. G., *et al.* (2010a). Regulation of synaptic vesicle recycling by complex formation between intersectin 1 and the clathrin adaptor complex AP2. Proc Natl Acad Sci U S A *107*, 4206-4211.

Pechstein, A., Shupliakov, O., and Haucke, V. (2010b). Intersectin 1: a versatile actor in the synaptic vesicle cycle. Biochem Soc Trans *38*, 181-186.

Perez-Otano, I., Lujan, R., Tavalin, S. J., Plomann, M., Modregger, J., Liu, X. B., Jones, E. G., Heinemann, S. F., Lo, D. C., and Ehlers, M. D. (2006). Endocytosis and synaptic removal of NR3A-containing NMDA receptors by PACSIN1/syndapin1.

Nat Neurosci *9*, 611-621.

Peter, B. J., Kent, H. M., Mills, I. G., Vallis, Y., Butler, P. J., Evans, P. R., and McMahon, H. T. (2004). BAR domains as sensors of membrane curvature: the amphiphysin BAR structure. Science *303*, 495-499.

Plomann, M., Lange, R., Vopper, G., Cremer, H., Heinlein, U. A., Scheff, S., Baldwin, S. A., Leitges, M., Cramer, M., Paulsson, M., and Barthels, D. (1998). PACSIN, a brain protein that is upregulated upon differentiation into neuronal cells. Eur J Biochem *256*, 201-211.

Plomann, M., Wittmann, J. G., and Rudolph, M. G. (2010). A hinge in the distal end of the PACSIN 2 F-BAR domain may contribute to membrane-curvature sensing. J Mol Biol *400*, 129-136.

Praefcke, G. J., and McMahon, H. T. (2004). The dynamin superfamily: universal membrane tubulation and fission molecules? Nat Rev Mol Cell Biol *5*, 133-147.

Qualmann, B., and Kelly, R. B. (2000). Syndapin isoforms participate in receptor-mediated endocytosis and actin organization. J Cell Biol *148*, 1047-1062.

Qualmann, B., and Kessels, M. M. (2002). Endocytosis and the cytoskeleton. Int Rev Cytol *220*, 93-144.

Qualmann, B., and Kessels, M. M. (2009). New players in actin polymerization--WH2-domain-containing actin nucleators. Trends Cell Biol *19*, 276-285.

Qualmann, B., Roos, J., DiGregorio, P. J., and Kelly, R. B. (1999). Syndapin I, a synaptic dynamin-binding protein that associates with the neural Wiskott-Aldrich syndrome protein. Mol Biol Cell *10*, 501-513.

Quinlan, M. E., Heuser, J. E., Kerkhoff, E., and Mullins, R. D. (2005). Drosophila Spire is an actin nucleation factor. Nature *433*, 382-388.

Ramachandran, R., and Schmid, S. L. (2008). Real-time detection reveals that effectors couple dynamin's GTP-dependent conformational changes to the membrane. Embo J *27*, 27-37.

Ramachandran, R., Surka, M., Chappie, J. S., Fowler, D. M., Foss, T. R., Song, B. D., and Schmid, S. L. (2007). The dynamin middle domain is critical for tetramerization and higher-order self-assembly. Embo J *26*, 559-566.

Ramjaun, A. R., and McPherson, P. S. (1998). Multiple amphiphysin II splice variants display differential clathrin binding: identification of two distinct clathrin-binding sites. J Neurochem *70*, 2369-2376.

Ramjaun, A. R., Philie, J., de Heuvel, E., and McPherson, P. S. (1999). The N terminus of amphiphysin II mediates dimerization and plasma membrane targeting. J Biol Chem *274*, 19785-19791.

Rao, Y., Bian, C., Yuan, C., Li, Y., Chen, L., Ye, X., Huang, Z., and Huang, M.

(2006). An open conformation of switch I revealed by Sar1-GDP crystal structure at low Mg2+. Biochem Biophys Res Commun *348*, 908-915.

Rao, Y., Ma, Q., Vahedi-Faridi, A., Sundborger, A., Pechstein, A., Puchkov, D., Luo, L., Shupliakov, O., Saenger, W., and Haucke, V. (2010). Molecular basis for SH3 domain regulation of F-BAR-mediated membrane deformation. Proc Natl Acad Sci U S A *107*, 8213-8218.

Raucher, D., and Sheetz, M. P. (2000). Cell spreading and lamellipodial extension rate is regulated by membrane tension. J Cell Biol *148*, 127-136.

Razani, B., and Lisanti, M. P. (2001). Caveolins and caveolae: molecular and functional relationships. Exp Cell Res *271*, 36-44.

Razani, B., Woodman, S. E., and Lisanti, M. P. (2002). Caveolae: from cell biology to animal physiology. Pharmacol Rev *54*, 431-467.

Regan-Klapisz, E., Sorokina, I., Voortman, J., de Keizer, P., Roovers, R. C., Verheesen, P., Urbe, S., Fallon, L., Fon, E. A., Verkleij, A., *et al.* (2005). Ubiquilin recruits Eps15 into ubiquitin-rich cytoplasmic aggregates via a UIM-UBL interaction. J Cell Sci *118*, 4437-4450.

Reider, A., Barker, S. L., Mishra, S. K., Im, Y. J., Maldonado-Baez, L., Hurley, J. H., Traub, L. M., and Wendland, B. (2009). Syp1 is a conserved endocytic adaptor that contains domains involved in cargo selection and membrane tubulation. Embo J *28*, 3103-3116.

Ren, G., Vajjhala, P., Lee, J. S., Winsor, B., and Munn, A. L. (2006). The BAR domain proteins: molding membranes in fission, fusion, and phagy. Microbiol Mol Biol Rev *70*, 37-120.

Renault, L., Bugyi, B., and Carlier, M. F. (2008). Spire and Cordon-bleu: multifunctional regulators of actin dynamics. Trends Cell Biol *18*, 494-504.

Rikhy, R., Kumar, V., Mittal, R., and Krishnan, K. S. (2002). Endophilin is critically required for synapse formation and function in Drosophila melanogaster. J Neurosci *22*, 7478-7484.

Ringstad, N., Gad, H., Low, P., Di Paolo, G., Brodin, L., Shupliakov, O., and De Camilli, P. (1999). Endophilin/SH3p4 is required for the transition from early to late stages in clathrin-mediated synaptic vesicle endocytosis. Neuron *24*, 143-154.

Rizzoli, S. O., and Jahn, R. (2007). Kiss-and-run, collapse and 'readily retrievable' vesicles. Traffic *8*, 1137-1144.

Robertson, A. M., and Allan, V. J. (2000). Brefeldin A-dependent membrane tubule formation reconstituted in vitro is driven by a cell cycle-regulated microtubule motor. Mol Biol Cell *11*, 941-955.

Rodal, A. A., Motola-Barnes, R. N., and Littleton, J. T. (2008). Nervous wreck and Cdc42 cooperate to regulate endocytic actin assembly during synaptic growth. J Neurosci *28*, 8316-8325.

Roux, A., Cappello, G., Cartaud, J., Prost, J., Goud, B., and Bassereau, P. (2002). A minimal system allowing tubulation with molecular motors pulling on giant liposomes. Proc Natl Acad Sci U S A *99*, 5394-5399.

Roux, A., Uyhazi, K., Frost, A., and De Camilli, P. (2006). GTP-dependent twisting of dynamin implicates constriction and tension in membrane fission. Nature *441*, 528-531.

Rumpf, J., Simon, B., Groemping, Y., and Sattler, M. (2008). 1H, 13C, and 15N chemical shift assignments for the Eps15-EH2-stonin 2 complex. Biomol NMR Assign *2*, 55-58.

Russell, C., and Stagg, S. M. (2009). New Insights into the Structural Mechanisms of the COPII Coat. Traffic.

Saarikangas, J., Zhao, H., Pykalainen, A., Laurinmaki, P., Mattila, P. K., Kinnunen, P. K., Butcher, S. J., and Lappalainen, P. (2009). Molecular mechanisms of membrane deformation by I-BAR domain proteins. Curr Biol *19*, 95-107.

Sakamuro, D., Elliott, K. J., Wechsler-Reya, R., and Prendergast, G. C. (1996). BIN1 is a novel MYC-interacting protein with features of a tumour suppressor. Nat Genet *14*, 69-77.

Sato, K., Ernstrom, G. G., Watanabe, S., Weimer, R. M., Chen, C. H., Sato, M., Siddiqui, A., Jorgensen, E. M., and Grant, B. D. (2009). Differential requirements for clathrin in receptor-mediated endocytosis and maintenance of synaptic vesicle pools. Proc Natl Acad Sci U S A *106*, 1139-1144.

Scherer, P. E., Okamoto, T., Chun, M., Nishimoto, I., Lodish, H. F., and Lisanti, M. P. (1996). Identification, sequence, and expression of caveolin-2 defines a caveolin gene family. Proc Natl Acad Sci U S A *93*, 131-135.

Schneider, S. W. (2001). Kiss and run mechanism in exocytosis. J Membr Biol *181*, 67-76.

Schneider, T. R., and Sheldrick, G. M. (2002). Substructure solution with SHELXD. Acta Crystallogr D Biol Crystallogr *58*, 1772-1779.

Sever, S. (2002). Dynamin and endocytosis. Curr Opin Cell Biol *14*, 463-467.

Shao, Y., Akmentin, W., Toledo-Aral, J. J., Rosenbaum, J., Valdez, G., Cabot, J. B., Hilbush, B. S., and Halegoua, S. (2002). Pincher, a pinocytic chaperone for nerve growth factor/TrkA signaling endosomes. J Cell Biol *157*, 679-691.

She, B. R., Liou, G. G., and Lin-Chao, S. (2002). Association of the growth-arrest-specific protein Gas7 with F-actin induces reorganization of microfilaments and promotes membrane outgrowth. Exp Cell Res *273*, 34-44.

Sheldrick, G. M. (2008). A short history of SHELX. Acta Crystallogr A *64*, 112-122.

Shemesh, T., Luini, A., Malhotra, V., Burger, K. N., and Kozlov, M. M. (2003). Prefission constriction of Golgi tubular carriers driven by local lipid metabolism: a

theoretical model. Biophys J *85*, 3813-3827.

Shimada, A., Niwa, H., Tsujita, K., Suetsugu, S., Nitta, K., Hanawa-Suetsugu, K., Akasaka, R., Nishino, Y., Toyama, M., Chen, L., *et al.* (2007). Curved EFC/F-BAR-domain dimers are joined end to end into a filament for membrane invagination in endocytosis. Cell *129*, 761-772.

Shpetner, H. S., Herskovits, J. S., and Vallee, R. B. (1996). A binding site for SH3 domains targets dynamin to coated pits. J Biol Chem *271*, 13-16.

Shpetner, H. S., and Vallee, R. B. (1989). Identification of dynamin, a novel mechanochemical enzyme that mediates interactions between microtubules. Cell *59*, 421-432.

Shupliakov, O., Bloom, O., Gustafsson, J. S., Kjaerulff, O., Low, P., Tomilin, N., Pieribone, V. A., Greengard, P., and Brodin, L. (2002). Impaired recycling of synaptic vesicles after acute perturbation of the presynaptic actin cytoskeleton. Proc Natl Acad Sci U S A *99*, 14476-14481.

Shupliakov, O., Low, P., Grabs, D., Gad, H., Chen, H., David, C., Takei, K., De Camilli, P., and Brodin, L. (1997). Synaptic vesicle endocytosis impaired by disruption of dynamin-SH3 domain interactions. Science *276*, 259-263.

Sivadon, P., Bauer, F., Aigle, M., and Crouzet, M. (1995). Actin cytoskeleton and budding pattern are altered in the yeast rvs161 mutant: the Rvs161 protein shares common domains with the brain protein amphiphysin. Mol Gen Genet *246*, 485-495.

Slepnev, V. I., Ochoa, G. C., Butler, M. H., and De Camilli, P. (2000). Tandem arrangement of the clathrin and AP-2 binding domains in amphiphysin 1 and disruption of clathrin coat function by amphiphysin fragments comprising these sites. J Biol Chem *275*, 17583-17589.

Slepnev, V. I., Ochoa, G. C., Butler, M. H., Grabs, D., and De Camilli, P. (1998). Role of phosphorylation in regulation of the assembly of endocytic coat complexes. Science *281*, 821-824.

Small, J. V., and Celis, J. E. (1978). Filament arrangements in negatively stained cultured cells: the organization of actin. Cytobiologie *16*, 308-325.

Sobolevsky, A. I., Rosconi, M. P., and Gouaux, E. (2009). X-ray structure, symmetry and mechanism of an AMPA-subtype glutamate receptor. Nature *462*, 745-756.

Soderling, S. H., Binns, K. L., Wayman, G. A., Davee, S. M., Ong, S. H., Pawson, T., and Scott, J. D. (2002). The WRP component of the WAVE-1 complex attenuates Rac-mediated signalling. Nat Cell Biol *4*, 970-975.

Soulet, F., Yarar, D., Leonard, M., and Schmid, S. L. (2005). SNX9 regulates dynamin assembly and is required for efficient clathrin-mediated endocytosis. Mol Biol Cell *16*, 2058-2067.

Spencer, S., Dowbenko, D., Cheng, J., Li, W., Brush, J., Utzig, S., Simanis, V., and Lasky, L. A. (1997). PSTPIP: a tyrosine phosphorylated cleavage furrow-associated

protein that is a substrate for a PEST tyrosine phosphatase. J Cell Biol *138*, 845-860.

Stagg, S. M., Gurkan, C., Fowler, D. M., LaPointe, P., Foss, T. R., Potter, C. S., Carragher, B., and Balch, W. E. (2006). Structure of the Sec13/31 COPII coat cage. Nature *439*, 234-238.

Stagg, S. M., LaPointe, P., Razvi, A., Gurkan, C., Potter, C. S., Carragher, B., and Balch, W. E. (2008). Structural basis for cargo regulation of COPII coat assembly. Cell *134*, 474-484.

Stowell, M. H., Marks, B., Wigge, P., and McMahon, H. T. (1999). Nucleotide-dependent conformational changes in dynamin: evidence for a mechanochemical molecular spring. Nat Cell Biol *1*, 27-32.

Suetsugu, S. (2009). The direction of actin polymerization for vesicle fission suggested from membranes tubulated by the EFC/F-BAR domain protein FBP17. FEBS Lett *583*, 3401-3404.

Suetsugu, S., Kurisu, S., Oikawa, T., Yamazaki, D., Oda, A., and Takenawa, T. (2006a). Optimization of WAVE2 complex-induced actin polymerization by membrane-bound IRSp53, PIP(3), and Rac. J Cell Biol *173*, 571-585.

Suetsugu, S., Murayama, K., Sakamoto, A., Hanawa-Suetsugu, K., Seto, A., Oikawa, T., Mishima, C., Shirouzu, M., Takenawa, T., and Yokoyama, S. (2006b). The RAC binding domain/IRSp53-MIM homology domain of IRSp53 induces RAC-dependent membrane deformation. J Biol Chem *281*, 35347-35358.

Suetsugu, S., Toyooka, K., and Senju, Y. (2009). Subcellular membrane curvature mediated by the BAR domain superfamily proteins. Semin Cell Dev Biol.

Suntio, T., Shmelev, A., Lund, M., and Makarow, M. (1999). The sorting determinant guiding Hsp150 to the COPI-independent transport pathway in yeast. J Cell Sci *112 (Pt 22)*, 3889-3898.

Svitkina, T. M., Bulanova, E. A., Chaga, O. Y., Vignjevic, D. M., Kojima, S., Vasiliev, J. M., and Borisy, G. G. (2003). Mechanism of filopodia initiation by reorganization of a dendritic network. J Cell Biol *160*, 409-421.

Sweitzer, S. M., and Hinshaw, J. E. (1998). Dynamin undergoes a GTP-dependent conformational change causing vesiculation. Cell *93*, 1021-1029.

Takano, K., Toyooka, K., and Suetsugu, S. (2008). EFC/F-BAR proteins and the N-WASP-WIP complex induce membrane curvature-dependent actin polymerization. Embo J *27*, 2817-2828.

Takei, K., McPherson, P. S., Schmid, S. L., and De Camilli, P. (1995). Tubular membrane invaginations coated by dynamin rings are induced by GTP-gamma S in nerve terminals. Nature *374*, 186-190.

Takei, K., Slepnev, V. I., Haucke, V., and De Camilli, P. (1999). Functional partnership between amphiphysin and dynamin in clathrin-mediated endocytosis. Nat Cell Biol *1*, 33-39.

Takenawa, T., and Suetsugu, S. (2007). The WASP-WAVE protein network: connecting the membrane to the cytoskeleton. Nat Rev Mol Cell Biol *8*, 37-48.

Tang, Z., Scherer, P. E., Okamoto, T., Song, K., Chu, C., Kohtz, D. S., Nishimoto, I., Lodish, H. F., and Lisanti, M. P. (1996). Molecular cloning of caveolin-3, a novel member of the caveolin gene family expressed predominantly in muscle. J Biol Chem *271*, 2255-2261.

Tarricone, C., Xiao, B., Justin, N., Walker, P. A., Rittinger, K., Gamblin, S. J., and Smerdon, S. J. (2001). The structural basis of Arfaptin-mediated cross-talk between Rac and Arf signalling pathways. Nature *411*, 215-219.

Tebar, F., Confalonieri, S., Carter, R. E., Di Fiore, P. P., and Sorkin, A. (1997). Eps15 is constitutively oligomerized due to homophilic interaction of its coiled-coil region. J Biol Chem *272*, 15413-15418.

Teng, H., and Wilkinson, R. S. (2000). Clathrin-mediated endocytosis near active zones in snake motor boutons. J Neurosci *20*, 7986-7993.

Tsuboi, S., Takada, H., Hara, T., Mochizuki, N., Funyu, T., Saitoh, H., Terayama, Y., Yamaya, K., Ohyama, C., Nonoyama, S., and Ochs, H. D. (2009). FBP17 Mediates a Common Molecular Step in the Formation of Podosomes and Phagocytic Cups in Macrophages. J Biol Chem *284*, 8548-8556.

Tsuboi, T., and Rutter, G. A. (2003). Multiple forms of "kiss-and-run" exocytosis revealed by evanescent wave microscopy. Curr Biol *13*, 563-567.

Tsujita, K., Suetsugu, S., Sasaki, N., Furutani, M., Oikawa, T., and Takenawa, T. (2006). Coordination between the actin cytoskeleton and membrane deformation by a novel membrane tubulation domain of PCH proteins is involved in endocytosis. J Cell Biol *172*, 269-279.

Udell, C. M., Samayawardhena, L. A., Kawakami, Y., Kawakami, T., and Craig, A. W. (2006). Fer and Fps/Fes participate in a Lyn-dependent pathway from FcepsilonRI to platelet-endothelial cell adhesion molecule 1 to limit mast cell activation. J Biol Chem *281*, 20949-20957.

Unwin, N. (2005). Refined structure of the nicotinic acetylcholine receptor at 4A resolution. J Mol Biol *346*, 967-989.

Vale, R. D., and Hotani, H. (1988). Formation of membrane networks in vitro by kinesin-driven microtubule movement. J Cell Biol *107*, 2233-2241.

van Bergen En Henegouwen, P. M. (2009). Eps15: a multifunctional adaptor protein regulating intracellular trafficking. Cell Commun Signal *7*, 24.

Van Duyne, G. D., Standaert, R. F., Karplus, P. A., Schreiber, S. L., and Clardy, J. (1993). Atomic structures of the human immunophilin FKBP-12 complexes with FK506 and rapamycin. J Mol Biol *229*, 105-124.

Vartiainen, M. K., and Machesky, L. M. (2004). The WASP-Arp2/3 pathway: genetic insights. Curr Opin Cell Biol *16*, 174-181.

Vogt, D. L., Gray, C. D., Young, W. S., 3rd, Orellana, S. A., and Malouf, A. T. (2007). ARHGAP4 is a novel RhoGAP that mediates inhibition of cell motility and axon outgrowth. Mol Cell Neurosci *36*, 332-342.

Wang, D. S., and Shaw, G. (1995). The association of the C-terminal region of beta I sigma II spectrin to brain membranes is mediated by a PH domain, does not require membrane proteins, and coincides with a inositol-1,4,5 triphosphate binding site. Biochem Biophys Res Commun *217*, 608-615.

Wang, H., Traub, L. M., Weixel, K. M., Hawryluk, M. J., Shah, N., Edinger, R. S., Perry, C. J., Kester, L., Butterworth, M. B., Peters, K. W., *et al.* (2006). Clathrin-mediated endocytosis of the epithelial sodium channel. Role of epsin. J Biol Chem *281*, 14129-14135.

Wang, Q., Kaan, H. Y., Hooda, R. N., Goh, S. L., and Sondermann, H. (2008). Structure and plasticity of Endophilin and Sorting Nexin 9. Structure *16*, 1574-1587.

Wang, Q., Navarro, M. V., Peng, G., Molinelli, E., Goh, S. L., Judson, B. L., Rajashankar, K. R., and Sondermann, H. (2009a). Molecular mechanism of membrane constriction and tubulation mediated by the F-BAR protein Pacsin/Syndapin. Proc Natl Acad Sci U S A *106*, 12700-12705.

Wang, Y., Huang, Y., Wang, J., Cheng, C., Huang, W., Lu, P., Xu, Y. N., Wang, P., Yan, N., and Shi, Y. (2009b). Structure of the formate transporter FocA reveals a pentameric aquaporin-like channel. Nature *462*, 467-472.

Warnock, D. E., Terlecky, L. J., and Schmid, S. L. (1995). Dynamin GTPase is stimulated by crosslinking through the C-terminal proline-rich domain. Embo J *14*, 1322-1328.

Wasiak, S., Quinn, C. C., Ritter, B., de Heuvel, E., Baranes, D., Plomann, M., and McPherson, P. S. (2001). The Ras/Rac guanine nucleotide exchange factor mammalian Son-of-sevenless interacts with PACSIN 1/syndapin I, a regulator of endocytosis and the actin cytoskeleton. J Biol Chem *276*, 26622-26628.

Waterman-Storer, C. M., and Salmon, E. D. (1998). Endoplasmic reticulum membrane tubules are distributed by microtubules in living cells using three distinct mechanisms. Curr Biol *8*, 798-806.

Wenk, M. R., and De Camilli, P. (2004). Protein-lipid interactions and phosphoinositide metabolism in membrane traffic: insights from vesicle recycling in nerve terminals. Proc Natl Acad Sci U S A *101*, 8262-8269.

Wieffer, M., Maritzen, T., and Haucke, V. (2009). SnapShot: endocytic trafficking. Cell *137*, 382 e381-383.

Wigge, P., Kohler, K., Vallis, Y., Doyle, C. A., Owen, D., Hunt, S. P., and McMahon, H. T. (1997). Amphiphysin heterodimers: potential role in clathrin-mediated endocytosis. Mol Biol Cell *8*, 2003-2015.

Williams, T. M., and Lisanti, M. P. (2004). The caveolin proteins. Genome Biol *5*, 214.

Winckler, B., and Schafer, D. A. (2007). Cordon-bleu: a new taste in actin nucleation. Cell *131*, 236-238.

Wong, H. K., Liu, X. B., Matos, M. F., Chan, S. F., Perez-Otano, I., Boysen, M., Cui, J., Nakanishi, N., Trimmer, J. S., Jones, E. G., *et al.* (2002). Temporal and regional expression of NMDA receptor subunit NR3A in the mammalian brain. J Comp Neurol *450*, 303-317.

Wong, K., Ren, X. R., Huang, Y. Z., Xie, Y., Liu, G., Saito, H., Tang, H., Wen, L., Brady-Kalnay, S. M., Mei, L., *et al.* (2001). Signal transduction in neuronal migration: roles of GTPase activating proteins and the small GTPase Cdc42 in the Slit-Robo pathway. Cell *107*, 209-221.

Wu, M., Huang, B., Graham, M., Raimondi, A., Heuser, J. E., Zhuang, X., and De Camilli, P. (2010). Coupling between clathrin-dependent endocytic budding and F-BAR-dependent tubulation in a cell-free system. Nat Cell Biol *12*, 902-908.

Wu, Y., Dowbenko, D., and Lasky, L. A. (1998a). PSTPIP 2, a second tyrosine phosphorylated, cytoskeletal-associated protein that binds a PEST-type protein-tyrosine phosphatase. J Biol Chem *273*, 30487-30496.

Wu, Y., Spencer, S. D., and Lasky, L. A. (1998b). Tyrosine phosphorylation regulates the SH3-mediated binding of the Wiskott-Aldrich syndrome protein to PSTPIP, a cytoskeletal-associated protein. J Biol Chem *273*, 5765-5770.

Yamabhai, M., Hoffman, N. G., Hardison, N. L., McPherson, P. S., Castagnoli, L., Cesareni, G., and Kay, B. K. (1998). Intersectin, a novel adaptor protein with two Eps15 homology and five Src homology 3 domains. J Biol Chem *273*, 31401-31407.

Yamada, H., Padilla-Parra, S., Park, S. J., Itoh, T., Chaineau, M., Monaldi, I., Cremona, O., Benfenati, F., De Camilli, P., Coppey-Moisan, M., *et al.* (2009). Dynamic interaction of amphiphysin with N-WASP regulates actin assembly. J Biol Chem *284*, 34244-34256.

Yamagishi, A., Masuda, M., Ohki, T., Onishi, H., and Mochizuki, N. (2004). A novel actin bundling/filopodium-forming domain conserved in insulin receptor tyrosine kinase substrate p53 and missing in metastasis protein. J Biol Chem *279*, 14929-14936.

Yap, C. C., Lasiecka, Z. M., Caplan, S., and Winckler, B. (2010). Alterations of EHD1/EHD4 protein levels interfere with L1/NgCAM endocytosis in neurons and disrupt axonal targeting. J Neurosci *30*, 6646-6657.

Yarar, D., Waterman-Storer, C. M., and Schmid, S. L. (2005). A dynamic actin cytoskeleton functions at multiple stages of clathrin-mediated endocytosis. Mol Biol Cell *16*, 964-975.

Yoon, Y., Tong, J., Lee, P. J., Albanese, A., Bhardwaj, N., Kallberg, M., Digman, M. A., Lu, H., Gratton, E., Shin, Y. K., and Cho, W. (2010). Molecular basis of the potent membrane-remodeling activity of the epsin 1 N-terminal homology domain. J Biol Chem *285*, 531-540.

Yoshida, Y., Kinuta, M., Abe, T., Liang, S., Araki, K., Cremona, O., Di Paolo, G., Moriyama, Y., Yasuda, T., De Camilli, P., and Takei, K. (2004). The stimulatory action of amphiphysin on dynamin function is dependent on lipid bilayer curvature. Embo J *23*, 3483-3491.

You, J. J., and Lin-Chao, S. (2010). Gas7 functions with N-WASP to regulate the neurite outgrowth of hippocampal neurons. J Biol Chem *285*, 11652-11666.

Zakharenko, S., and Popov, S. (1998). Dynamics of axonal microtubules regulate the topology of new membrane insertion into the growing neurites. J Cell Biol *143*, 1077-1086.

Zhang, P., and Hinshaw, J. E. (2001). Three-dimensional reconstruction of dynamin in the constricted state. Nat Cell Biol *3*, 922-926.

Appendix

a) List of Figures

b) List of Primers

Constructs	Mutations & Truncations	Vector	Primer Sequence 5'—3' *
Syndapin 1-FL	---	pET-28a(+)	TAATGCTAGCATGTCTGGCTCCTACGATGAGGCCT
			GGCTGAATTCCTATATAGCCTCAACGTAGTTGGC
Syndapin 1-(1-337)	---	pET-28a(+)	TAATGCTAGCATGTCTGGCTCCTACGATGAGGCCT
			GGCTGAATTCCTACTGGGATGTGGATTCTACAGCCCCAGT
Syndapin 1-(1-337)	K145E,K146E, K148E	pET-28a(+)	CAGAAGCCCTGGGCTGAAGAGATGGAGGAGCTAGAGCTAG
			CTAGCTCTAGCTCCTCCATCTCTTCAGCCCAGGGCTTCTG
Syndapin 1	Q396R,E397R	pET-28a(+)	TATGACTACGACGGTAGGAGGCAGGATGAGCTCAGCTTC
			GAAGCTGAGCTCATCCTGCCTCCTACCGTCGTAGTCATA
Endophilin 1-(1-256)	---	pET-28a(+)	ATAAGGATCCATGTCGGTGGCAGGGCTGAAGAAGCA
			ATCCCTCGAGCTACTGATATTCCCTTCTTGGTTGAGATGAAG
Amphiphysin 1-(1-245)	---	pET-28a(+)	ATAAGGATCCATGGCCGACATCAAGACGGGCATCT
			ATATCTCGAGCTAAATGCTGAAGGCCTTGTCAGCGTG
EHD1-(401-534)	---	pET-28a(+)	GTATCATATGGAGTCCCTGATGCCTTCCCAGGTGGT
			TGATGGATCCGAGTCCCTGATGCCTTCCCAGGTGGT
Dynamin 1-(509-864)	---	pET-28a(+)	TACTCATATGAAGACTTCAGGGAACCAGGATGAGAT
			TTACGAATTCTTAGAGGTCGAAGGGGGGCCTGGGGC
Syndapin 1-(340-441)	---	pGEX-2T	TCATGGATCCGACCGTGGCAGTGTTAGCAGCTAT
			GACTGAATTCCTATATAGCCTCAACGTAGTTGGCAG
Syndapin 1-(379-441)	---	pGEX-2T	TAATGGATCCGAGGATGATGCCAAGGGAGTTCGT
			GACTGAATTCCTATATAGCCTCAACGTAGTTGGCAG
Syndapin 1-SH3 domain	E400R	pGEX-2T	GACGGTCAGGAGCAGGATCGGCTCAGCTTCAAGGCC
			GGCCTTGAAGCTGAGCCGATCCTGCTCCTGACCGTC
Syndapin 1-SH3 domain	P434L	pGEX-2T	TAATGGATCCGAGGATGATGCCAAGGGAGTTCGT
			TGATGGATCCCTATATAGCCTCAACGTAGTTGGCAAGATAG

Syndapin 1-SH3 domain	D394R,E400R	pGEX-2T	TATGACTACCGCGGTCAGGAGCAGGATAG GCTCAGCTTCAAG
			CTTGAAGCTGAGCCTATCCTGCTCCTGAC CGCGGTAGTCATA
Syndapin 1-SH3 domain	Q396R,E397R	pGEX-2T	TATGACTACGACGGTAGGAGGCAGGATGA GCTCAGCTTC
			GAAGCTGAGCTCATCCTGCCTCCTACCGT CGTAGTCATA
Endophilin 1-SH3 domain	---	pGEX-4T-1	CCGGAATTCCCCAAACCTCCAGGTGTC
			TCCGCTCGAGCTAATGGGGCAGAGCAACC A
Syndapin 1-FL	---	pEGFP-C1	TGATGAATTCCACCATGTCTGGCTCCTACG ATGAGGCCT
			TGATGGATCCCTATATAGCCTCAACGTAGT TGGC
Syndapin 1	I122F,M123F	pEGFP-C1	GCCTATCACAAGCAGGGTGGCTTCAAGGA G
			CTCCTTGAAGCCACCCTGCTTGTGATAGG C
Syndapin 1	K127E,K130E	pEGFP-C1	ATGGGTGGCTTCGAGGAGACGGAAGAGG CCGAGGA
			TCCTCGGCCTCTTCCGTCTCCTCGAAGCC ACCCAT
Syndapin 1-(1-304)	---	pEGFP-C1	TGATGAATTCCACCATGTCTGGCTCCTACG ATGAGGCCT
			TGATGGATCCCTATGGGTTCCACTCCTCGA ACTGCGGCC
Syndapin 1-(1-304)	I122F,M123F	pEGFP-C1	GCCTATCACAAGCAGGGTGGCTTCAAGGA G
			CTCCTTGAAGCCACCCTGCTTGTGATAGG C
Syndapin 1-(1-304)	I122T,M123Q	pEGFP-C1	TATCACAAGCAGACCCAGGGTGGCTTCAA GGA
			TCCTTGAAGCCACCCTGGGTCTGCTTGTG ATAG
Syndapin 1-(1-304)	K127E,K130E	pEGFP-C1	ATGGGTGGCTTCGAGGAGACGGAAGAGG CCGAGGA
			TCCTCGGCCTCTTCCGTCTCCTCGAAGCC ACCCAT
Syndapin 1-(1-304)	K145E,K146E, K148E	pEGFP-C1	CAGAAGCCCTGGGCTGAAGAGATGGAGG AGCTAGAGCTAG
			CTAGCTCTAGCTCCTCCATCTCTTCAGCCC AGGGCTTCTG
Syndapin 1-SH3 domain	---	pmCherry-N1	CATCAAGCTTATGGAGGATGATGCCAAGG GAGTTCGT
			TGATGGTACCAGTATAGCCTCAACGTAGTT GGCAG
Syndapin 1-SH3 domain	D394R,E400R	pmCherry-N1	TATGACTACCGCGGTCAGGAGCAGGATAG GCTCAGCTTCAAG
			CTTGAAGCTGAGCCTATCCTGCTCCTGAC CGCGGTAGTCATA
Syndapin 1-SH3 domain	Q396R,E397R	pmCherry-N1	TATGACTACGACGGTAGGAGGCAGGATGA GCTCAGCTTC
			GAAGCTGAGCTCATCCTGCCTCCTACCGT CGTAGTCATA

* A pair of primers for each construct: forward and reverse primer

c) List of Abbreviations

2xYT	2x Yeast trypton
ABBA	Actin-bundling protein with BAIAP2 homology
ADAM	A Metalloprotease And Disintegrins
Amp	Ampicillin
AMPAR	α-amino-3-hydroxy-5-methyl-4-isoxazolepropionic acid receptor
ANTH domain	AP180 N-terminal homology domain
AP2	Adaptor protein complex 2
ARH	Autosomal Recessive Hypercholesterolemia
BAR	Bin, amphiphysin, Rvs domain
BSA	Bovine serum albumin
C2 domain	protein kinase C conserved region 2 domain
CCD	Charge-coupled device
CCP	Clathrin-coated pit
CCV	Clathrin-coated vesicle
CHAPS	3-[(3-Cholamidopropyl)dimethylammonio]-1-propanesulfonate
CIP	Calf intestinal phosphatase
CIP4	Cdc42-interacting protein-4
CNS	Cental nervous system
Cobl	Cordon-Bleu
COP	Coat protein complex
DAB2	Disabled homolog 2
Dbl domain	Duffy-binding-like domain
DH domain	Dbl homology domain
DLP1	dynamin-like protein1
DMEM	Dulbecco’s modified Eagle’s medium
DMSO	Dimethyl sulfoxide
DPF	Aspartate-Proline-Phenylalanine
EDTA	Ethylenediaminetetraacetic Acid
EH	Eps15 homology domain
EHD	Eps15 homology domain protein
EM	Electron microscopy

ENTH domain	Epsin N-terminal homology domain
ER	Endoplasmic reticulum
EtBr	Ethidium bromide
F-BAR	Fer/CIP4 homology (FCH)-BAR domain
FBP17	formin-binding protein-17
FCHO	FCH domain-only domain
FCS	Fetal calf serum
FERM domain	4.1-ezrin, radixin, and moesin homology domain
FH2	Formin-homology-2 domain
FL	Full-length
FYVE domain	Fab1, YOTB, Vac1 (vesicle transport protein), and EEA1 domain
GAP	GTPase activating protein
GBP1	Guanylate-binding protein 1
GED	GTPase effector domain
GFP	Green fluorescent protein
GRAF	GTPase regulator associated with focal adhesion kinase
GST	Glutathione-S-Transferase
GTP	Guanosine-5'-triphosphate
HBSS	Hank's buffered salt solution
HCl	Hydrogen chloride
HEPES	4-(2-hydroxyethyl)-1-piperazineethanesulfonic acid
HR1	Protein kinase C-related kinase homology region
I-BAR	Inverse-BAR domain
IPTG	Isopropyl-β-D-thiogalactopyranoside
IRTKS/BAIAP2L1	Insulin receptor tyrosine kinase substrate
Kan	Kanamycin
KIND	Kinase non-catalytic C-lobe domain
LB medium	Luria–Bertani medium
MAD	Multiple anomalous dispersion
MIM	Missing-in-metastasis
MIR	Multiple isomorphous replacement
MR	Molecular replacement
MPD	2-methylpentan-2,4-diol

N-BAR	BAR domain with a N-terminal amphipathic helix
NEB	New England Biolabs
Ni-NTA	Nickel-nitrilotriacetic acid
NLS	Nuclear localization signal
NMDAR	N-methyl-D-aspartic acid receptor
NMJ	Neuromuscular junction
NPF	Asn-Pro-Phe peptide
N-WASP	Neural Wiskott-Aldrich syndrome protein
Nwk	Nervous Wreck
OD	Optical density
OPA1	Optic atrophy 1
PACSIN	Protein kinase C and casein kinase 2 substrate in neurons
PBS	Phosphate buffered saline
PCH	Pombe Cdc15 homology domain
PCR	Polymerase Chain Reaction
PDB	Protein Data Bank
PEG	polyethylene glycol
PH domain	Pleckstrin homology domain
PI	Phosphatidylinositol
PI(4,5)P2	Phosphatidylinositol (4,5)-bisphosphate
PMSF	Phenylmethanesulfonyl fluoride
PRD	Proline-rich domain
PSTPIP	Proline-serinethreonine phosphatase-interacting proteins
PTB domain	Phosphotyrosine binding-domain
PX domain	Phox homology domains
RFP	Red fluorescent protein
Scar	Suppressor of cyclic AMP receptor
SDS	Sodium dodecyl sulfate
SDS-PAGE	SDS polyacrylamide gel electrophoresis
SH2 domain	SRC Homology 2 Domain
SH3 domain	SRC Homology 3 Domain
SNX	Sorting Nexin
Sos	Son-of-sevenless

SPR	Surface Plasmon Resonance
srGAP	Slit-Robo Rho GTPase activating protein
SV	Synaptical vesicle
TBE	Tris-boronacid-EDTA
TNF	Tumour necrosis factor
Toca-1	transactivator of cytoskeletal assembly-1
Tris	2-amino-2-hydroxymethyl-propane-1,3-diol
Triton X-100	Octylphenol ethylene oxide condensate
UIM	Ubiquitin-interacting Motif
UV	Ultraviolet
WAVE	WASP family Verprolin-homologous protein
WH2 domain	WASP homology domain-2
W/O	Without
WT	Wild type
w/v	Weight per volume
w/w	Weight per weight
µHD	µ-homology domain

d) Curriculum vitae

For reasons of data protection,
the curriculum vitae is not included in the online version

e) Publications

1. **Rao, Y.,** Ma, Q., Vahedi-Faridi, A., Sundborger, A., Pechstein, A., Puchkov, D., Luo, L., Shupliakov, O., Saenger, W., and Haucke, V. (2010). Molecular basis for SH3 domain regulation of F-BAR-mediated membrane deformation. Proc Natl Acad Sci U S A *107*, 8213-8218.

2. **Rao, Y.,** Bian, C., Yuan, C., Li, Y., Chen, L., Ye, X., Huang, Z., and Huang, M. (2006). An open conformation of switch I revealed by Sar1-GDP crystal structure at low Mg2+. Biochem Biophys Res Commun *348*, 908-915.

3. **Rao, Y.,** Yuan, C., Bian, C., Hou, X., Li, Y., Zhao, G., Ye, X., Huang, Z., and Huang, M. (2006). Crystal Structure of Sar1[H79G]-GDP Which Provides Insight into the Coat-controlled GTP Hydrolysis in the Disassembly of COP II. Chinese J Struct Chem *25*, 854-860.